SFB/CPP-10-122
TTP10-48
MZ-TH/10-44
November 2010

$\bar{B}_s \to \phi\rho^0$ and $\bar{B}_s \to \phi\pi^0$ as a handle on isospin-violating New Physics

Lars Hofer[a,b], Dominik Scherer[a] and Leonardo Vernazza[c*]

[a] *Institut für Theoretische Teilchenphysik, Karlsruhe Institute of Technology, D–76128 Karlsruhe, Germany*

[b] *Institut für Theoretische Physik und Astrophysik, Universität Würzburg, D–97074 Würzburg, Germany*

[c] *Institut für Physik (THEP), Johannes Gutenberg-Universität, D–55099 Mainz, Germany*

Abstract

The 2.5σ discrepancy between theory and experiment observed in the difference $A_{\rm CP}(B^- \to \pi^0 K^-) - A_{\rm CP}(\bar{B}^0 \to \pi^+ K^-)$ can be explained by a new electroweak penguin amplitude. Motivated by this result, we analyse the purely isospin-violating decays $\bar{B}_s \to \phi\rho^0$ and $\bar{B}_s \to \phi\pi^0$, which are dominated by electroweak penguins, and show that in presence of a new electroweak penguin amplitude their branching ratio can be enhanced by up to an order of magnitude, without violating any constraints from other hadronic B decays. This makes them very interesting modes for LHCb and future B factories. We perform both a model-independent analysis and a study within realistic New Physics models such as a modified-Z^0-penguin scenario, a model with an additional Z' boson and the MSSM. In the latter cases the new amplitude can be correlated with other flavour phenomena, such as semileptonic B decays and B_s-$\bar{B}_s$ mixing, which impose stringent constraints on the enhancement of the two B_s decays. In particular we find that, contrary to claims in the literature, electroweak penguins in the MSSM can reduce the discrepancy in the $B \to \pi K$ modes only marginally. As byproducts we update the SM predictions to $\mathrm{Br}(\bar{B}_s \to \phi\pi^0) = 1.6^{+1.1}_{-0.3} \cdot 10^{-7}$ and $\mathrm{Br}(\bar{B}_s \to \phi\rho^0) = 4.4^{+2.7}_{-0.7} \cdot 10^{-7}$ and perform a state-of-the-art analysis of $B \to \pi K$ amplitudes in QCD factorisation.

[*] Alexander-von-Humboldt Fellow

1 Introduction

At present flavour physics has entered a new exciting era. The new experiment LHCb and the planned super-B-factories will bring the precision of Standard Model (SM) tests and the scope of searches for New Physics (NP) to unseen heights. Particularly important thereby are flavour-changing neutral current (FCNC) decays, which in the SM are highly-suppressed electroweak loop processes. In this work we present a phenomenological analysis of two hadronic FCNC decays, namely $\bar{B}_s \to \phi\rho^0$ and $\bar{B}_s \to \phi\pi^0$. We argue that within the next years these decays will become very interesting objects for experimental analyses of the electroweak penguin sector. Up to now, this sector has been tested in hadronic decays only in $B \to \pi K$ modes, and the discrepancies found between the SM prediction and experimental measurements is the main motivation for our work.

The four $B \to \pi K$ decay channels, first observed by the CLEO experiment in the late 1990s [1,2], have become by now a classic in flavour physics thanks to the precise measurements by BABAR and BELLE. This is also reflected in the large number of theoretical studies of these decays in the SM and various extensions of it. Charged and neutral B mesons can decay to a πK final state due to a weak process at the partonic level, $b \to s\bar{q}q$ with $q = u, d$. This process is dominated by an FCNC loop governed by the CKM factor $V_{ts}^* V_{tb}$ and receives, in the $q = u$ case, also a small tree-level contribution involving the smaller CKM factor $V_{us}^* V_{ub}$. The $B \to \pi K$ branching fractions are therefore small, of order $\mathcal{O}(10^{-6})$, and sensitive to new FCNCs arising in extensions of the SM. For this reason they are, together with the corresponding CP asymmetries, important observables for tests of the SM flavour structure and for NP searches.

With the data of the B factories having become more and more precise, some discrepancies between $B \to \pi K$ measurements and SM predictions have occurred, provoking speculations on a "$B \to \pi K$ puzzle". To date, the measurements of the branching fractions have fluctuated towards the SM predictions, the latter still suffering from large hadronic uncertainties, and only the CP asymmetries show an unexpected behavior [3–5] manifesting itself in the quantity

$$\Delta A_{\rm CP} \equiv A_{\rm CP}(B^- \to \pi^0 K^-) - A_{\rm CP}(\bar{B}^0 \to \pi^+ K^-). \tag{1}$$

For this observable we find in the framework of QCD factorisation (QCDF)

$$\Delta A_{\rm CP} \stackrel{\rm SM}{=} 1.9^{+5.8}_{-4.8}\,\% \tag{2}$$

as the SM prediction, which differs significantly from the experimental value

$$\Delta A_{\rm CP} \stackrel{\rm exp.}{=} (14.8 \pm 2.8)\%. \quad [6] \tag{3}$$

Adopting a frequentist approach where we consider a theoretical "error bar" as a range of values definitely containing the true theory result but without assigning any statistical meaning to it [7], this amounts to a 2.5σ discrepancy.

A point which has received much attention in the literature (see e.g. [8] and references therein) is the fact that the formerly observed discrepancies as well as the currently existing anomaly in $\Delta A_{\rm CP}$ suggest a violation of the strong isospin symmetry beyond the amount expected in the SM. This has often been interpreted as a hint for enhanced electroweak penguins (EW penguins) [9–11]. We will give a brief overview and discuss the current status of this topic in section 2.1. Whether the 2.5σ discrepancy in $\Delta A_{\rm CP}$ is a hint for NP in EW penguins or a non-perturbative hadronic effect or simply a statistical fluctuation is controversial. The point that we want to make is that, in order to assess this question, it is highly desirable to obtain further information from other hadronic decays which are sensitive to EW penguin contributions. For this reason we study the *purely* isospin-violating decays $\bar{B}_s \to \phi\rho^0$ and $\bar{B}_s \to \phi\pi^0$, which are dominated by EW penguins. If NP in this sector exists at a level where it can explain the $\Delta A_{\rm CP}$ puzzle, it could be clearly visible in these purely isospin-violating decays. The upcoming new generation of flavour experiments will have the opportunity to detect these modes for the first time and to measure their branching fractions. The aim of our work is to provide a detailed analysis from the theory side, both in the SM and beyond.

Since the decays $\bar{B}_s \to \phi\rho^0$ and $\bar{B}_s \to \phi\pi^0$ are not related to other decay modes via flavour symmetries, the non-perturbative part of their decay amplitudes has to be determined from first principles. This can be achieved using the framework of QCDF [12–16]. This method amounts to a calculation of the hadronic matrix elements up to corrections of order $\Lambda_{\rm QCD}/m_B$, where $\Lambda_{\rm QCD} \sim \mathcal{O}(200\,{\rm MeV})$ is a typical non-perturbative energy scale of strong interactions. We will use this method throughout the paper in all analyses of B decays to light mesons.

The plan of the paper is as follows: In Chapter 2, we discuss the issue of isospin-violation in $B \to \pi K$ decays and the phenomenology of $\bar{B}_s \to \phi\rho^0$ and $\bar{B}_s \to \phi\pi^0$. As a byproduct we provide simple formulas which allow for an easy calculation of various observables concerning these decay modes, taking into account NP effects in EW penguins. Chapter 3 contains a detailed quantitative analysis of $\bar{B}_s \to \phi\rho^0$ and $\bar{B}_s \to \phi\pi^0$ in different scenarios of a model-independent parameterisation of NP in EW penguins. This analysis is performed in light of our present knowledge on EW penguins from other B decays, in particular $B \to \pi K$. It is complemented in Chapter 4 with studies of particular extensions of the SM which feature enhanced EW penguins. We conclude in Chapter 5. We keep the main body of the paper free of technicalities and refer the reader interested in technical details to the appendices.

2 Isospin-violation in hadronic B decays

2.1 The $B \to \pi K$ modes

The $B \to \pi K$ decays are dominated by the isospin-conserving QCD penguin amplitude. Nevertheless, they receive small contributions from the tree and the EW penguin amplitude, which are isospin-violating. Combining measurements of the four different decay modes $B^- \to \pi^- \bar{K}^0$, $B^- \to \pi^0 K^-$, $\bar{B}^0 \to \pi^+ K^-$ and $\bar{B}^0 \to \pi^0 \bar{K}^0$, it is possible to construct observables in which the leading contribution from the QCD penguin drops out, so that they are sensitive to isospin violation.

The mesons participating in $B \to \pi K$ decays transform under isospin rotations as

$$(\bar{B}^0, -B^-)_{1/2}\,, \qquad (\bar{K}^0, -K^-)_{1/2}\,, \qquad (\pi^+, -\pi^0, -\pi^-)_1\,. \tag{4}$$

Furthermore we can assign isospin to the operators appearing in the effective Hamiltonian

$$\mathcal{H}_{\rm eff} = \frac{G_F}{\sqrt{2}} \sum_{p=u,c} \lambda_p^{(s)} \left(C_1 Q_1^p + C_2 Q_2^p + \sum_{i=3}^{10} C_i Q_i + C_{7\gamma} Q_{7\gamma} + C_{8g} Q_{8g} \right) + \text{h.c.}, \tag{5}$$

which mediates the $B \to \pi K$ transitions. Here $\lambda_p^{(s)} = V_{pb} {V_{ps}}^*$ represents a product of elements of the quark mixing (CKM) matrix, $Q_{1,2}^p$ are the so-called current-current operators, $Q_{3,\ldots,6}$ are QCD penguin operators, $Q_{7\gamma}$ and Q_{8g} represent the electromagnetic and chromomagnetic operators and

$$Q_7 = (\bar{s}_\alpha b_\alpha)_{V-A} \textstyle\sum_q \frac{3}{2} e_q (\bar{q}_\beta q_\beta)_{V+A}, \qquad Q_8 = (\bar{s}_\alpha b_\beta)_{V-A} \textstyle\sum_q \frac{3}{2} e_q (\bar{q}_\beta q_\alpha)_{V+A}, \tag{6}$$

$$Q_9 = (\bar{s}_\alpha b_\alpha)_{V-A} \textstyle\sum_q \frac{3}{2} e_q (\bar{q}_\beta q_\beta)_{V-A}, \qquad Q_{10} = (\bar{s}_\alpha b_\beta)_{V-A} \textstyle\sum_q \frac{3}{2} e_q (\bar{q}_\beta q_\alpha)_{V-A}, \tag{7}$$

are the EW penguin operators (α, β denote colours). The latter are of great importance for our work. We define the operators as in [14] so that $C_1(m_W) = 1$ at leading-order. Containing $\bar{u}u$- and $\bar{d}d$-bilinears, the operators Q_1,...,Q_{10} can be distributed among

$$\mathcal{H}_{\rm eff} \;=\; \mathcal{H}_{\rm eff}^{\Delta I=1} \;+\; \mathcal{H}_{\rm eff}^{\Delta I=0} \tag{8}$$

according to the decomposition $1/2 \otimes 1/2 = 1 \oplus 0$ [17]. Since the QCD penguin operators $Q_{3,\ldots,6}$ involve the isosinglet combination $(\bar{u}u + \bar{d}d)$, they contribute solely to $\mathcal{H}_{\rm eff}^{\Delta I=0}$ whereas the other operators give contributions to both parts of $\mathcal{H}_{\rm eff}$. The $B \to \pi K$ decays thus follow the isospin pattern

$$1/2 \;\stackrel{\Delta I=1,0}{\longrightarrow}\; 1 \otimes 1/2 \;=\; 3/2 \oplus 1/2, \tag{9}$$

implying that all four decay amplitudes can be decomposed into three independent isospin amplitudes, $\mathcal{A}_{1/2}^{\Delta I=0}$, $\mathcal{A}_{1/2}^{\Delta I=1}$ and $\mathcal{A}_{3/2}^{\Delta I=1}$ with the lower index denoting the total isospin of the final state.

One finds that $B \to \pi K$ is dominated by the QCD penguin contribution and thus $|\mathcal{A}_{1/2}^{\Delta I=0}| \gg |\mathcal{A}_{3/2,\,1/2}^{\Delta I=1}|$. To a first approximation, all the decay modes can be described by the amplitude $\mathcal{A}_{1/2}^{\Delta I=0}$ only, dictating the relative size of the branching fractions to be $1:2:1:2$ (in the same order as in tab. 1).

The isospin-invariant amplitudes receive contributions from various SM quark diagrams. It is only at the level of these diagrams that the pattern of CP violation can be

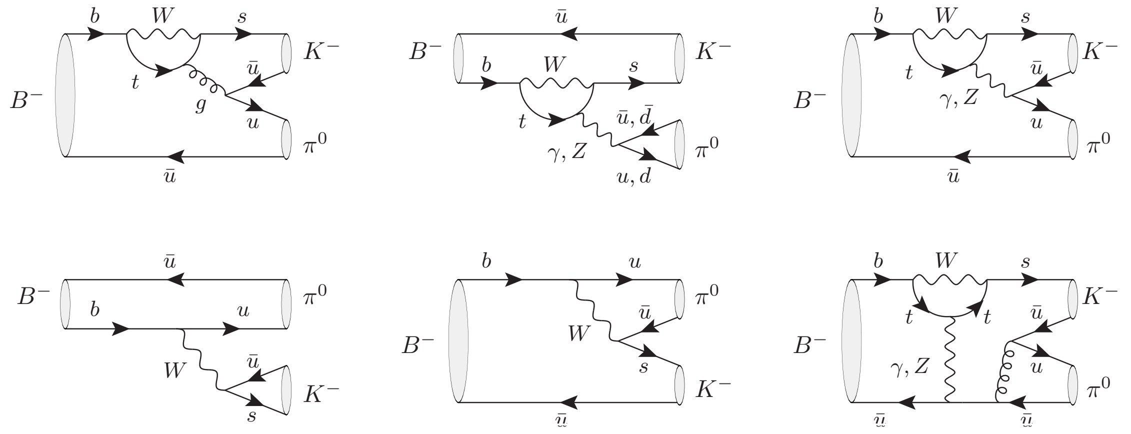

Figure 1: Diagrams representing the topological parameterisation in eq. (10) for $B^- \to \pi^0 K^-$. First line from left to right: QCD penguin (P), colour-allowed EW penguin ($r_{\rm EW}$), colour-suppressed EW penguin ($r_{\rm EW}^{\rm C}$). Second line from left to right: colour-allowed tree ($r_{\rm T}$), colour-suppressed tree ($r_{\rm C}$), EW penguin annihilation ($r_{\rm EW}^{\rm A}$).

correctly implemented, i.e. that the amplitudes $\mathcal{A}_{1/2}^{\Delta I=0}$, $\mathcal{A}_{3/2,\,1/2}^{\Delta I=1}$ can be related to their CP-conjugated counterparts $\overline{\mathcal{A}}_{1/2}^{\Delta I=0}$, $\overline{\mathcal{A}}_{3/2,\,1/2}^{\Delta I=1}$. This suggests an alternative parameterisation of the amplitudes in terms of the topologies of the underlying quark-level transitions [18,19]:

$$
\begin{aligned}
\mathcal{A}(B^- \to \pi^- \bar{K}^0) &\simeq P\left(1 - \frac{1}{3} r_{\rm EW}^{C} + \frac{2}{3} r_{\rm EW}^{\rm A}\right), \\
\sqrt{2}\,\mathcal{A}(B^- \to \pi^0 K^-) &\simeq P\left(1 + r_{\rm EW} + \frac{2}{3} r_{\rm EW}^{C} + \frac{2}{3} r_{\rm EW}^{\rm A} - (r_{\rm T} + r_{\rm C}) e^{-i\gamma}\right), \\
\mathcal{A}(\bar{B}^0 \to \pi^+ K^-) &\simeq P\left(1 + \frac{2}{3} r_{\rm EW}^{C} - \frac{1}{3} r_{\rm EW}^{\rm A} - r_{\rm T} e^{-i\gamma}\right), \\
\sqrt{2}\,\mathcal{A}(\bar{B}^0 \to \pi^0 \bar{K}^0) &\simeq -P\left(1 - r_{\rm EW} - \frac{1}{3} r_{\rm EW}^{C} - \frac{1}{3} r_{\rm EW}^{\rm A} + r_{\rm C} e^{-i\gamma}\right).
\end{aligned} \tag{10}
$$

This topological parameterisation is illustrated by the corresponding Feynman diagrams for $B^- \to \pi^0 K^-$ in fig. 1. In eq. (10) we have factored out the dominant QCD penguin amplitude P and neglected penguin amplitudes suppressed by $|V_{us}^* V_{ub}|/|V_{cs}^* V_{cb}|$. The dependence on the weak CKM phase γ has been made explicit, while strong phases are contained in the ratios r_i which fulfill $|r_i| < 1$. These quantities denote corrections from different types of Feynman diagrams: $r_{\rm T}$ and $r_{\rm C}$ stem from colour-allowed and colour-suppressed tree diagrams, $r_{\rm EW}$ and $r_{\rm EW}^{\rm C}$ from colour-allowed and colour-suppressed EW penguins, respectively. Annihilation via QCD penguin diagrams is absorbed into P whereas weak annihilation via EW penguin diagrams is parameterised by $r_{\rm EW}^{\rm A}$ and colour-suppressed tree annihilation is neglected. With our QCDF setup explained in

Appendix A and the expressions of the ratios from Appendix B we obtain

$$\begin{aligned}
r_{\mathrm{T}} &= 0.17^{+0.07}_{-0.06} + 0.03^{+0.03}_{-0.10}\, i\,, \\
r_{\mathrm{C}} &= 0.07^{+0.04}_{-0.06} + (-0.01)^{+0.03}_{-0.05}\, i\,, \\
r_{\mathrm{EW}} &= 0.13^{+0.05}_{-0.05} + 0.02^{+0.02}_{-0.07}\, i\,, \\
r_{\mathrm{EW}}^{\mathrm{C}} &= 0.04^{+0.02}_{-0.03} + (-0.01)^{+0.02}_{-0.03}\, i\,, \\
r_{\mathrm{EW}}^{\mathrm{A}} &= 0.007^{+0.002}_{-0.010} + (-0.004)^{+0.011}_{-0.003}\, i\,.
\end{aligned} \tag{11}$$

The result displays the typical features of QCDF predictions, namely small strong phases and large uncertainties of colour-suppressed topologies. The smallness of the r_i reflects the domination of the isospin-conserving QCD penguin and justifies the expansion of physical observables in the r_i. Among the isospin-violating contributions the colour-allowed tree gives the largest corrections followed by the EW penguin which dominates over the colour-suppressed tree. The colour-suppressed EW penguin ratio $r_{\mathrm{EW}}^{\mathrm{C}}$ and especially the EW penguin annihilation ratio $r_{\mathrm{EW}}^{\mathrm{A}}$ are quite small and consequently they have been omitted in most analyses of $B \to \pi K$ decays. In particular, the possibility of having NP in the EW penguin annihilation amplitude $r_{\mathrm{EW}}^{\mathrm{A}}$ has to our knowledge not been considered so far. However, we want to point out that such an approximation is not valid in the analysis of CP asymmetries: non-vanishing direct CP asymmetries are caused by the interference of parts of the decay amplitude with different weak and strong phases. Consequently direct CP asymmetries in $B \to \pi K$ cannot be generated by the QCD penguin amplitude alone and are automatically sensitive to subleading contributions, encoded in the imaginary parts of the r_i coefficients. These, in turn, are generated in QCDF either perturbatively at $\mathcal{O}(\alpha_s)$ or non-perturbatively at $\mathcal{O}(\Lambda_{\mathrm{QCD}}/m_B)$. At $\mathcal{O}(\alpha_s)$ the colour-suppression of $r_{\mathrm{EW}}^{\mathrm{C}}$ is not present anymore and the $\Lambda_{\mathrm{QCD}}/m_B$ - suppressed $r_{\mathrm{EW}}^{\mathrm{A}}$ can compete as well. Therefore we keep $r_{\mathrm{EW}}^{\mathrm{C}}$ and $r_{\mathrm{EW}}^{\mathrm{A}}$ in our calculation and we will see in later chapters that we can indeed have a large NP contribution in these amplitudes.

One can easily see from eqs. (10,11) that the two amplitudes involved in ΔA_{CP} differ only by the subdominant contributions r_{C}, r_{EW} and $r_{\mathrm{EW}}^{\mathrm{A}}$, all of which are isospin-violating. Turning to the CP asymmetries, one finds in the SM

$$\begin{aligned}
A_{\mathrm{CP}}(B^- \to \pi^0 K^-) &\simeq -2\,\mathrm{Im}\,(r_{\mathrm{T}} + r_{\mathrm{C}}) \sin\gamma, \\
A_{\mathrm{CP}}(\bar{B}^0 \to \pi^+ K^-) &\simeq -2\,\mathrm{Im}(r_{\mathrm{T}}) \sin\gamma,
\end{aligned} \tag{12}$$

with terms quadratic in the r_i being neglected. Thus the only possible explanation for a large ΔA_{CP} in the SM seems to be a large imaginary part of r_{C}, i.e. a large absolute value and large strong phase of the colour-suppressed tree amplitude, generated by some hadronic effects at the low scale Λ_{QCD} which can hardly be calculated perturbatively. However, QCDF predicts only a small $\mathrm{Im}(r_{\mathrm{C}})$, insufficient to explain the data, even when all the theory uncertainties are included. Therefore one is tempted to conclude that the discrepancy in ΔA_{CP} is not due to our lack of understanding of strong interactions but due to isospin-violating NP.

Observable	Theory	Experiment
$\mathrm{Br}(\bar{B}^0 \to \pi^0 \bar{K}^0) \cdot 10^{-6}$	$5.8^{+5.7}_{-3.6}$	$9.5^{+0.5}_{-0.5}$
$\mathrm{Br}(\bar{B}^0 \to \pi^+ \bar{K}^-) \cdot 10^{-6}$	$14.0^{+12.1}_{-7.8}$	$19.4^{+0.6}_{-0.6}$
$\mathrm{Br}(B^- \to \pi^0 \bar{K}^-) \cdot 10^{-6}$	$9.6^{+7.3}_{-4.9}$	$12.9^{+0.6}_{-0.6}$
$\mathrm{Br}(B^- \to \pi^- \bar{K}^0) \cdot 10^{-6}$	$15.7^{+13.7}_{-8.9}$	$23.1^{+1.0}_{-1.0}$
$R_c(\pi K)$	$1.22^{+0.17}_{-0.15}$	$1.12^{+0.07}_{-0.07}$
$R_n(\pi K)$	$1.22^{+0.18}_{-0.16}$	$1.02^{+0.06}_{-0.06}$
$R_c^K(\pi K)$	$1.27^{+0.12}_{-0.11}$	$1.24^{+0.07}_{-0.07}$
$R_n^K(\pi K)$	$1.27^{+0.13}_{-0.15}$	$1.13^{+0.08}_{-0.07}$
$R_c^\pi(\pi K)$	$1.04^{+0.10}_{-0.08}$	$1.11^{+0.06}_{-0.06}$
$R_n^\pi(\pi K)$	$1.55^{+0.38}_{-0.31}$	$1.26^{+0.09}_{-0.09}$
$R(\pi K)$	$1.02^{+0.02}_{-0.02}$	$1.05^{+0.05}_{-0.05}$
$A_{\mathrm{CP}}(\bar{B}^0 \to \pi^0 \bar{K}^0)$	$-0.003^{+0.057}_{-0.108}$	$-0.01^{+0.10}_{-0.10}$
$A_{\mathrm{CP}}(\bar{B}^0 \to \pi^+ \bar{K}^-)$	$-0.047^{+0.187}_{-0.047}$	$-0.098^{+0.012}_{-0.011}$
$A_{\mathrm{CP}}(B^- \to \pi^0 \bar{K}^-)$	$-0.028^{+0.221}_{-0.059}$	$0.050^{+0.025}_{-0.025}$
$A_{\mathrm{CP}}(B^- \to \pi^- \bar{K}^0)$	$0.003^{+0.012}_{-0.003}$	$0.009^{+0.025}_{-0.025}$
$\Delta A_{\mathrm{CP}} = \Delta A_{\mathrm{CP}}^-$	$0.019^{+0.058}_{-0.048}$	$0.148^{+0.027}_{-0.028}$
ΔA_{CP}^0	$0.006^{+0.118}_{-0.057}$	$0.019^{+0.103}_{-0.103}$
$S_{\mathrm{CP}}(\bar{B}^0 \to \pi^0 \bar{K}^0)$	$0.80^{+0.06}_{-0.08}$	$0.57^{+0.17}_{-0.17}$

Table 1: Theoretical vs. experimental results for $\bar{B} \to \pi \bar{K}$ decays. The experimental data is taken from [6]. The original results can be found in [20–34].

For this reason, ΔA_{CP} has been studied in various NP models in recent publications [5,35–43]. The main ingredient of these analyses is usually an enhancement of the EW penguin topologies by effects of virtual heavy particles. Such contributions can be included into the amplitudes (10) by the replacements

$$r_{\mathrm{EW}} \to r_{\mathrm{EW}} + \tilde{r}_{\mathrm{EW}} e^{-i\delta}, \qquad r_{\mathrm{EW}}^{\mathrm{C}} \to r_{\mathrm{EW}}^{\mathrm{C}} + \tilde{r}_{\mathrm{EW}}^{\mathrm{C}} e^{-i\delta}, \qquad r_{\mathrm{EW}}^{\mathrm{A}} \to r_{\mathrm{EW}}^{\mathrm{A}} + \tilde{r}_{\mathrm{EW}}^{\mathrm{A}} e^{-i\delta}, \tag{13}$$

where δ is a new weak phase and $\tilde{r}_{\mathrm{EW}}^{(i)}$ are complex numbers including a strong phase. The CP asymmetries then become

$$\begin{aligned} A_{\mathrm{CP}}(B^- \to \pi^0 K^-) &\simeq -2\,\mathrm{Im}\,(r_{\mathrm{T}} + r_{\mathrm{C}}) \sin\gamma + 2\,\mathrm{Im}\left(\tilde{r}_{\mathrm{EW}} + \frac{2}{3}\tilde{r}_{\mathrm{EW}}^{\mathrm{C}} + \frac{2}{3}\tilde{r}_{\mathrm{EW}}^{\mathrm{A}}\right) \sin\delta, \\ A_{\mathrm{CP}}(\bar{B}^0 \to \pi^+ K^-) &\simeq -2\,\mathrm{Im}(r_{\mathrm{T}}) \sin\gamma + 2\,\mathrm{Im}\left(\frac{2}{3}\tilde{r}_{\mathrm{EW}}^{\mathrm{C}} - \frac{1}{3}\tilde{r}_{\mathrm{EW}}^{\mathrm{A}}\right) \sin\delta, \end{aligned} \tag{14}$$

such that

$$\Delta A_{\mathrm{CP}} \simeq -2\,\mathrm{Im}\,(r_{\mathrm{C}}) \sin\gamma + 2\,\mathrm{Im}\left(\tilde{r}_{\mathrm{EW}} + \tilde{r}_{\mathrm{EW}}^{\mathrm{A}}\right) \sin\delta \tag{15}$$

can turn out to be much larger than in the SM. The observed discrepancy can be solved by a $\tilde{r}_{\rm EW}$ or a $\tilde{r}^{A}_{\rm EW}$ term comparable in size to the corresponding SM term $r_{\rm EW}$.

Apart from $\Delta A_{\rm CP}$ one can also construct other observables from the $B \to \pi K$ data which are sensitive to isospin violation, for example certain ratios of branching fractions. Even though tensions with experimental data in these observables raised the formulation of a "$B \to \pi K$ puzzle" in the first place [8,9,11,44–46], in the meantime these quantities are in reasonable agreement with the SM predictions. However, they serve as important constraints for NP in EW penguins and we define and discuss them in Appendix B. Note in particular that the quantity $\Delta A^0_{\rm CP}$ defined there, which is the difference of the two remaining CP asymmetries not appearing in $\Delta A_{\rm CP}$, probes the same combination of $\mathrm{Im}(\tilde{r}_{\rm EW})$ and $\mathrm{Im}(\tilde{r}^{\rm A}_{\rm EW})$ as $\Delta A_{\rm CP}$. Unfortunately, data on $A_{\rm CP}(B^- \to \bar{K}^0\pi^-)$ and especially on $A_{\rm CP}(\bar{B}^0 \to \bar{K}^0\pi^0)$ are not good enough yet to gain any information from these observables. Experimental results and SM predictions for the $B \to \pi K$ observables are given in tab. 1.

The main problem which makes it difficult to single out a possible NP contribution in $B \to \pi K$ decays is evident from (10): the colour-allowed EW penguin contributions and colour-suppressed tree contributions enter the amplitudes in (10) exclusively in the combination

$$r_{\rm EW} \, - \, r_{\rm C}\, e^{-i\gamma}. \tag{16}$$

This implies that colour-allowed EW penguins and colour-suppressed trees are inextricably linked with each other, reflecting the fact that the topological parameterisation contains some redundancy. Physical effects found in any experiment cannot unambiguously be attributed to one or the other partner of this topology pair. A new EW penguin contribution $\tilde{r}_{\rm EW}e^{-i\delta}$ can be probed only in one of the four physical combinations

$$\begin{aligned}
&\mathrm{Re}(\tilde{r}_{\rm EW})\cos\delta \,-\, \mathrm{Re}(r_{\rm C})\cos\gamma \,+\, \mathrm{Re}(r_{\rm EW})\,,\\
&\mathrm{Im}(\tilde{r}_{\rm EW})\sin\delta \,-\, \mathrm{Im}(r_{\rm C})\sin\gamma\,,\\
&\mathrm{Im}(\tilde{r}_{\rm EW})\cos\delta \,-\, \mathrm{Im}(r_{\rm C})\cos\gamma \,+\, \mathrm{Im}(r_{\rm EW})\,,\\
&\mathrm{Re}(\tilde{r}_{\rm EW})\sin\delta \,-\, \mathrm{Re}(r_{\rm C})\sin\gamma\,.
\end{aligned} \tag{17}$$

Therefore, probing $\tilde{r}_{\rm EW}e^{-i\delta}$ is challenged by the large hadronic uncertainties in the QCDF prediction for $r_{\rm C}$, which can mimic or hide such a NP signal.

The perspective of our work is the following: In order to find out whether the $\Delta A_{\rm CP}$ discrepancy really is a manifestation of isospin-violating physics beyond the SM, one should also study other observables on which such a kind of NP could have a large impact and see whether similar effects appear in measurements of these observables. Our proposal in this work is to test the hypothesis of isospin-violating NP by looking at processes which are highly sensitive to it, namely *purely isospin-violating B_s decays.*

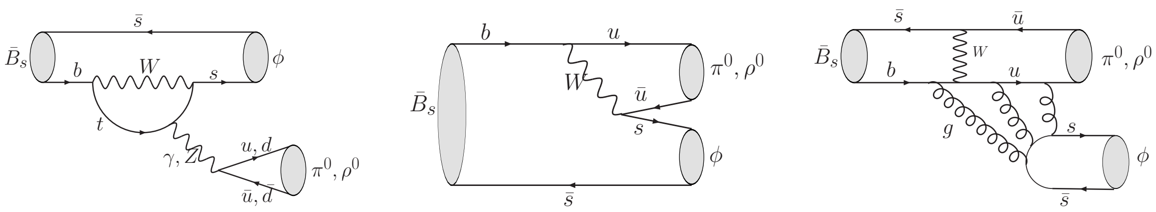

Figure 2: penguin, tree and annihilation topologies contributing to $\bar{B}_s \to \phi\rho^0, \phi\pi^0$

2.2 Purely isospin-violating B_s decays

EW penguin contributions to hadronic B decays are usually overshadowed by the larger QCD penguins. This problem can be avoided if one succeeds in probing exclusively the $\Delta I = 1$ part of the effective Hamiltonian which is orthogonal to the QCD penguin operators. To achieve this for $B \to \pi K$, we had to single out the $\Delta I = 1$ part of the transition in eq. (9) by combining different isospin-related decay modes, for example by considering the observable $\Delta A_{\rm CP}$. Our proposal now is to consider decays to which QCD penguins do not contribute at all, i.e. pure $\Delta I = 1$ decays, where no such procedure is needed.

There are no two-body decays of the B^0 or $B^\pm$ meson with this property. In these cases the final state would have to be a pure $|3/2, \pm 1/2\rangle$ isospin state which cannot be constructed out of two mesons. The B_s meson, on the other hand, is an isosinglet and it can decay as

$$0 \stackrel{\Delta I=1}{\longrightarrow} 0 \otimes 1 \, = \, 1\,. \tag{18}$$

The final state must consist of an isospin triplet, i.e. π^0 or ρ^0, and an isosinglet, i.e. a meson with the flavour structure $s\bar{s}$. In order to avoid complications stemming from $\eta - \eta'$-mixing, we restrict ourselves to the vector-meson ϕ which is to a good approximation a pure $s\bar{s}$ state. This leaves us with the two $\Delta I = 1$ channels

$$\boxed{\bar{B}_s \to \phi\rho^0 \qquad \text{and} \qquad \bar{B}_s \to \phi\pi^0.}$$

So far only an upper limit $\text{Br}(\bar{B}_s \to \phi\rho^0) \leq 6.17 \cdot 10^{-4}$ exists [47] and no detailed theory analysis of $\bar{B}_s \to \phi\rho^0, \phi\pi^0$ has been published. Only the SM branching fractions and CP asymmetries have been calculated in general surveys on B decays to light mesons [15,16]. In addition, $\bar{B}_s \to \phi\pi^0$ has been suggested as a tool for γ measurements from the mixing-induced CP asymmetry [48]. Since in the era of LHCb and super B-factories these two processes will become interesting objects for tests of isospin-violation and potential NP we will in the following study their phenomenology in full detail, in the SM and beyond.

In the SM only three basic topologies are present in these decays, depicted in fig. 2:

- EW penguins
- CKM- and colour-suppressed tree diagrams

- Singlet-annihilation diagrams.

Since the flavour-structure of π^0 and ρ^0 excludes their production via gluon-exchange, annihilation can only contribute if the ϕ meson (the flavour singlet) in the final state is produced from gluons and the second meson comes from weak (as depicted in fig. 2) or electromagnetic interactions. Since the ϕ is colour-neutral and it is odd under charge-conjugation, at least three gluons are needed, so that the singlet-annihilation amplitude is formally of higher-order in α_s and does not appear in QCDF at the next-to-leading order $\mathcal{O}(\alpha_s^1)$ [15]. However, annihilation topologies in general do not factorise and cannot be calculated perturbatively, because the exchanged gluons may be soft. This means that we can, from a theoretical point of view, only rely on the suppression of these contributions by Λ/m_B, where Λ is a non-perturbative scale, and by $1/N_c$. This leads to the expectation that both the tree and the EW penguin amplitudes can receive corrections of $10\% - 20\%$ from singlet-annihilation. However, we can also argue from a phenomenological point of view that ϕ-production from three gluons is suppressed by the OZI rule [49–52] and should thus be only a small effect, even though this rule is theoretically not well understood. In short, our reasoning leads us to the conclusion that in order to test NP in $\bar{B}_s \to \phi\rho^0, \phi\pi^0$, we have to look for new effects which are much larger than this intrinsic uncertainty.

In all our calculations of $\bar{B}_s \to \phi\rho^0, \phi\pi^0$ we use the full QCDF decay amplitudes, see refs. [15,16]. However, since these are quite involved, we now quote simple approximative formulas which can be used as building blocks for an easy calculation of various observables such as branching fractions, CP asymmetries and polarisation fractions. Neglecting singlet-annihilation we can parameterise the amplitudes in analogy to eq. (10) as

$$\sqrt{2}\mathcal{A}(\bar{B}_s \to \phi M_2) \;=\; P_{\rm EW}^{M_2}\left(1 - r_{\rm C}^{M_2} e^{-i\gamma}\right), \tag{19}$$

with M_2 representing a π^0, a longitudinal ρ^0 or a ρ^0 with negative helicity. The positive helicity amplitude can be neglected in the SM because of its $\Lambda_{\rm QCD}^2/m_B^2-$suppression. We have factored out the EW penguin amplitude $P_{\rm EW}^{M_2}$ anticipating its dominance over the colour-suppressed tree represented by the tree-to-penguin ratio $r_{\rm C}^{M_2}$. A new contribution to the $B \to \pi K$ amplitudes of the form (13) would also enter the $\bar{B}_s \to \phi\pi^0, \phi\rho^0$ amplitude (19) modifying it as

$$\sqrt{2}\, A(\bar{B}_s \to \phi M_2) \;=\; P_{\rm EW}^{M_2}\left(1 \,-\, r_{\rm C}^{M_2}\, e^{-i\gamma} \,+\, \tilde{r}_{\rm EW}^{M_2}\, e^{-i\delta}\right) \tag{20}$$

where $\tilde{r}_{\rm EW}^{M_2}$ contains a strong phase and δ is the weak phase introduced in (13). If we assume the new contribution to be of the order of the SM EW penguin, as required by a solution of the "$\Delta A_{\rm CP}$-puzzle", we have $|\tilde{r}_{\rm EW}^{M_2}| \sim \mathcal{O}(1)$ and expect a large enhancement of the $\bar{B}_s \to \phi\pi^0, \phi\rho^0$ branching fractions, up to an order of magnitude. In order to obtain the same effect within the SM one would have to assume an even larger enhancement of the soft non-perturbative physics entering the colour-suppressed tree topology in $r_{\rm C}^{M_2}$.

Choosing a phase convention such that $P_{\rm EW}^{M_2}$ is real, we find

$$P_{\rm EW}^{\pi} \;=\; 6.45^{+1.87}_{-0.54}\cdot 10^{-9}, \qquad P_{\rm EW}^{\rho,0} \;=\; 9.95^{+2.83}_{-0.79}\cdot 10^{-9}, \qquad P_{\rm EW}^{\rho,-} \;=\; 4.27^{+1.34}_{-0.81}\cdot 10^{-9}. \tag{21}$$

for the isotriplet meson being π^0, longitudinal ρ^0 and ρ^0 with negative helicity, respectively. We further have

$$
\begin{aligned}
r_{\rm C}^{\pi} &= 0.41^{+0.37}_{-0.41} \, - \, 0.13^{+0.30}_{-0.30}\, i\,,\\
r_{\rm C}^{\rho,0} &= 0.39^{+0.35}_{-0.39} \, - \, 0.13^{+0.28}_{-0.29}\, i\,,\\
r_{\rm C}^{\rho,-} &= 0.21^{+0.49}_{-0.46} \, + \, 0.15^{+0.45}_{-0.45}\, i\,.
\end{aligned} \tag{22}
$$

Inserting these numbers into eq. (19) we obtain a good approximation of the SM amplitudes for the $\bar{B}_s$ decays. Replacing $\gamma \to -\gamma$ in eq. (19) yields the corresponding CP-conjugated amplitudes (B_s decays). Subsequently one can use the formulas in Appendix A.4 to convert the amplitudes into physical observables. In section 3.1 we extend these prescriptions to physics beyond the SM.

One should keep in mind that the numbers above are calculated using state-of-the-art values for the non-perturbative input parameters, summarised in Appendix A.3. They are based on lattice QCD, QCD sum rules and experimental data. Since our knowledge on these parameters is hopefully going to improve in the future it is desirable to have an additional parameterisation of the decay amplitudes where the non-perturbative input can be changed. We find the dominant sources of theory uncertainties to be (ordered by importance)

- the form factors $A_0^{B_s\to\phi}(0)$ and $F_\pm^{B_s\to\phi}(0)$,
- the CKM angle γ,
- the non-factorisable spectator-scattering amplitudes, parameterised by the complex number X_H and the first inverse moment λ_{B_s} of the B_s-meson light-cone distribution amplitude.

The remaining uncertainties, stemming from decay constants, Gegenbauer moments, quark masses and CKM parameters, are much less important so we do not need to display them explicitly. Setting the less important theory parameters to their default values we arrive at the following approximate expressions for the quantities in eqs. (21,22):

$$
\begin{aligned}
P_{\rm EW}^{\pi} &= 17.0\, A_0^{B_s\to\phi}(0)\cdot 10^{-9}, & r_{\rm C}^{\pi} &= -0.12i - 0.02 + \frac{0.01\mathrm{GeV}(1+X_H)}{A_0^{B_s\to\phi}(0)\lambda_{B_s}}\\
P_{\rm EW}^{\rho,0} &= 26.2\, A_0^{B_s\to\phi}(0)\cdot 10^{-9}, & r_{\rm C}^{\rho,0} &= -0.13i - 0.02 + \frac{0.01\mathrm{GeV}(1+X_H)}{A_0^{B_s\to\phi}(0)\lambda_{B_s}}\\
P_{\rm EW}^{\rho,-} &= 6.6\, F_-^{B_s\to\phi}(0)\cdot 10^{-9}, & r_{\rm C}^{\rho,-} &= 0.14i - 0.06 - \frac{0.02\mathrm{GeV}(1-X_H)}{F_-^{B_s\to\phi}(0)\lambda_{B_s}}
\end{aligned} \tag{23}
$$

The tree topologies $r_{\rm C}^{M_2}$ suffer from the large spectator-scattering uncertainties due to a strong cancellation between the leading-order and QCD vertex corrections. Again one can insert these formulas into eq. (19), this time with arbitrary values and uncertainties for the form factors and spectator-scattering parameters, and use the definitions in Appendix A.4 to calculate physical observables. CP conjugation again amounts to replacement $\gamma \to -\gamma$.

We conclude this section quoting our QCDF results for the SM values of the $\bar{B}_s \to \phi\pi^0, \phi\rho^0$ observables. As for the CP-averaged branching fractions we obtain

$$\mathrm{Br}(\bar{B}_s \to \phi\pi^0) \,=\, 1.6^{+1.1}_{-0.3} \cdot 10^{-7}, \qquad \mathrm{Br}(\bar{B}_s \to \phi\rho^0) \,=\, 4.4^{+2.7}_{-0.7} \cdot 10^{-7}. \tag{24}$$

For comparison we also quote the approximate result according to (23):

$$\mathrm{Br}(\bar{B}_s \to \phi\pi^0) \,=\, 1.6^{+1.0}_{-0.3} \cdot 10^{-7}, \qquad \mathrm{Br}(\bar{B}_s \to \phi\rho^0) \,=\, 4.4^{+2.4}_{-0.7} \cdot 10^{-7}. \tag{25}$$

The smallness of the SM branching ratios compared to other hadronic B decays is due to the absence of QCD penguins and non-suppressed tree-level contributions. The measurement of these branching fractions is thus challenging and has not been achieved yet. However we will show in later chapters that NP in EW penguins has the chance to enhance the BRs by up to an order of magnitude, such that this measurement is a very interesting project. We expect that LHCb will be able to measure $\mathrm{Br}(\bar{B}_s \to \phi\rho^0)$ while the $\bar{B}_s \to \phi\pi^0$ mode is more suitable for a super B-factory where a full reconstruction can cure the notorious difficulties with the identification of neutral pions. The branching ratio $\mathrm{Br}(\bar{B}_s \to \phi\rho^0)$ is dominated by the longitudinal polarisation state as can be seen in

$$\mathrm{Br}(\bar{B}_s \to \phi_L\rho^0_L) \,=\, 3.7^{+2.5}_{-0.7} \cdot 10^{-7} \tag{26}$$

and the longitudinal polarisation fraction

$$f_{\mathrm{L}} \,=\, 0.84^{+0.08}_{-0.11}\,. \tag{27}$$

As stated above, one of the main sources of uncertainty in the QCDF predictions is the form factor $A_0^{B_s\to\phi}$. It can in principle be eliminated by considering the ratios

$$\frac{\mathrm{Br}(\bar{B}_s \to \phi\rho^0)}{\mathrm{Br}(\bar{B}_s \to \phi\pi^0)} = 2.83^{+0.35}_{-0.23}, \qquad \frac{\mathrm{Br}(\bar{B}_s \to \phi_L\rho^0_L)}{\mathrm{Br}(\bar{B}_s \to \phi\pi^0)} = 2.38^{+0.10}_{-0.08}\,. \tag{28}$$

NP could still be visible in these ratios because in many scenarios it enters $\bar{B}_s \to \phi\rho^0$ and $\bar{B}_s \to \phi\pi^0$ in different ways. The cancellation of $A_0^{B_s\to\phi}$ also occurs in the ratios

$$\begin{aligned}
&\frac{\mathrm{Br}(\bar{B}_s \to \phi\pi^0)}{\mathrm{Br}(\bar{B}_s \to \phi\phi)} = 0.007^{+0.008}_{-0.004}, \\
&\frac{\mathrm{Br}(\bar{B}_s \to \phi\rho^0)}{\mathrm{Br}(\bar{B}_s \to \phi\phi)} = 0.020^{+0.023}_{-0.010}, \quad \frac{\mathrm{Br}(\bar{B}_s \to \phi_L\rho^0_L)}{\mathrm{Br}(\bar{B}_s \to \phi\phi)} = 0.017^{+0.019}_{-0.009}.
\end{aligned} \tag{29}$$

There however this gain is compensated by additional uncertainties arising from the QCD-penguin-dominated decay $\bar{B}_s \to \phi\phi$. The experimental benefit in these last ratios is that at LHCb absolute branching ratios cannot be measured because the absolute number of B_s mesons is unknown. Finally, we find the direct CP asymmetries to be very uncertain:

$$A_{\rm CP}^{\rm dir}(\bar{B}_s \to \phi\rho^0) = 0.19^{+0.53}_{-0.61}, \qquad A_{\rm CP}^{\rm dir}(\bar{B}_s \to \phi\pi^0) = 0.27^{+0.50}_{-0.62}. \tag{30}$$

Due to the smallness of the branching ratios, these CP asymmetries are also difficult to access experimentally, therefore we will not consider them any further.

3 Model-independent analysis

In the previous chapter we proposed to test the hypothesis of NP in the EW penguin sector, as suggested by the discrepancy in the $B \to \pi K$ observable $\Delta A_{\rm CP}$, by a measurement of the decays $\bar{B}_s \to \phi\pi^0, \phi\rho^0$. In this chapter we support our proposal by a quantitative analysis pursuing the following strategy: We parameterise NP in EW penguins in a model-independent way by adding corresponding terms to the Wilson coefficients $C_7^{(\prime)}, ..., C_{10}^{(\prime)}$. By performing a χ^2-fit we determine the NP parameters in such a way that they describe well the $B \to \pi K$ data. In particular they should allow for a solution of the $\Delta A_{\rm CP}$ discrepancy. Further hadronic decays like $B \to \rho K, \pi K^*, \rho K^*$ are used to impose additional constraints at the $2\,\sigma$ level. With respect to the resulting fit we study the decays $\bar{B}_s \to \phi\pi^0, \phi\rho^0$ and quantify a potential enhancement of their branching fractions. Note that such an exhaustive analysis, correlating different hadronic decay modes with sensitivity to isospin violation, is only possible if hadronic matrix elements are calculated from first principles like in the framework of QCDF. A method based on flavour symmetries, as it has been used in most studies of $B \to \pi K$ decays so far, could not achieve this. In particular, the decays $\bar{B}_s \to \phi\pi^0, \phi\rho^0$, which are our main interest, are not related to any other decay via $SU(3)_F$ so their branching fractions cannot be predicted in this way.

3.1 Modified EW penguin coefficients

In the SM the Wilson coefficients $C_7, ..., C_{10}$ obey the hierarchy $|C_9| \gg |C_7| \gg |C_8|, |C_{10}|$ at the electroweak scale. This is because C_9 receives $1/\sin^2\theta_W$-enhanced contributions from Z-penguin and box diagrams in contrast to C_7, while $C_{8,10}$ are generated for the first time at two-loop level due to their colour structure. For our model-independent analysis we consider arbitrary NP contributions to the coefficients C_7 and C_9 as well as to their mirror counterparts C_7' and C_9'. Normalizing the new coefficients to the SM value $C_9^{\rm LO}$ defined in eq. (59) in the appendix, we have

$$C_{7,9}^{(\prime)\rm NP}(m_W) = C_9^{\rm LO}(m_W)\, q_{7,9}^{(\prime)}, \qquad q_{7,9}^{(\prime)} = |q_{7,9}^{(\prime)}| e^{i\phi_{7,9}^{(\prime)}}, \tag{31}$$

where $\phi_{7,9}^{(\prime)}$ are new weak phases. The coefficient $C_9^{\rm LO}$ contains the parts of $C_9^{\rm SM}$ enhanced by m_t^2/M_W^2 and $1/\sin^2\theta_W$, as explained in Appendix A.1. There we also describe the

	$C_i^{\rm NP}(m_b)/\alpha$	$C_i^{\rm NP\,\prime}(m_b)/\alpha$
C_7	$-0.966\,q_7 + 0.009\,q_9$	$-0.966\,q_7' + 0.009\,q_9'$
C_8	$-0.387\,q_7 + 0.002\,q_9$	$-0.387\,q_7' + 0.002\,q_9'$
C_9	$0.010\,q_7 - 1.167\,q_9$	$0.010\,q_7' - 1.167\,q_9'$
C_{10}	$-0.001\,q_7 + 0.268\,q_9$	$-0.001\,q_7' + 0.268\,q_9'$

Table 2: NLO short-distance coefficients of the EW penguin operators at the scale m_b. Modifications to other short-distance coefficients are negligible.

scheme which we use for the renormalisation group evolution. Applying it to the NP coefficients leads to the low-scale values displayed in tab. 2. They can be compared to the dominant SM coefficient $C_9^{\rm SM}(m_b)/\alpha = -1.203$.

In our analysis we will study several different scenarios. First, we consider the cases where only one of the coefficients q_7, q_9, q_7', q_9' is different from zero. This means we assume the dominance of an individual NP operator as it has also been done for example in ref. [40]. Second, we consider the possibilities of having $q_7 = q_9$, $q_7' = q_9'$, $q_7 = q_9'$ and $q_7' = q_9$. Finally, we study parity-symmetric new contributions corresponding to the three cases $q_7 = q_7'$, $q_9 = q_9'$ and $q_7 = q_7' = q_9 = q_9'$. Each of these scenarios can be described by means of two real parameters, the absolute value $|q|$ and phase ϕ of the NP contribution under consideration. This reduced number of free parameters allows us to perform a fit to $B \to \pi K$ data and to draw meaningful conclusions on the $\bar{B}_s \to \phi\pi^0, \phi\rho^0$ decays. The study of this large set of well-motivated simplified scenarios is assumed to represent all relevant features of the general framework with unrelated q_7, q_9, q_7', q_9'.

Our main motivation for adding NP to the coefficients $C_7^{(\prime)}, C_9^{(\prime)}$ was the claim that the $\Delta A_{\rm CP}$ discrepancy can be solved in this way, namely by generating the terms $\tilde{r}_{\rm EW}$, $\tilde{r}_{\rm EW}^{\rm C}$, $\tilde{r}_{\rm EW}^{\rm A}$ introduced in (13). Introducing individual terms for each respective Wilson coefficient, we obtain

$$\begin{aligned}
\sum_{i=7,9,7',9'} \tilde{r}_{{\rm EW},\,i}\, e^{-i\delta_i} &= (q_7 - q_7')\,\left[(-0.12)^{+0.04}_{-0.05} + (-0.02)^{+0.07}_{-0.02}\, i\right] + \\
&\quad (q_9 - q_9')\,\left[0.12^{+0.05}_{-0.04} + 0.02^{+0.02}_{-0.07}\, i\right]\,, \\
\sum_{i=7,9,7',9'} \tilde{r}^{\rm C}_{{\rm EW},\,i}\, e^{-i\delta_i} &= (q_7 - q_7')\,\left[0.10^{+0.03}_{-0.02} + 0.01^{+0.01}_{-0.06}\, i\right] + \\
&\quad (q_9 - q_9')\,\left[0.04^{+0.02}_{-0.03} + (-0.005)^{+0.016}_{-0.026}\, i\right]\,, \\
\sum_{i=7,9,7',9'} \tilde{r}^{\rm A}_{{\rm EW},\,i}\, e^{-i\delta_i} &= (q_7 - q_7')\,\left[0.03^{+0.04}_{-0.07} + (-0.06)^{+0.12}_{-0.01}\, i\right] + \\
&\quad (q_9 - q_9')\,\left[0.007^{+0.003}_{-0.010} + (-0.006)^{+0.012}_{-0.003}\, i\right]\,. \qquad (32)
\end{aligned}$$

Let us briefly discuss the main characteristics of these coefficients:

- First of all, note that parity-symmetric models obviously do not contribute to $B \to \pi K$ at all. This general feature of B decays into two pseudoscalar mesons (PP decays) follows from eq. (63). Therefore such a scenario cannot solve the $\Delta A_{\rm CP}$ discrepancy.

- The contributions $\tilde{r}_{{\rm EW},\,7^{(\prime)}}$ and $\tilde{r}_{{\rm EW},\,9^{(\prime)}}$ tend to cancel each other. Hence in the scenarios with $q_7 = q_9$ and $q_7' = q_9'$ only a negligible new colour-allowed EW penguin contribution is generated.

- Whereas ${\rm Re}(\tilde{r}^{\rm C}_{{\rm EW},\,9^{(\prime)}})$ features the typical colour-suppression with respect to ${\rm Re}(\tilde{r}_{{\rm EW},\,9^{(\prime)}})$, this pattern is not obeyed by the $q_7^{(\prime)}$ terms. This is due to a conspirative interplay of the large mixing of $C_7^{(\prime)}$ into $C_8^{(\prime)}$ (compare tab. 2), constructive interference of the new $C_7^{(\prime)}$ and $C_8^{(\prime)}$ contributions in the QCDF coefficient $a_8^{(\prime)}$ and a chiral enhancement factor $r_\chi^{\pi,K} \approx 1.5$ multiplying $a_8^{(\prime)}$ in eq. (61) for the topological amplitude. None of these three effects is present in the $q_9^{(\prime)}$ case.

- The annihilation coefficient $\tilde{r}^{\rm A}_{{\rm EW},\,7^{(\prime)}}$ develops a large imaginary part. In scenarios with non-vanishing $q_7^{(\prime)}$ this term gives the dominant contribution to $\Delta A_{\rm CP}$.

From eq. (15) we see that the $\Delta A_{\rm CP}$ discrepancy can be solved either through $\tilde{r}_{\rm EW}$ or through $\tilde{r}^{\rm A}_{\rm EW}$. Except for the parity-symmetric models, all the scenarios mentioned above can achieve such a solution. In fig. 3 this is illustrated for the cases with a single q_7 or q_9 and for the $q_7 = q_9$ scenario. Graphs for the respective mirror scenarios are obtained by a 180° rotation. The yellow region contains those points of the $({\rm Re}(q_i), {\rm Im}(q_i))$ - plane for which the theory error band overlaps with the experimental $1\,\sigma$ region, whereas the blue region represents those points for which also the experimental central value lies within the theory error interval. The red circle illustrates the minimal $|q|$ - value needed to reduce the $\Delta A_{\rm CP}$ tension below the $1\,\sigma$ level. For the three scenarios in fig. 3 we read off $|q_7| \gtrsim 0.3$, $|q_9| \gtrsim 0.8$ and $|q_7| = |q_9| \gtrsim 0.4$. The fact that in the $q_7 = q_9$ case only a small NP contribution is needed, in spite of the absence of $\tilde{r}_{\rm EW}$, demonstrates the importance of the annihilation term $\tilde{r}^{\rm A}_{\rm EW}$. Finally, we like to stress that the solution of the $\Delta A_{\rm CP}$ discrepancy via a minimal $|q|$ - value requires the adjustment of the phase ϕ to a certain value. Realistic scenarios avoiding such a fine-tuning have larger $|q|$ - values, typically $|q| \sim 1$.

Our main goal is to study the impact of such a NP scenario on the decays $\bar{B}_s \to \phi\pi^0, \phi\rho^0$. The NP contributions to $C_7^{(\prime)}, ..., C_{10}^{(\prime)}$ generate the $\widetilde{r}^{M_2}_{\rm EW}$ - terms introduced in eq. (20). Introducing again individual terms for contributions from the various Wilson

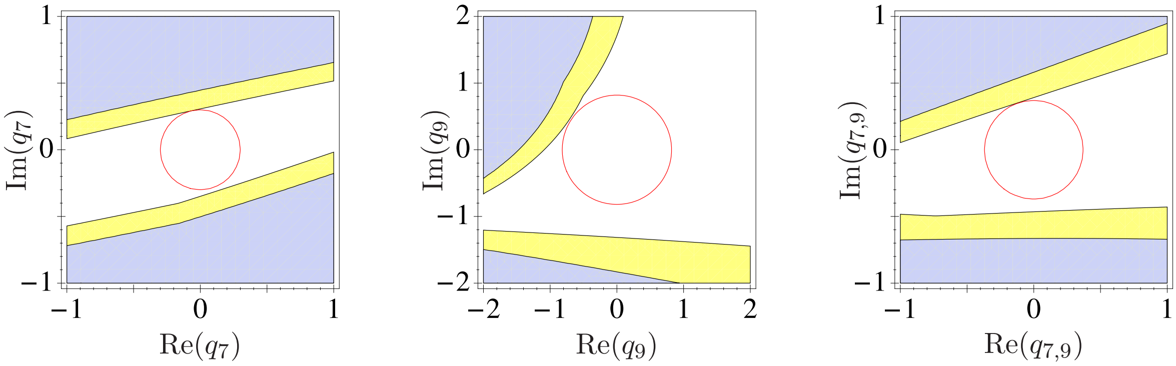

Figure 3: NP contribution needed to solve the $\Delta A_{\rm CP}$ discrepancy in the three scenarios (from left to right) with single q_7, single q_9 and equal $q_7 = q_9$ contribution. Yellow region: Theory error band and experimental $1\,\sigma$ region overlap. Blue region: Theory error band and experimental central value overlap. Red circle: Minimal magnitude of the NP contribution needed to reduce the $\Delta A_{\rm CP}$ discrepancy below the $1\,\sigma$ level.

coefficients, they read for the four different amplitudes

$$\begin{aligned}
\sum_{i=7,9,7',9'} \tilde{r}^{\pi}_{\text{EW},\,i}\, e^{-i\delta_i} &= -0.9\,\left(q_7 + q_7' - q_9 - q_9'\right), \\
\sum_{i=7,9,7',9'} \tilde{r}^{\rho,0}_{\text{EW},\,i}\, e^{-i\delta_i} &= 0.9\,\left(q_7 - q_7' + q_9 - q_9'\right), \\
\sum_{i=7,9,7',9'} \tilde{r}^{\rho,-}_{\text{EW},\,i}\, e^{-i\delta_i} &= -0.6\,\left(q_7 + q_9\right), \\
\sum_{i=7,9,7',9'} \tilde{r}^{\rho,+}_{\text{EW},\,i}\, e^{-i\delta_i} &= 0.6\,\left(q_7' + q_9'\right) \times P^{\rho,-}_{\text{EW}}/P^{\rho,+}_{\text{EW}}\,,
\end{aligned} \tag{33}$$

where we have neglected $q_{7,9}$-contributions to $\tilde{r}^{\rho,+}_{\text{EW}}$ and $q'_{7,9}$-contributions to $\tilde{r}^{\rho,-}_{\text{EW}}$ according to their $\Lambda^2_{\text{QCD}}/m_B^2$ suppression. The SM EW penguin amplitude $P^{\rho,+}_{\text{EW}}$ drops out of the total expression (20) of the amplitude, $P^{\rho,-}_{\text{EW}}$ is given in eq. (21). The parameters $\tilde{r}^{M_2}_{\text{EW}}$ develop only very small strong phases and uncertainties not indicated in (33). This is because they are ratios of equal topologies such that uncertainties and strong phases approximately cancel.

We have stated the expression (33) for two reasons: Firstly we want to show the main consequences of non-vanishing $q^{(\prime)}_{7,9}$ for the $\bar{B}_s \to \phi\pi^0, \phi\rho^0$ decays. We see that for $|q_i| = \mathcal{O}(1)$ indeed new contributions with the magnitude of the leading SM EW penguin are generated. While parity-symmetric NP was invisible in $B \to \pi K$, it could be detected in $\bar{B}_s \to \phi\pi^0$ and in principle also in $\bar{B}_s \to \phi\rho^0$ due to the different interference patterns of $\tilde{r}^{\rho,-}_{\text{EW}}$ and $\tilde{r}^{\rho,+}_{\text{EW}}$ with the corresponding SM contributions. Furthermore, left- and right-handed NP could be distinguished by a polarisation measurement of $\bar{B}_s \to \phi\rho^0$. This general feature of decays to vector-vector final states has been pointed out by Kagan

[53]. Note that the question of left- vs. right-handed NP cannot be answered from $B \to \pi K$ alone since, as we have seen, the two scenarios differ only by a rotation in the NP parameter space.

The second benefit of expression (33) is that it allows for a simple calculation of $\bar{B}_s \to \phi\pi, \phi\rho$ observables to a very good accuracy. In this way it permits a study of these decays without the extensive implementation of QCDF. One simply evaluates the amplitude eq. (20) inserting eqs. (21,22) - or alternatively eq. (23) - and the NP part from eq. (33). The CP-conjugated amplitude is obtained by flipping the sign of γ and replacing the q_i by their complex conjugates. Subsequently one can use the formulas in Appendix A.4 to calculate observables.

3.2 Fit to $B \to \pi K$ data and constraints from other decays

The four $B \to \pi K$ channels are the most precisely measured hadronic $b \to s$ decays. For this reason, we use experimental information from these channels as input for our quantitative NP analysis by performing a fit of $q_7^{(\prime)}$ and $q_9^{(\prime)}$ to $B \to \pi K$ data. This fit will be an indication for values of the $q_i^{(\prime)}$ that are realistic to expect and consequently will enable us to find an expected size of enhancement of the branching ratios of $\bar{B}_s \to \phi\rho^0$ and $\bar{B}_s \to \phi\pi^0$. In the treatment of theoretical and experimental uncertainties in the fit we follow the Rfit scheme [7]. More details on this issue are given in Appendix C.

Since $B \to \pi K$ decays are greatly dominated by QCD penguins and since they suffer from large theoretical uncertainties, it is obvious that NP effects residing in EW penguins are difficult to find in branching ratios and direct CP asymmetries. It is more useful to consider instead particular combinations of these basic observables which highlight the isospin-violating contributions and can be predicted with a better precision. For example, it is difficult to see a need for isospin-violating NP by looking at the two CP asymmetries entering in $\Delta A_{\rm CP}$ (see tab. 1) since both of them have more than 100% theoretical uncertainty, reflecting the difficulty of predicting strong phases in QCDF. In the difference $\Delta A_{\rm CP}$, the theory uncertainties cancel to a large extent such that the discrepancy with experimental data becomes clearer. Moreover, in realistic models a new contribution in the EW penguin sector comes usually in combination with NP of comparable size in the QCD penguins since the new contribution in general matches onto a linear combination of the QCD and EW penguin operators. By considering mainly isospin violating observables, one reduces the sensitivity to additional effects from new contributions to $C_3, ..., C_6$ which we did not include in our parameterisation (31).

For our $B \to \pi K$ fit, we use suitable ratios of branching fractions and differences of CP asymmetries as well as the mixing-induced CP asymmetry in $\bar{B}^0 \to \pi^0\bar{K}^0$ as input. The definitions of these quantities are summarised in Appendix B. Many of these quantities have also been considered in the past in the context of flavour symmetry analyses of $B \to \pi K$ decays. A summary of theoretical predictions vs. experimental results for all these observables as well as for the $B \to \pi K$ branching fractions and CP asymmetries is provided in tab. 1. At present none of these quantities deviates from the SM prediction by more than 1σ apart from $\Delta A_{\rm CP}$. We thus expect $\Delta A_{\rm CP}$ (and to a lower degree also $S_{\rm CP}$) to pull the fit towards non-zero values of the $q_i^{(\prime)}$ whereas the other observables will favor values close to the origin of the complex plane.

In addition to the fit we consider constraints on the NP parameters arising from a large number of hadronic B decays. To this end we compare the theoretical prediction of an observable as a function of the $q_i^{(\prime)}$ to its measured value and extract a 2σ-constraint as follows:

$$\text{Point}[\text{q}_{7,9}^{(\prime)}\text{ space}] = \begin{cases} \text{allowed} \quad \text{if} \begin{cases} (x_{\rm theo} + \sigma_{\rm theo,\,sup}) > (x_{\rm exp} - 2\sigma_{\rm exp,\,inf}) \\ \text{and } (x_{\rm theo} - \sigma_{\rm theo,\,inf}) < (x_{\rm exp} + 2\sigma_{\rm exp,\,sup}), \end{cases} \\ \text{excluded} \quad \text{otherwise.} \end{cases} \tag{34}$$

Here $(x_{\rm theo})^{+\sigma_{\rm theo,\,sup}}_{-\sigma_{\rm theo,\,inf}}$ represents the theoretical prediction for the respective physical observable. The uncertainty does not imply a particular probability distribution but the true value is supposed to lie within the error interval. For the experimental value $x_{\rm exp} \pm \sigma_{\rm exp}$ a Gaussian error is assumed.

This procedure is applied to data from $B \to \pi K$ as well as to data from the $B \to \rho K$, $B \to \pi K^*$ and $B \to \rho K^{(*)}$ decay channels, which are simply the pseudoscalar-vector (PV) and vector-vector (VV) modes corresponding to $\bar{B} \to \pi K$. The PV and VV modes turn out to be more sensitive to isospin-violating flavour topologies than their PP counterparts because the leading QCD penguin amplitude is smaller. Experimental information on these decays, however, is not (yet) as precise as the available data for the πK modes. Therefore we do not include the PV, VV modes into the fit but rather consider them only as constraints at the 2σ level. Nonetheless, the constraints from $B \to \rho K$ and $B \to \pi K^\star$ give some information complementary to the one from $B \to \pi K$ because they test different chirality structures than $B \to \pi K$ and are therefore sensitive to other linear combinations of the $q_{7,9}^{(\prime)}$. Moreover, we apply eq. (34) also to data from $B \to K^{(*)}\phi$, $\bar{B}_s \to \phi\phi$ and $\bar{B}_s \to \bar{K}K$ decays even if they only carry a small sensitivity to EW penguins.

3.3 Results of the model-independent analysis

We now discuss the results of the analysis outlined in the previous section. The aim is to make predictions for the B_s decays in combination with the regions of the $q_{7,9}^{(\prime)}$ parameter space which are preferred, or not yet excluded, by experimental data from $\bar{B} \to \pi K$ and related decays.

In figs. 4,5 we present graphs showing the enhancement $\text{Br}^{\rm SM+NP}/\text{Br}^{\rm SM}$ of the $\bar{B}_s \to \phi\rho^0, \phi\pi^0$ branching ratios as a function of the parameters $q_i^{(\prime)}$ in some representative scenarios. The displayed numbers are obtained with our default hadronic input. In order to be distinguishable from the SM, a particular scenario must at least provide a value for $\text{Br}^{\rm SM+NP}/\text{Br}^{\rm SM}$ which exceeds a potential enhancement factor faked by hadronic

Scenario	$\frac{\mathrm{Br}(\bar{B}_s\to\phi\pi^0)}{\mathrm{Br}^{\mathrm{SM}}(\bar{B}_s\to\phi\pi^0)}$	$\frac{\mathrm{Br}(\bar{B}_s\to\phi_L\rho_L^0)}{\mathrm{Br}^{\mathrm{SM}}(\bar{B}_s\to\phi_L\rho_L^0)}$	$\frac{\mathrm{Br}(\bar{B}_s\to\phi\rho^0)}{\mathrm{Br}^{\mathrm{SM}}(\bar{B}_s\to\phi\rho^0)}$
$q_7 \neq 0$	11.0 (18.7)	6.0 (9.9)	5.3 (8.4)
$q_9 \neq 0$	8.8 (16.4)	9.3 (17.0)	8.7 (15.1)
$q_7 = q_9 \neq 0$	1.0 (1.7)	11.5 (21.1)	10.8 (18.7)
$q_7' \neq 0$	8.3 (15.6)	8.8 (16.4)	8.4 (14.7)
$q_9' \neq 0$	6.2 (9.8)	2.8 (5.6)	2.7 (5.0)
$q_7' = q_9' \neq 0$	1.0 (1.7)	5.7 (8.9)	5.2 (7.9)
$q_7 = q_9' \neq 0$	1.0 (1.7)	1.0 (1.7)	1.6 (2.3)
$q_7' = q_9 \neq 0$	1.0 (1.7)	1.0 (1.7)	1.1 (1.8)
$q_7 = q_7' \neq 0$	29.5 (48.1)	1.0 (1.7)	2.1 (3.0)
$q_9 = q_9' \neq 0$	11.1 (20.5)	1.0 (1.7)	1.5 (2.2)
$q_7 = q_7' = q_9 = q_9' \neq 0$	1.0 (1.8)	1.0 (1.7)	2.3 (3.4)

Table 3: Maximal possible enhancement of branching ratios compatible with the constraints from $B \to \pi K, \rho K, \pi K^*, \rho K^*, \phi K, \phi K^*$ and $\bar{B}_s \to \phi\phi, \bar{K}K$ decays at the 2σ - level as well as the 1-σ confidence level from $B \to \pi K$ decays (method a)). We use the default SM value and the default (the maximal theoretical) total value of each branching ratio for an optimally chosen q_i value. Numbers in the second part of the table are obtained ignoring ΔA_{CP}.

uncertainties in the SM prediction. Parameter points for which the enhancement factor lies within the theory error band of the SM prediction are represented by the red-striped ring. The SM itself corresponds, of course, to the origin of the plots and is highlighted by a black dot.

In our sample models we introduced NP exclusively in the EW penguin operators. In realistic models, however, a new contribution in the EW penguin sector usually comes in combination with NP of comparable size in the QCD penguins since the new contribution in general matches onto a linear combination of the QCD and EW penguin operators. In order to account for this fact, we use the experimental data in two different ways:

a) We present a fit using isospin sensitive quantities in the $B \to \pi K$ decays, such as ratios of branching fractions and the differences of CP asymmetries as discussed in Appendix B and C, plus the time dependent CP asymmetry $S_{CP}(\bar{B}^0 \to \pi\bar{K}^0)$. In figs. 4,5 we individuate the 1σ region by a solid black line. At the same time we consider the constraints one obtains from all non-leptonic $B \to \pi K, \rho K, \pi K^*, \rho K^*, \phi K, \phi K^*$ and $\bar{B}_s \to \phi\phi, \bar{K}K$ decays at the 2σ - level and mark the allowed region by a (dark-)green area.

b) We exclude the time dependent CP asymmetry $S_{CP}(\bar{B}^0 \to \pi\bar{K}^0)$ from the fit and we restrict the constraints to the subset of observables which are particularly sensitive to isospin violation, see Appendix B. This procedure enlarges the 1σ confidence-level of the $B \to \pi K$ fit (indicated by the grey line) as well as the

Scenario	$\frac{\mathrm{Br}(\bar{B}_s\to\phi\pi^0)}{\mathrm{Br}^{\mathrm{SM}}(\bar{B}_s\to\phi\pi^0)}$	$\frac{\mathrm{Br}(\bar{B}_s\to\phi_L\rho_L^0)}{\mathrm{Br}^{\mathrm{SM}}(\bar{B}_s\to\phi_L\rho_L^0)}$	$\frac{\mathrm{Br}(\bar{B}_s\to\phi\rho^0)}{\mathrm{Br}^{\mathrm{SM}}(\bar{B}_s\to\phi\rho^0)}$
$q_7 \neq 0$	77.4 (134.1)	72.5 (117.6)	66.9 (104.7)
$q_9 \neq 0$	12.0 (21.9)	12.6 (22.8)	11.8 (20.3)
$q_7 = q_9 \neq 0$	1.0 (1.7)	52.9 (90.9)	49.4 (81.0)
$q_7' \neq 0$	56.6 (99.2)	59.5 (103.2)	54.0 (90.5)
$q_9' \neq 0$	13.0 (20.6)	13.0 (20.5)	11.7 (18.1)
$q_7' = q_9' \neq 0$	1.0 (1.8)	36.3 (58.2)	32.8 (51.2)
$q_7 = q_9' \neq 0$	1.0 (1.7)	1.0 (1.7)	2.5 (3.8)
$q_7' = q_9 \neq 0$	1.0 (0.0)	1.1 (1.8)	2.5 (3.8)
$q_7 = q_7' \neq 0$	76.0 (131.9)	1.0 (1.7)	3.8 (5.5)
$q_9 = q_9' \neq 0$	13.0 (20.6)	1.0 (1.7)	1.5 (2.2)
$q_7 = q_7' = q_9 = q_9' \neq 0$	1.0 (1.8)	1.0 (1.7)	4.0 (5.9)

Table 4: Maximal possible enhancement of branching ratios compatible with the constraints from isospin sensitive observables in $B \to \pi K, \rho K, \pi K^*$ decays at the 2σ - level as well as the 1-σ confidence level from $B \to \pi K$ decays, without including $S_{CP}(\bar{B}^0 \to \pi \bar{K}^0)$ (method b)). We use the default SM value and the default (the maximal theoretical) total value of each branching ratio for an optimally chosen q_i value. Numbers in the second part of the table are obtained ignoring ΔA_{CP}.

region of 2σ-allowed parameter points by the areas depicted by lighter colours in the figures.

Whereas the results from a) are valid only if NP is strictly limited to the electroweak penguin operators, the results from b) are expected to remain approximately valid also in presence of NP in QCD penguins, since such a kind of NP has only a minor impact on the quantities considered in b).

We find that the $B \to \pi K$ and related decays set quite strong constraints on the parameter space, especially in scenarios where $q_9 \neq 0$ or $q_9' \neq 0$. This basically rules out the possibility of having $|q_i| \gtrsim 5$, i.e. NP corrections cannot be much larger than the EW penguins of the SM. The fact that the SM point is always excluded at the $2\,\sigma$ level is a direct consequence of the ΔA_{CP} data. According to the sign pattern in Eq. (32), the $B \to \pi K$ fits of the primed and unprimed scenarios in figs. 4,5 are related to each other through rotation by 180°. The fit works best in the $q_9^{(\prime)}$ scenario where (using method a)) the best fit point is given by

$$|\hat{q}_9^{(\prime)}| \;=\; 1.9 \qquad\qquad \hat{\varphi}_9^{(\prime)} \;=\; -100^\circ\,(+180^\circ). \tag{35}$$

This parameter point yields a full agreement of all the $B \to \pi K$ observables with the experimental mean values (for S_{CP} the nearly exact value $S_{\mathrm{CP}} = 0.55$ is obtained). In the $q_7^{(\prime)} = q_9^{(\prime)}$ case a plateau of $\chi^2 = 0$ points arises due to the large theoretical errors. It turns out that the $B \to \pi K$ observables are not very sensitive to the $q_7^{(\prime)}$-only scenarios and so the fit does not work well here. Hence within the $q_7^{(\prime)}$-only setting one can mainly rely on the $2\,\sigma$ constraints. The total sets of constraints of the primed and unprimed scenarios are not anymore related to each other in a simple way since they involve PP decays subject to a $180°$ rotation together with PV decays which are unaffected by a $q_{7,9} \leftrightarrow q'_{7,9}$ exchange. It turns out that the constraints are stronger in the q'_9-only and in the $q'_7 = q'_9$ scenarios than in their unprimed counterparts and that the best fit regions are cut away in these cases.

From figs. 4,5 the enhancement $\mathrm{Br}^{\mathrm{SM+NP}}/\mathrm{Br}^{\mathrm{SM}}$ of the B_s branching fractions can be read off with respect to the different constraint- and fit-regions. A large enhancement of the $\bar{B}_s \to \phi\rho^0, \phi\pi^0$ branching ratio can be expected in many scenarios, especially in those involving $q_7^{(\prime)} \neq 0$. The fact that large parts of the allowed regions do not overlap with the SM uncertainty regions is encouraging. It means that, if such NP is realised in nature, it could be possible to probe it easily. In tabs. 3 and 4 we quote the maximal enhancement factors that can be obtained considering all points in parameter space which lie within the $1\,\sigma$ region of the $B \to \pi K$ fit and fulfill the additional $2\,\sigma$ constraints. The numbers in tab. 3 refer to input a) while the numbers in tab. 4 refer to input b). The first number in each cell represents $\mathrm{Br}^{\mathrm{SM+NP}}_{\mathrm{med}}/\mathrm{Br}^{\mathrm{SM}}_{\mathrm{med}}$ while the number in brackets represents $\mathrm{Br}^{\mathrm{SM+NP}}_{\mathrm{max}}/\mathrm{Br}^{\mathrm{SM}}_{\mathrm{med}}$, both evaluated for the q_i value which gives the largest enhancement. Here "max" and "med" refer to the upper limit of the theoretical uncertainty range and to our default value, respectively, according to our input given in Appendix A.3. Exploiting the theory error in favour of an enhancement, the number in brackets gives the absolutely maximal enhancement possible for each scenario whereas the first number gives a typical enhancement factor, but still for the most enhancing parameter point. Concerning the parity-symmetric scenarios one should have in mind that like the SM they violate ΔA_{CP} at the $> 2\,\sigma$ level since they have no impact on $B \to \pi K$ decays. The corresponding enhancement factors shown in tabs. 3,4 are obtained by ignoring ΔA_{CP} but taking into account all other constraints.

In most scenarios an enhancement of more than an order of magnitude is possible. Exceptions are $\bar{B}_s \to \phi\pi$ for $q_7^{(\prime)} = q_9^{(\prime)}$ and $\bar{B}_s \to \phi_L\rho_L$ for parity-symmetric models and have their origin in the pattern of eq. (33). Furthermore, effects in the q'_9 and the $q'_7 = q'_9$ scenarios are limited by the small allowed region resulting from the $B \to \pi K$ fit. Largest effects occur as expected in the scenarios which are least constrained by $B \to \pi K$, i.e. the single $q_7^{(\prime)}$ and the parity-symmetric models. Especially in these cases a $\bar{B}_s \to \phi\pi$ measurement would complement $B \to \pi K$ data and, while the parity-symmetric models lack the motivation via the ΔA_{CP} discrepancy, the q'_7 setting resolves it with ease (see Fig. 3). Moreover, we like to stress that $B \to \pi K$ data alone cannot distinguish among opposite-parity scenarios because such scenarios generate equal results for the $B \to \pi K$ observables (for $180°$-rotated parameter points). Therefore an analysis of $B \to \pi K$ should for example be supported by the analysis of a PV decay, suggesting $\bar{B}_s \to \phi\pi^0$ as an ideal candidate.

We have seen that NP in the EW penguin coefficients allows for an enhancement

Observable	$\lvert q_9\rvert = 1.9$, $\phi_9 = -100°$,
$\mathrm{Br}(\bar{B}_s \to \phi\pi^0)\cdot 10^{-6}$	$0.35^{+0.41}_{-0.19}$
$\mathrm{Br}_L(\bar{B}_s \to \phi\rho^0)\cdot 10^{-6}$	$0.90^{+0.98}_{-0.46}$
$\mathrm{Br}(\bar{B}_s \to \phi\rho^0)\cdot 10^{-6}$	$1.13^{+0.95}_{-0.38}$

Table 5: Values of various observables at our best fit point in the scenario $q_9 \neq 0$.

of $\mathrm{Br}(\bar{B}_s \to \phi\pi, \phi\rho)$ of more than an order of magnitude. According to the simple topological structure of these decays, the observation of such an effect would be a clear and unambiguous signal for such a scenario. It is interesting to raise also the reversed question, i.e. whether the absence of such an effect would rule out a NP solution of the ΔA_{CP} discrepancy, at least for a specific scenario. This is, however, not compulsory. In nearly all the considered settings there are points within the $1\,\sigma$ region of the $B \to \pi K$ fit which do not generate an enhancement of $\mathrm{Br}(\bar{B}_s \to \phi\pi, \phi\rho)$. The only exception is the q_9'-only case: Here an enhancement factor of at least 2.1 would occur in $\bar{B}_s \to \phi\pi$. This time we have exploited the theoretical error in disfavour of an enhancement (for the default value the factor is 2.7). Finally we provide in tab. 5 the $\bar{B}_s \to \phi\pi, \phi\rho$ branching ratios for the best fit points in the q_9-only scenario.

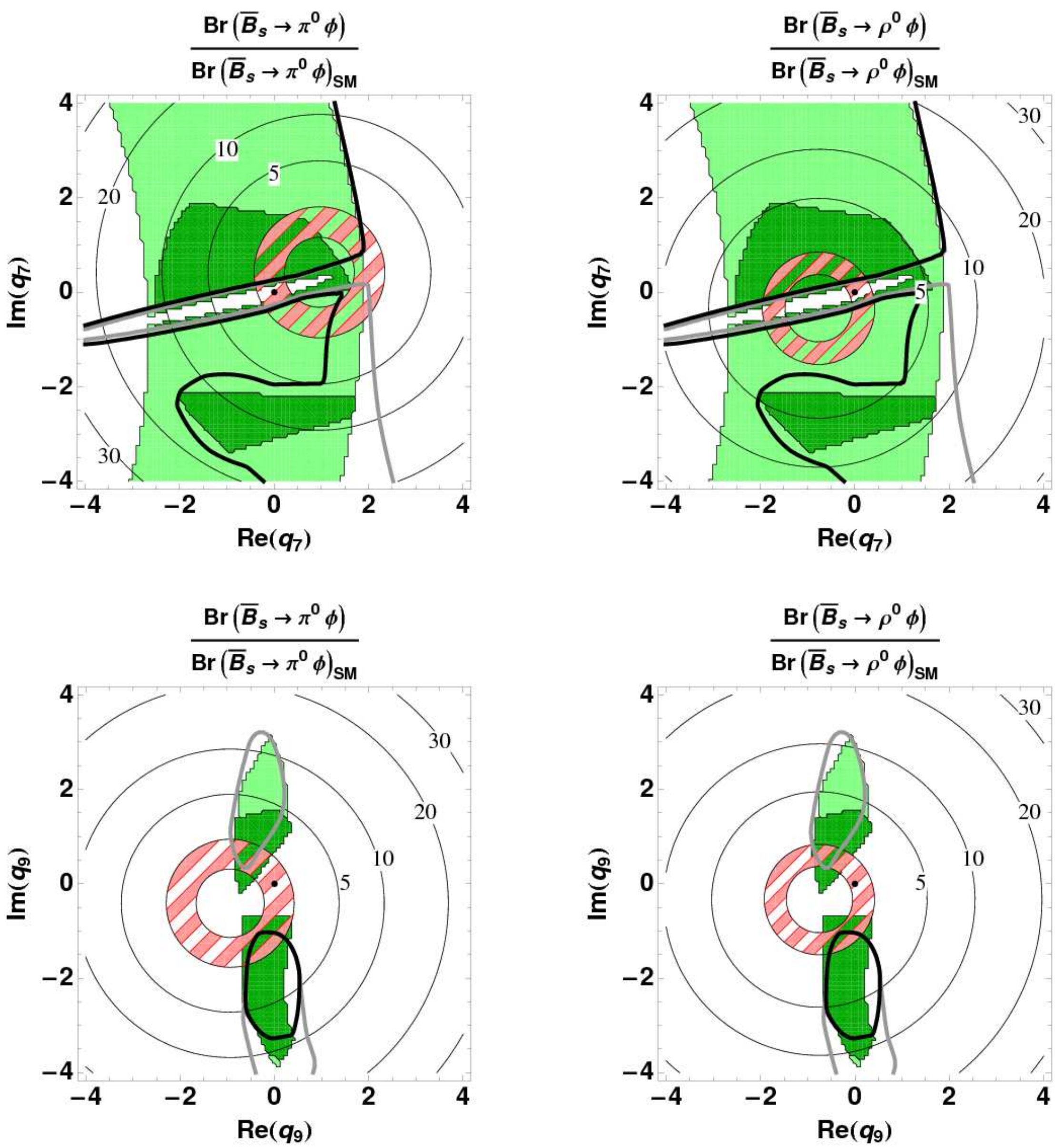

Figure 4: Enhancement factors of the $\bar{B}_s \to \phi\rho^0, \phi\pi^0$ branching ratios with respect to their SM values. The black dot represents the SM result while the red striped region shows the theoretical uncertainty in the SM. The dark green area is the region allowed by the $2\,\sigma$ constraints from $\bar{B} \to \pi K^{(*)}, \rho K^{(*)}, \phi K^{(*)}$ and $\bar{B}_s \to \phi\phi, \bar{K}K$ decays; for comparison, the light green area represents the area allowed by constraints from isospin-sensitive observables only, considering only $\bar{B} \to \pi K, \pi K^{(*)}, \rho K$ decays. The solid black line represents the 1σ CL of the fit with $S_{CP}(\bar{B}^0 \to \pi \bar{K}^0)$, while the solid grey line represents the 1σ CL of the fit without it. Here the scenarios $q_7 \neq 0$ (upper row) and $q_9 \neq 0$ (lower row) are displayed. For the q_7-scenario the 1σ region of the fit is the region to the left of the black (grey) curve.

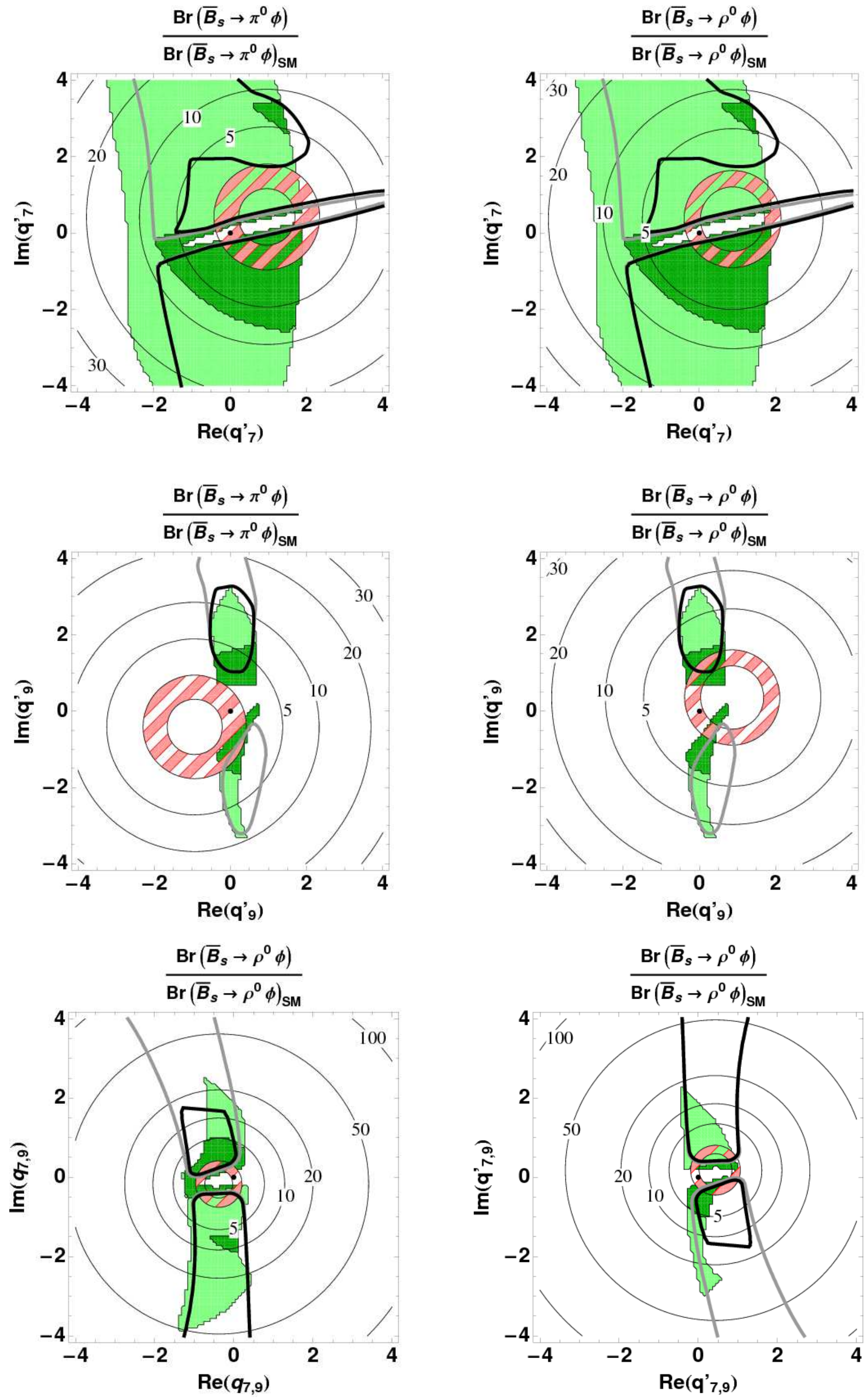

Figure 5: Enhancement factors of the $\bar{B}_s \to \phi\rho^0, \phi\pi^0$ branching ratios with respect to their SM values. The meaning of the contours and regions is the same as in fig. 4. Here the scenarios $q'_7 \neq 0$ (upper row) and $q'_9 \neq 0$ (center row) and $q_7 = q_9 \neq 0$ and $q'_7 = q'_9 \neq 0$ (lower row) are displayed. For the q'_7-scenario the 1σ region of the fit is the region to the right of the black (grey) curve.

4 Analysis of viable New-Physics models

In view of the results in chapter 3, the question arises which concrete models for NP can provide a large new EW penguin amplitude without being excluded by present data. In this section we consider a number of well-motivated NP models. The main difference with respect to the model-independent analysis is the possibility of adding constraints from other flavour processes beyond the hadronic B modes, e.g. the semileptonic decay $\bar{B} \to X_s e^+ e^-$, the radiative decay $\bar{B} \to X_s \gamma$ and B_s-$\bar{B}_s$ mixing. These processes usually yield tight constraints on new flavour structures and it has to be investigated if the effects in $B \to \pi K$ and $\bar{B}_s \to \phi\rho^0, \phi\pi^0$ survive these constraints.

4.1 Constraints from semileptonic decays and B_s-$\bar{B}_s$ mixing

Before turning to the models we summarise here how we implement constraints from semileptonic B decays and B_s-$\bar{B}_s$ mixing. The inclusive semileptonic decay $\bar{B} \to X_s e^+ e^-$ is generated by electroweak interactions and therefore correlated to the hadronic EW penguins in many models. We describe it by the effective Hamiltonian (5), adding the operators

$$Q_{9V} = (\bar{s}_\alpha b_\alpha)_{V-A} (\bar{l}l)_V \qquad \text{and} \qquad Q_{10A} = (\bar{s}_\alpha b_\alpha)_{V-A} (\bar{l}l)_A \tag{36}$$

and the corresponding mirror copies Q'_{9V}, Q'_{10A}. The SM expressions for the Wilson coefficients can be found e.g. in refs. [54,55]. Following [54] and extending the formulae therein to include effects of the mirror operators, we use the effective Hamiltonian to calculate the ratio

$$R_{e^+e^-}(q^2) \equiv \frac{\frac{d}{dq^2}\Gamma(b \to s\, e^+ e^-)}{\Gamma(b \to c\, e \bar{\nu})}, \tag{37}$$

where $q^2 = (p_{e^+} + p_{e^-})^2$ is the squared invariant mass of the lepton pair. This ratio has the advantage that its theoretical uncertainty is considerably reduced with respect to the simple branching fraction. We integrate over a continuum region below the ψ resonances to find the integrated ratio

$$R_{e^+e^-}|_{[1,6]} \equiv \int_{1\mathrm{GeV}^2}^{6\mathrm{GeV}^2} R_{e^+e^-}(q^2) dq^2, \tag{38}$$

which we can finally compare to the experimental result [56–59]

$$\mathrm{Br}_{e^+e^-}|_{[1,6]} = (1.60 \pm 0.51) \cdot 10^{-6}, \tag{39}$$

also normalized to the semileptonic decay. We require $R_{e^+e^-}|_{[1,6]}$ to be compatible with experimental data according to (34).

Besides the inclusive $\bar{B} \to X_s e^+ e^-$, also the exclusive mode $\bar{B} \to K^* l^+ l^-$ has been found to be a useful constraint for NP [60–62]. Here we focus only on the forward-backward asymmetry A_{FB} of this process [60], which gives a constraint complementary to that of $R_{e^+e^-}|_{[1,6]}$. In the light of present experimental data we require the sign of $A_{\rm FB}(q^2)$ integrated over $q^2 > 14$ GeV^2 to be negative.

For completeness we note that we use a renormalisation-group evolution analogous to the one of the EW penguin operators, treating the parts of C_{9V} and C_{10A} enhanced by $x_{tW} = m_t^2/M_W^2$ and/or $1/\sin^2\theta_W$ as leading order. This results in the following initial conditions at the scale $\mu \sim \mathcal{O}(M_W)$:

$$\begin{aligned}
C_{9V}^{(0)} &= \frac{\alpha}{2\pi}\left(\frac{Y_0(x_{tW})}{\sin^2\theta_W} - \frac{x_{tW}}{2}\right),\\
C_{9V}^{(1)} &= \frac{\alpha}{2\pi}\left(-4Z_0(x_{tW}) + \frac{x_{tW}}{2} + \frac{4}{9}\right) + \frac{\alpha}{2\pi}\frac{\alpha_s}{4\pi}\left(\frac{Y_1(x_{tW})}{\sin^2\theta_W} - 4x_{tW}\left(\frac{4}{3} - \frac{\pi^2}{6}\right)\right),\\
C_{10A}^{(0)} &= -\frac{\alpha}{2\pi}\frac{Y_0(x_{tW})}{\sin^2\theta_W}, \qquad\qquad C_{10A}^{(1)} = -\frac{\alpha}{2\pi}\frac{\alpha_s}{4\pi}\frac{Y_1(x_{tW})}{\sin^2\theta_W}.
\end{aligned} \tag{40}$$

The functions $Y_{0,1}$ and Z_0 can be found e.g. in [63].

Finally, we consider constraints coming from B_s-$\bar{B}_s$ mixing, which is described by the effective weak Hamiltonian

$$\mathcal{H}_{\rm eff}^{(2)} = \frac{G_F^2 M_W^2}{4\pi^2}(\lambda_t^{(s)})^2 \sum_i C_i\, Q_i\,, \tag{41}$$

with the operators [64]

$$\begin{aligned}
Q^{\rm VLL} &= (\bar{s}_\alpha\gamma^\mu P_L b_\alpha)(\bar{s}_\beta\gamma_\mu P_L b_\beta),\\
Q_1^{\rm SLL} &= (\bar{s}_\alpha P_L b_\alpha)(\bar{s}_\beta P_L b_\beta), \qquad Q_2^{\rm SLL} = (\bar{s}_\alpha\sigma^{\mu\nu} P_L b_\alpha)(\bar{s}_\beta\sigma_{\mu\nu} P_L b_\beta),\\
Q_1^{\rm LR} &= (\bar{s}_\alpha\gamma^\mu P_L b_\alpha)(\bar{s}_\beta\gamma_\mu P_L b_\beta), \qquad Q_2^{\rm LR} = (\bar{s}_\alpha P_L b_\alpha)(\bar{s}_\beta P_R b_\beta)
\end{aligned} \tag{42}$$

and the mirror copies $Q^{\rm VRR}$, $Q_1^{\rm SRR}$ and $Q_2^{\rm SRR}$. In the SM only $C^{\rm VLL} \neq 0$, while in extensions of the SM all operators can receive contributions. The matrix element relevant for B_s-$\bar{B}_s$ mixing,

$$M_{12}^{B_s} = \frac{1}{2m_{B_s}}\langle B_s^0|\mathcal{H}_{\rm eff}^{(2)}|\bar{B}_s^0\rangle, \tag{43}$$

is evaluated using lattice results from ref. [65]. Besides the B_s-$\bar{B}_s$ mass difference

$$\Delta M_s = 2|M_{12}^{B_s}| \overset{\rm exp.}{=} (17.77 \pm 0.12)\,{\rm ps}^{-1} \quad [66], \tag{44}$$

we use the quantity [67]

$$\Delta_s \equiv \frac{M_{12}^{B_s}}{M_{12}^{B_s,\rm SM}} = |\Delta_s|e^{i\phi_s}, \tag{45}$$

as additional constraint. This observable has been analysed in ref. [68] in different generic NP scenarios and evidence for a NP contribution with a large new weak phase has been found. A fit of Δ_s and the analogous quantity Δ_d to data shows a $3.6\,\sigma$ discrepancy for the SM value $\Delta_s = 1$. In our study of the Z' models we take those points of the NP parameter space as excluded which give a Δ_s outside the $2\,\sigma$ region drawn in fig. 9 of ref. [68].

4.2 The modified-Z^0-penguin scenario

The simplest class of models with large new contributions to EW penguins comprises models with a modified $Z\bar{s}b$ coupling. Such a FCNC coupling can either be generated by integrating out new heavy particles, e.g. in supersymmetric models or fourth-generation models, or it can exist at tree-level in more exotic scenarios like models with non-sequential quarks, see e.g. ref. [69]. Consequences for hadronic B decays have been considered for example in [70], more detailed analyses of the motivation and the effects in flavour physics have been performed in [44,71].

4.2.1 Effective Theory

Our parameterisation of the $Z\bar{s}b$ coupling follows ref. [70]. At the electroweak scale we have an effective theory with the Lagrangian

$$\mathcal{L}_Z^{eff} = -\frac{g}{4\cos\theta_W} \sum_{I\neq J} \bar{d}_I \left[\kappa_L^{IJ}\gamma^\mu(1-\gamma_5) + \kappa_R^{IJ}\gamma^\mu(1+\gamma_5)\right] d_J Z_\mu, \tag{46}$$

where I, J are generation indices. Since the flavour-violating couplings are expected to be small, the flavour-diagonal couplings of the Z bosons are to a first approximation the same as in the SM. Matching tree-level diagrams with Z exchange onto the $\Delta B = \Delta S = 1$ effective Hamiltonian adds new contributions δC_i to the SM Wilson coefficients C_i and generates also coefficients C_i' of the mirror operators. The resulting contributions at the electroweak scale read

$$\begin{aligned}
\delta C_3 &= \frac{1}{6}\frac{\kappa_L^{sb}}{\lambda_t^{(s)}}\,, & C_5' &= \frac{1}{6}\frac{\kappa_R^{sb}}{\lambda_t^{(s)}}\,,\\
\delta C_7 &= \frac{2}{3}\frac{\kappa_L^{sb}}{\lambda_t^{(s)}}\sin^2\theta_W\,, & C_7' &= -\frac{2}{3}\frac{\kappa_R^{sb}}{\lambda_t^{(s)}}\cos^2\theta_W\,,\\
\delta C_9 &= -\frac{2}{3}\frac{\kappa_L^{sb}}{\lambda_t^{(s)}}\cos^2\theta_W\,, & C_9' &= \frac{2}{3}\frac{\kappa_R^{sb}}{\lambda_t^{(s)}}\sin^2\theta_W\,.
\end{aligned} \tag{47}$$

They reach the size of the dominant SM Wilson coefficient $C_9(\mu_W)$ if

$$|\kappa_{L,R}^{sb}| \sim |\kappa_{\rm SM}| \equiv \frac{\alpha}{\pi\sin^2\theta_W}\,\lambda_t^{(s)}\,C_0(x_{tW}) \sim 0.00035\,, \tag{48}$$

where $C_0(x)$ is a loop function, see e.g. ref. [63]. Such a scenario corresponds to $q_i \sim \mathcal{O}(1)$ in our model-independent analysis, thus we expect significant effects in hadronic B decays for such values of $\kappa_{L,R}^{sb}$.

From the Lagrangian (46) and the SM coupling of the Z to leptons we also obtain corrections to the short-distance coefficients of the semileptonic operators (36), namely

$$\delta C_{9V} = -\frac{\kappa_L^{sb}}{\lambda_t^{(s)}}\left(2\sin^2\theta_W - \frac{1}{2}\right), \qquad C'_{9V} = -\frac{\kappa_R^{sb}}{\lambda_t^{(s)}}\left(2\sin^2\theta_W - \frac{1}{2}\right),$$
$$\delta C_{10A} = -\frac{\kappa_L^{sb}}{\lambda_t^{(s)}}\left(\frac{1}{2}\right), \qquad C'_{10A} = -\frac{\kappa_R^{sb}}{\lambda_t^{(s)}}\left(\frac{1}{2}\right). \tag{49}$$

This enables us to study constraints on $\kappa_{L,R}^{sb}$ from semileptonic B decays as indicated in the previous section.

Diagrams with Z-exchange contribute also to B_s-$\bar{B}_s$ mixing via the Wilson coefficients

$$\delta C_1^{\mathrm{VLL}} = \frac{4\pi^2}{\sqrt{2}\,G_F M_W^2}\left(\frac{\kappa_L^{sb}}{\lambda_t^{(s)}}\right)^2, \qquad C_1^{\mathrm{VRR}} = \frac{4\pi^2}{\sqrt{2}\,G_F M_W^2}\left(\frac{\kappa_R^{sb}}{\lambda_t^{(s)}}\right)^2,$$
$$C_1^{\mathrm{LR}} = \frac{8\pi^2}{\sqrt{2}\,G_F M_W^2}\,\frac{\kappa_L^{sb}}{\lambda_t^{(s)}}\frac{\kappa_R^{sb}}{\lambda_t^{(s)}}. \tag{50}$$

Explaining the discrepancy in Δ_s defined in eq. (45) with the help of these new contributions would push the couplings $\kappa_{L,R}^{sb}$ to large values. Note, however, that in most realistic cases the couplings $\kappa_{L,R}^{sb}$ are loop-induced with the consequence of eq. (50) actually representing two-loop effects. Usually such scenarios provide also one-loop contributions from box diagrams which then are more likely to account for the Δ_s discrepancy. Therefore we prefer not to include Δ_s as a constraint into our analysis and regard a potential relaxation of the Δ_s discrepancy only as a bonus feature.

4.2.2 Results

In our study of the modified Z coupling we consider the three special cases of non-vanishing κ_L^{sb} only, κ_R^{sb} only and $\kappa_L^{sb} = \kappa_R^{sb}$, similarly to the model-independent analysis. Since $\cos^2\theta_W \gg \sin^2\theta_W$, the κ_L^{sb} scenario shares its most important features with the q_9 setup of the model-independent study and the same holds for κ_R^{sb} and q'_7. This expectation is confirmed by the graphs in fig. 6, we only note that we get a 180° rotation due to the signs of δC_9 and C'_7. We have again marked the 1σ - region of the $B \to \pi K$ fit by a black line (as well as the additional 3σ - black dotted line) and the region allowed by the $2\,\sigma$ constraints from all hadronic decay observables by a green area. The displayed regions refer to input a), as defined in section 3.3, while we have refrained from showing the corresponding regions for input b).

The main difference to the more general model-independent approach is that we now face additional constraints from semileptonic decays and B_s-$\bar{B}_s$ mixing. The allowed region for the former is given by the interior of the blue dashed curve, the allowed region

Scenario	$\frac{\mathrm{Br}(B_s\to\phi\pi^0)}{\mathrm{Br}^{\mathrm{SM}}(\bar{B}_s\to\phi\pi^0)}$	$\frac{\mathrm{Br}_L(B_s\to\phi\rho^0)}{\mathrm{Br}_L^{\mathrm{SM}}(\bar{B}_s\to\phi\rho^0)}$	$\frac{\mathrm{Br}(B_s\to\phi\rho^0)}{\mathrm{Br}^{\mathrm{SM}}(\bar{B}_s\to\phi\rho^0)}$
$\kappa_L^{sb} \neq 0$	10.3 (19.0)	3.6 (7.0)	3.4 (6.3)
$\kappa_R^{sb} \neq 0$	48.3 (84.6)	15.5 (28.2)	14.2 (24.8)
$\kappa_L^{sb} = \kappa_R^{sb}$	1.0 (1.7)	1.0 (1.7)	1.2 (1.8)
With additional semileptonic B decay constraints			
$\kappa_L^{sb} \neq 0$	1.6 (3.0)	1.1 (2.2)	1.1 (2.0)
$\kappa_R^{sb} \neq 0$	4.0 (6.5)	2.4 (3.9)	2.2 (3.5)
$\kappa_L^{sb} = \kappa_R^{sb}$	1.0 (1.7)	1.0 (1.7)	1.1 (1.7)

Table 6: Maximal possible enhancement of the B_s branching ratios in the modified-Z^0-penguin model. The upper part has been calculated with the method a) of the model-independent analysis, the lower part includes the 2σ constraints from semileptonic decays.

for the latter by the orange areas outside the zone preferred by the $B \to \pi K$ fit. We see that the Δ_s anomaly of B_s-$\bar{B}_s$ mixing cannot be resolved in a modified Z scenario when fulfilling at the same time the semileptonic constraints. This has already been noted in Ref. [72]. Here we recognise that also $B \to \pi K, \rho K, \pi K^*$ data are not compatible with a solution of Δ_s in this way. In the previous section we remarked that it is plausible to assign the explanation of Δ_s to other effects not directly related to the modified Z coupling. Pursuing this strategy, we are left with the semileptonic decays which are compatible with the $1\,\sigma$ region of the $B \to \pi K$ fit for all three cases but constrain the FCNC couplings $\kappa_{L,R}^{sb}$ to very small values as can be seen from fig. 6 where the coupling $\kappa_{L,R}^{sb}$ is normalised to $|\kappa_{\mathrm{SM}}|$ in Eq. (48).

As a consequence we expect no significant effects in $\bar{B}_s \to \phi\pi^0, \phi\rho^0$. This expectation is confirmed by fig. 6 and by the maximum enhancement factors given in tab. 6, which are determined in analogy to the ones in tab. 3. In the $\kappa_L^{sb} = \kappa_R^{sb}$ case no enhancement occurs at all because of the pattern in eq. (33): Equal contributions to C_7 and C_9' and to C_9 and C_7' cancel pairwise. The largest effect which one could gain in the other scenarios is a factor of ~ 4 in the case where only $\kappa_R^{sb} \neq 0$. Therefore an enhancement of $\bar{B}_s \to \phi\pi^0, \phi\rho^0$ due to a new modified Z contribution becomes indistinguishable in practice from the potential enhancement caused by a large non-factorisable SM effect. In fig. 6 this is reflected by the fact that the red-striped ring representing parameter points which reproduce the SM result for the B_s decays nearly fills the whole allowed region of the parameter space.

Our results can be summarised as follows: The constraints from semileptonic decays still allow for a solution of ΔA_{CP} via a modified Z coupling. This possibility would be excluded if an enhancement of $\bar{B}_s \to \phi\pi^0$ or $\bar{B}_s \to \phi\rho^0$ by an order of magnitude was found.

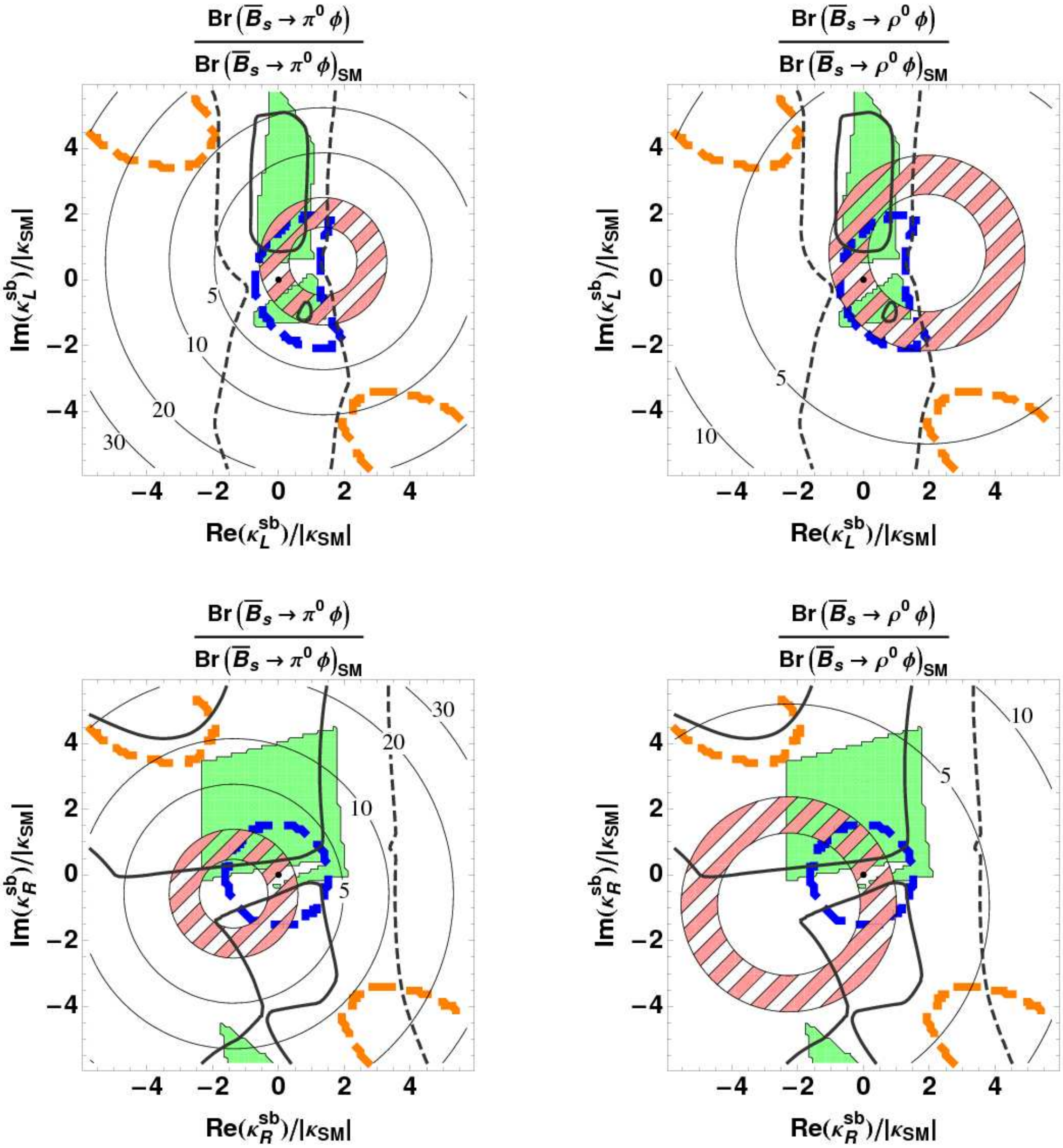

Figure 6: Enhancement factor for the $\bar{B}_s \to \phi\rho^0, \phi\pi^0$ branching ratios with respect to their SM values in the modified-Z^0-penguin scenario. The green area represents the region allowed by the 2σ constraints from all the considered hadronic decays, while the area inside the dashed blue line represents the region allowed by the 2σ constraint from semi-leptonic decays. The areas inside the dashed orange line represent the parameter values for which the modified-Z^0-penguin would solve Δ_s. See the text for further explanations.

4.3 Models with an additional $U(1)'$ gauge symmetry

The presence of a heavy Z' boson associated with an additional $U(1)'$ gauge symmetry is a well-motivated extension of the SM. This additional symmetry has not been invented to solve a particular problem of the SM, but rather occurs as a byproduct in many models like e.g. Grand Unified Theories, various models of dynamical symmetry breaking and Little Higgs models. In many scenarios the Z' boson is expected to have a mass at the TeV scale. It also appears in the form of a Kaluza-Klein excitation of the SM Z^0 boson in theories with extra dimensions. An extensive review about the physics of Z' gauge-bosons can be found in [73]. Here we are interested in implications for flavour physics as discussed in [70,74–76].

4.3.1 Effective Theory

We consider a model with an additional Z' gauge-boson, neglecting Z-Z' mixing and assuming the absence of exotic fermions which could mix with the SM fermions through non-universal Z' couplings. We write the general quark-antiquark-Z' coupling as [70,76]

$$\mathcal{L}_{Z'}^{eff} = -\frac{g_{U(1)'}}{2\sqrt{2}} \sum_{IJ} \bar{d}_I \left[\zeta_L^{IJ} \gamma^\mu (1-\gamma_5) + \zeta_R^{IJ} \gamma^\mu (1+\gamma_5) \right] d_J Z'_\mu . \tag{51}$$

and similarly for the up-type quarks. The couplings of interest are the flavour-changing $\zeta_{L,R}^{sb}$ as well as the flavour-conserving charges $\zeta_{L,R}^u \equiv \zeta_{L,R}^{uu}$ and $\zeta_{L,R}^d \equiv \zeta_{L,R}^{dd}$. Note that $SU(2)_L$ invariance implies $\zeta_L^u = \zeta_L^d \equiv \zeta_L^q$ whereas no restrictions hold in case of ζ_R^u, ζ_R^d. Following ref. [70] we introduce the parameter

$$\xi \equiv \frac{g_{U(1)'}^2}{g^2} \frac{M_W^2}{M_{Z'}^2} \tag{52}$$

with $g_{U(1)'}$ denoting the gauge coupling of the additional $U(1)'$ gauge group and $M_{Z'}$ being the mass of the Z'-boson. We then find the following additional contributions to the short-distance coefficients at the electroweak scale:

$$\begin{aligned}
\delta C_3 &= -\frac{\zeta_L^{sb}}{\lambda_t^{(s)}} \zeta_L^q \, \xi \,, & C_3' &= -\frac{1}{3} \frac{\zeta_R^{sb}}{\lambda_t^{(s)}} \left(\zeta_R^u + 2\zeta_R^d \right) \xi \,, \\
\delta C_5 &= -\frac{1}{3} \frac{\zeta_L^{sb}}{\lambda_t^{(s)}} \left(\zeta_R^u + 2\zeta_L^d \right) \xi \,, & C_5' &= -\frac{\zeta_R^{sb}}{\lambda_t^{(s)}} \zeta_L^q \, \xi \,, \\
\delta C_7 &= -\frac{2}{3} \frac{\zeta_L^{sb}}{\lambda_t^{(s)}} \left(\zeta_R^u - \zeta_R^d \right) \xi \,, & C_7' &= 0 \,, \\
\delta C_9 &= 0 \,, & C_9' &= -\frac{2}{3} \frac{\zeta_R^{sb}}{\lambda_t^{(s)}} \left(\zeta_R^u - \zeta_R^d \right) \xi \,.
\end{aligned} \tag{53}$$

Apart from ξ, FCNC transitions are controlled by the free parameters $\zeta_{L,R}^{IJ}$. Depending on them, the flavour-changing transitions contribute in general to both QCD and EW penguin operators, as well as to their mirror copies. Here we follow the approach of refs. [44,74–76] in which the main contribution is supposed to reside in the EW penguins, i.e. $|\delta C_{3,5}(\mu_W)| \ll |\delta C_7(\mu_W)|$, $|C'_{3,5}(\mu_W)| \ll |C'_7(\mu_W)|$. We implement this assumption by setting $\zeta_R^u + 2\zeta_R^d = \zeta_L^q = 0$. The constant $\zeta_R^u - \zeta_R^d$ can then be absorbed into a redefinition of $g_{U(1)'}$. After these simplifications we are left with only two non-zero coefficients

$$\delta C_7 = -\frac{2}{3}\frac{\widetilde{\zeta}_L^{sb}}{\lambda_t^{(s)}}, \qquad\qquad C'_9 = -\frac{2}{3}\frac{\widetilde{\zeta}_R^{sb}}{\lambda_t^{(s)}}, \tag{54}$$

where we have defined $\widetilde{\zeta}_{L,R}^{sb} \equiv \xi \zeta_{L,R}^{sb}$.

The coupling of the Z' boson to quarks is not related to its coupling to leptons. Therefore tight constraints from semileptonic decays, as we encountered in the case of a modified Z coupling, can be avoided here by simply switching off the Z' coupling to leptons. Such "leptophobic" Z' bosons can for example appear in models with a E_6 gauge symmetry (see e.g. ref. [77]). Since leptophobic Z' bosons avoid detection via traditional Drell-Yan processes, their mass is much less constrained allowing for larger values of the parameter ξ.

Besides constraints from hadronic B decays we have to face constraints from B_s-$\bar{B}_s$ mixing to which tree-level Z' exchange contributes. We find for the $\Delta B = 2$-Hamiltonian:

$$\begin{aligned}
\delta C_1^{\mathrm{VLL}} &= \frac{4\pi^2\sqrt{2}}{G_F M_W^2}\left(\frac{\widetilde{\zeta}_L^{sb}}{\lambda_t^{(s)}}\right)^2 \frac{1}{\xi}, \qquad\qquad C_1^{\mathrm{VRR}} = \frac{4\pi^2\sqrt{2}}{G_F M_W^2}\left(\frac{\widetilde{\zeta}_R^{sb}}{\lambda_t^{(s)}}\right)^2 \frac{1}{\xi}, \\
C_1^{\mathrm{LR}} &= \frac{8\pi^2\sqrt{2}}{G_F M_W^2}\left(\frac{\widetilde{\zeta}_L^{sb}}{\lambda_t^{(s)}}\right)\left(\frac{\widetilde{\zeta}_R^{sb}}{\lambda_t^{(s)}}\right)\frac{1}{\xi}.
\end{aligned} \tag{55}$$

In contrast to constraints from hadronic B decays, the B_s-$\bar{B}_s$ mixing constraint in the $(\mathrm{Re}(\widetilde{\zeta}_I^{sb}), \mathrm{Im}(\widetilde{\zeta}_I^{sb}))$ -plane depends on the parameter ξ determined by the coupling constant $g_{U(1)'}$ and the Z' mass $M_{Z'}$. It gets stronger for smaller ξ, i.e. for smaller $g_{U(1)'}$ and larger Z' mass $M_{Z'}$. This behaviour, which might seem counter-intuitive at first sight, has its origin in the dependence of the hadronic decays on the parameter combinations $\widetilde{\zeta}_I^{sb} = \xi\, \zeta_I^{sb}$. If one chooses smaller ξ values, one needs larger values of the FCNC couplings ζ_I^{sb} in order to obtain the same effects in the hadronic decays. Since the B_s-$\bar{B}_s$ mixing coefficients in (55) depend quadratically on the ζ_I^{sb}, this procedure sharpens their constraints.

4.3.2 Results

Considering eq. (54), one easily sees that the three scenarios $\tilde{\zeta}_L^{sb} \neq 0$, $\tilde{\zeta}_R^{sb} \neq 0$ and $\tilde{\zeta}_L^{sb} = \tilde{\zeta}_R^{sb} \neq 0$ correspond exactly to the scenarios $q_7 \neq 0$, $q'_9 \neq 0$ and $q_7 = q'_9 \neq 0$ in our model-independent analysis, except for a normalisation factor. In this way the

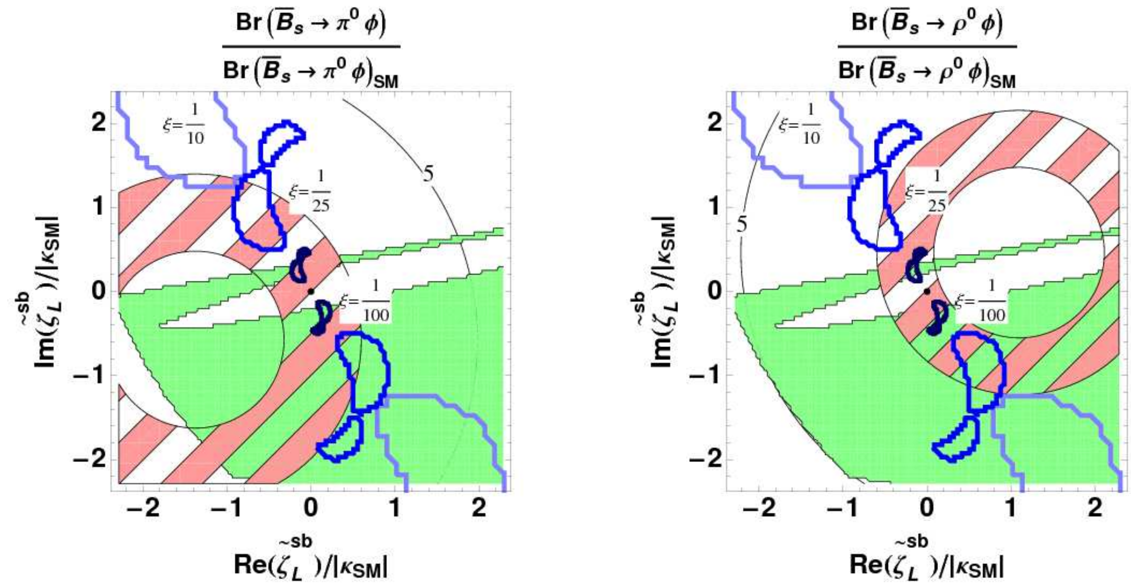

Figure 7: Enhancement factors of $\mathrm{Br}(\bar{B}_s \to \phi\pi^0)$ and $\mathrm{Br}(\bar{B}_s \to \phi\rho^0)$ for $\tilde{\zeta}_L^{sb} \neq 0$. The red-hatched ring corresponds to the SM uncertainty. The green area is allowed by the 2σ constraints from all hadronic B decays while the regions inside the blue lines are compatible with the constraint from B_s-$\bar{B}_s$ mixing. From the biggest to the smallest region they stand for the cases $\xi = 1/10$, $\xi = 1/25$ and $\xi = 1/100$, respectively.

exclusion regions from the $2\,\sigma$ constraints and the confidence levels from the fit can be immediately read off from figs. 4 and 5, provided one rescales the axes by an appropriate normalisation factor and rotates the pictures by 180° to take into account the minus signs in eq. (53).

In figs. 7 and 8 we present our results for the ζ_L^{sb} and the ζ_R^{sb} scenarios with the meanings of the green region and the red-striped ring being the same as in the preceeding sections. In addition the 2σ region for Δ_s is shown for different values of ξ. We recognise that there is very little overlap of the region allowed by hadronic constraints with the region preferred by Δ_s in the ζ_R^{sb} case. The same holds for the $\zeta_L^{sb} = \zeta_R^{sb}$ scenario not shown. This behaviour is easily understood: The observables $\Delta A_{\rm CP}$ and Δ_s both call for NP with a large imaginary part. The branching ratios of hadronic B decays depend linearly on the real part of $\zeta_{L,R}^{sb}$ at leading order, thus they pull the $\zeta_{L,R}^{sb}$ values towards the imaginary axis. The observable Δ_s, on the other hand, depends quadratically on $\zeta_{L,R}^{sb}$ and favours values on the diagonal $\mathrm{Re}(\tilde{\zeta}_{L,R}^{sb}) = -\mathrm{Im}(\tilde{\zeta}_{L,R}^{sb})$. For the ζ_L^{sb} setting this situation is relaxed due to the weak constraints from $B \to \pi K$ such that one can solve the two experimental discrepancies in $\Delta A_{\rm CP}$ and in Δ_s at the same time.

From the diagrams we see further that the B_s-$\bar{B}_s$ mixing constraint is very tight. It prohibits large effects in $\bar{B}_s \to \phi\pi^0, \phi\rho^0$ for realistic values of the parameter $\xi \lesssim 1/25$.

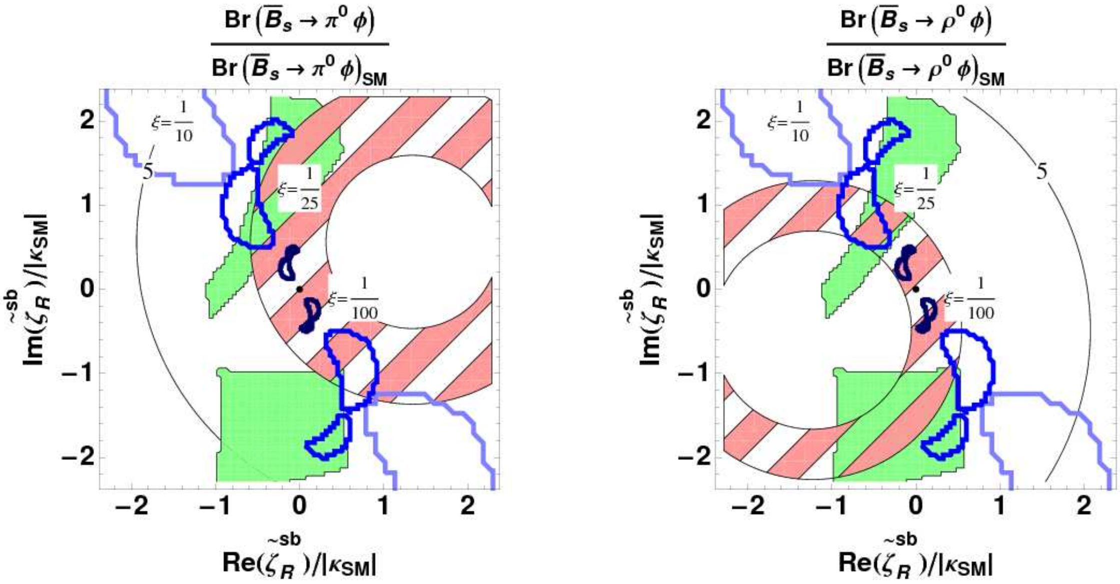

Figure 8: Enhancement factors of $\mathrm{Br}(\bar{B}_s \to \phi\pi^0)$ and $\mathrm{Br}(\bar{B}_s \to \phi\rho^0)$ for $\tilde{\zeta}_R^{sb} \neq 0$. The meaning of the coloured regions is the same as in fig. 7.

For $\xi = 1/25$, which would correspond for example to $g_{U(1)'} \sim g$ and $M_{Z'} \sim 400\mathrm{GeV}$, and for $\xi = 1/50$ we present the maximum enhancement factors in tab. 7. These numbers are obtained abandoning the $1\,\sigma$ region of the $B \to \pi K$ fit and requiring only agreement with the $2\,\sigma$ constraints. We find that enhancement of a factor ~ 5 is possible in the ζ_L^{sb} and ζ_R^{sb} scenarios whereas no effect can occur in the $\zeta_L^{sb} = \zeta_R^{sb}$ case because of eq. (33). For $\xi = 1/100$ the constraints from B_s-$\bar{B}_s$ mixing become so strong that no effect in $\bar{B}_s \to \phi\pi^0, \phi\rho^0$ would be detectable. A measurement of a significant enhancement would therefore set a lower limit on ξ, equivalent to an upper limit on the Z' mass.

4.4 MSSM

Supersymmetric effects in B decays have been studied in an enormous number of publications but most often hadronic decays have not been considered in such studies because of their large theoretical uncertainties. In the MSSM with conserved R-parity, all new flavour-changing interactions can be related to the squark mass matrices and enter all kinds of B decays via loops with virtual squarks and gauginos/higgsinos. Therefore one can expect supersymmetric contributions to be of roughly the same size in hadronic modes as they are in leptonic, semileptonic or radiative modes, so their effects will be most easily found where the uncertainties are smallest. However, once hints for supersymmetry are found in clean decay channels, one will also look for confirmations of these observations in other modes. Therefore we find it interesting to study the possible size of

Scenario		$\frac{\mathrm{Br}(B_s\to\phi\pi^0)}{\mathrm{Br}^{\mathrm{SM}}(\bar{B}_s\to\phi\pi^0)}$	$\frac{\mathrm{Br}_L(B_s\to\phi\rho^0)}{\mathrm{Br}_L^{\mathrm{SM}}(\bar{B}_s\to\phi\rho^0)}$	$\frac{\mathrm{Br}(B_s\to\phi\rho^0)}{\mathrm{Br}^{\mathrm{SM}}(\bar{B}_s\to\phi\rho^0)}$
$\xi = \frac{1}{25}$	$\tilde{\zeta}_L^{sb} \neq 0$	2.5 (4.9)	3.6 (5.6)	3.3 (4.9)
	$\tilde{\zeta}_R^{sb} \neq 0$	3.6 (5.7)	3.7 (5.7)	3.4 (5.1)
	$\tilde{\zeta}_L^{sb} = \tilde{\zeta}_R^{sb}$	1.0 (1.7)	1.0 (1.7)	1.1 (1.8)
$\xi = \frac{1}{50}$	$\tilde{\zeta}_L^{sb} \neq 0$	1.9 (3.7)	2.6 (4.0)	2.4 (3.6)
	$\tilde{\zeta}_R^{sb} \neq 0$	2.6 (4.1)	2.6 (4.1)	2.4 (3.7)
	$\tilde{\zeta}_L^{sb} = \tilde{\zeta}_R^{sb}$	1.0 (1.7)	1.0 (1.7)	1.1 (1.8)

Table 7: Maximal possible enhancement of the B_s branching ratios compatible with the constraints from all other hadronic decays and B_s-$\bar{B}_s$ mixing for the Z' model.

isospin-violation in the MSSM and whether large effects in the rare decays $\bar{B}_s \to \phi\rho^0$ and $\bar{B}_s \to \phi\pi^0$ can be expected or not, taking into account present experimental constraints on supersymmetric flavour-violation. Besides, we investigate whether the deviation of the ΔA_{CP} measurement from the SM prediction can be explained in the MSSM, as it has been claimed recently [78,79].

Throughout this chapter, we use the MSSM conventions of the SUSY Les Houches Accords (SLHA) [80,81] and diagonalise the sparticle mass matrices exactly. We do not make use of the mass-insertion approximation (MIA), which means that we are not limited to the case where off-diagonal elements in the mass matrices are small with respect to the diagonal elements.

4.4.1 Flavour-violation in the down-squark sector

First we consider the scenario where flavour-violation arises in the down-squark sector, i.e. where the 6×6 down-squark mass matrix contains flavour-violating elements. In this case we expect the largest SUSY effects in $b \to s$ transitions to stem from gluino-(down-)squark loops since these loops come with the strong gauge coupling α_s. Neutralino-squark loops arise from exactly the same off-diagonal elements but are suppressed by weak couplings, so they can be neglected to a first approximation.

The authors of ref. [70] have analysed such a scenario and have found that a significant amount of isospin-violation can only occur via $b \to s\bar{q}q$ box diagrams with virtual gluinos and down squarks ($q = u, d$) and not from photon- or Z-penguin diagrams. A necessary condition therein is that the SUSY-breaking masses of the right-handed first-generation squarks, $m^2_{\tilde{u}}$ and $m^2_{\tilde{d}}$, are very different from each other. Recently, this idea has been seized in ref. [82] and studied in the light of new data, especially measurements of CP asymmetries in $B \to \pi K$ decays and of B_s-$\bar{B}_s$ oscillations. It was found that the $B \to \pi K$ data can only be reproduced in a tiny region of the parameter space of the model.

In contrast to these findings the authors of ref. [78] have found a large impact of the gluino-mediated photon penguin in a mass-insertion calculation and state that sufficient isospin-violation is generated to explain the ΔA_{CP} data. However we find that this results from a missing factor $-\alpha/6\pi$ in eq. (41) of ref. [78]. We have performed a scan over the MSSM parameter space without using the mass-insertion approximation. Our full results for the $\Delta B = 1$ Wilson coefficients are written down in Appendix D. We found the gluino-mediated photon penguin to yield corrections below the 3% level to the SM coefficients of the EW penguin operators for all the points which allow for a diagonalisation of the squark mass-matrices with eigenvalues greater than $(100\,\mathrm{GeV})^2$ and satisfy the experimental constraints from $b \to s\gamma$. Such corrections are negligible for the prediction of ΔA_{CP}.

We conclude that we find no sizeable enhancement of EW penguins in the MSSM with flavour-violation in the down-sector. Neither can we explain the ΔA_{CP} discrepancy in this scenario nor can we expect large NP effects in the decays $\bar{B}_s \to \phi\pi^0$ and $\bar{B}_s \to \phi\rho^0$.

4.4.2 Flavour-violation in the up-squark sector

Supersymmetric flavour-violation can also arise in the up-sector via off-diagonal elements in the hermitian 6×6 up-squark mass matrix. In this scenario, penguin and box diagrams with virtual charginos and up-type squarks can provide sizeable contributions to B decays. We have calculated all of these diagrams, our full results for the $\Delta B = 1$ Wilson coefficients are written down in Appendix D.

The small Yukawa couplings occuring in the quark-squark-chargino couplings and in the squark mass matrix strongly suppress the effect of certain off-diagonal elements of this matrix. The only relevant flavour-violating entries for $b \to s$ transitions are therefore those corresponding to $\tilde{c}_L - \tilde{t}_L$ and $\tilde{c}_L - \tilde{t}_R$ mixing. We define them via

$$\hat{m}^2_{\tilde{Q}} \equiv m^2_{\tilde{q}} \begin{pmatrix} 1 & 0 & 0 \\ 0 & 1 & \delta^{uLL*}_{32} \\ 0 & \delta^{uLL}_{32} & 1 \end{pmatrix} \tag{56}$$

and

$$(\mathcal{M}^2_{\tilde{u}})_{62} = \frac{v_u}{\sqrt{2}} (\hat{T}_U)_{32} \equiv \delta^{uRL}_{32} m^2_{\tilde{q}}. \tag{57}$$

with a generic squark mass $m_{\tilde{q}}$. The remaining flavour-conserving elements are specified by $\hat{m}^2_{\tilde{u}} = \mathrm{Diag}(m^2_{\tilde{q}}, m^2_{\tilde{q}}, m^2_{\tilde{t}_R})$, $(\hat{T}_U)_{ii} = (\hat{T}_U)_{33}\delta_{i3}$ and $\tan\beta = 10$.

We have performed a scan over the free parameters in the value ranges defined in the table in fig. 10 to identify possible sources of large isospin-violation. In fig. 9 we plot the Z-penguin contribution to $|q_7|$ and $|q_9|$ (q_i is defined in eq. (31)) over the sum of all contributions to $|q_7|$ and $|q_9|$ for 30000 random points. We see that considering the Z-penguin only is a very good approximation for all points yielding large isospin-violation. In this way our scenario is essentially equivalent to the one with a left-handed flavour-changing Z coupling κ^{sb}_L discussed in sec. 4.2 and we will stay in this approximation in the following. Since a non-vanishing κ^{sb}_L breaks electroweak symmetry [71] it must involve

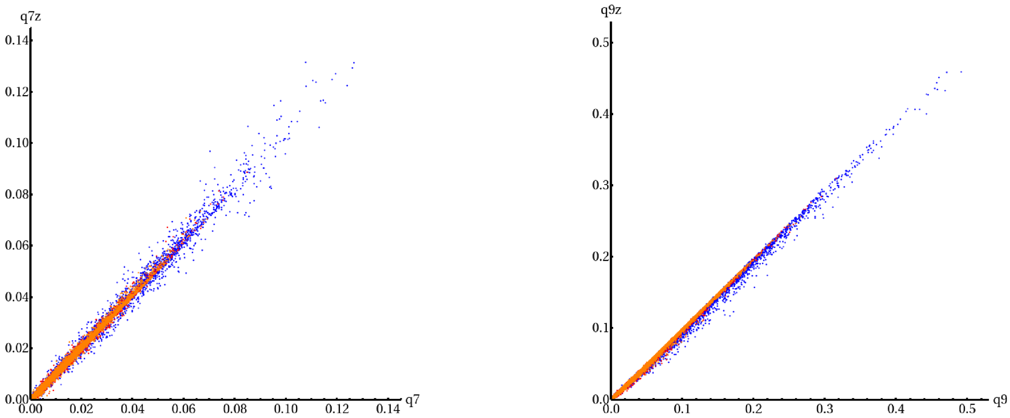

Figure 9: Left: (Right:) Z-penguin contribution to $|q_7|$ ($|q_9|$) over the full $|q_7|$ ($|q_9|$) for 30000 points in the MSSM parameter space. Blue: points excluded by the bound on $|C_{7\gamma}|$. Red: points excluded by $\mathrm{Br}(\bar{B} \to X_s\gamma)$. Orange: points passing all constraints. Not displayed: points excluded by lower bounds on squark and chargino masses.

the vacuum expectation values $v_{u,d}$. Therefore it is almost exclusively sensitive to δ_{32}^{uRL} and not to δ_{32}^{uLL} and we will neglect the latter in the following.

Having calculated the MSSM mass spectrum for a given parameter point we apply the following constraints:

- physical squark and chargino masses ≥ 100 GeV ,
- $\mathrm{Br}(\bar{B} \to X_s\gamma)$ compatible with data at the 2σ level,
- chargino contribution $|C_{7\gamma}^{\chi}| \leq |C_{7\gamma}^{\mathrm{SM}}| \approx 0.22$.

The last constraint ensures that fine-tuned points passing the $\mathrm{Br}(\bar{B} \to X_s\gamma)$ constraint are not considered.

It has been suggested [79] that a non-vanishing δ_{32}^{uRL} can generate isospin-violating effects large enough to explain the ΔA_{CP} discrepancy within the QCDF framework. This would clearly be an interesting perspective for supersymmetric effects in purely isospin-violating decays. However, we cannot confirm this statement in our framework. In fig. 9 we find that C_9 can be enhanced by about 25% and C_7 by about 8% with respect to the SM in the presence of a non-vanishing δ_{32}^{uRL}. In section 3 we have seen that a 25% effect in C_9 or an 8% effect in C_7 are not enough to generate a large ΔA_{CP} and are also not sufficient to enhance the branching fractions of $\bar{B}_s \to \phi\pi^0$ and $\bar{B}_s \to \phi\rho^0$ sizeably. A NP effect of this size would be hidden in the theoretical uncertainty and thus be unobservable. These findings are illustrated in figs. 10 and 11, where we display on the one hand a figure similar to fig. 3 in the complex κ_L^{sb} plane and on the other hand a zoomed version of the upper plots in fig. 6. To both figures we add the κ_L^{sb} values resulting from chargino-induced flavour-violating Z couplings in a scan over 30000

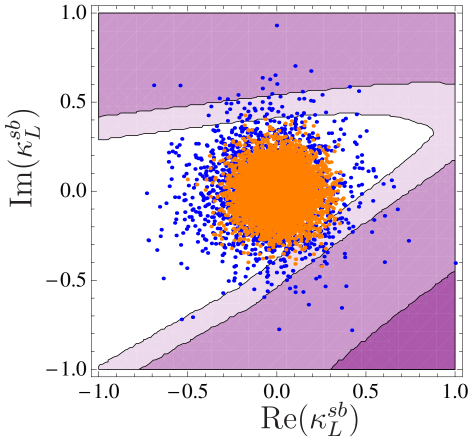

$m_{\tilde{q}}$, $m_{\tilde{t}_R}$, $(\hat{T}_U)_{33}$	200 GeV	1000 GeV
M_2, μ	100 GeV	1000 GeV
$\lvert\delta_{32}^{uLL}\rvert$, $\lvert\delta_{32}^{uRL}\rvert$	0	1
$\arg(\delta_{32}^{uLL})$, $\arg(\delta_{32}^{uRL})$	0	2π

Figure 10: Discrepancy between $\Delta A_{\rm CP}$ in theory and experiment as a function of $\kappa_L^{sb}/|\kappa_{\rm SM}|$ as defined in sec. 4.2. From light to dark the coloured regions denote 2.2σ, 2σ and 1σ. On top we add the $\kappa_L^{sb}/|\kappa_{\rm SM}|$ values resulting from chargino-induced flavour-violating Z couplings in a parameter scan as defined in the table. Blue (orange): Points (not) excluded by the bound on $|C_{7\gamma}|$. Not displayed: Points excluded by the lower bounds on SUSY masses.

points in the MSSM parameter space as defined in the table in fig. 10 to illustrate the statements of the last paragraph.

We note that there is an important difference between our calculation and the one of [79], namely the treatment of strong phases. We obtain all of these phases directly from QCDF, where they are suppressed by either $\alpha_s(m_b)$ or $\Lambda_{\rm QCD}/m_B$. Thus we typically find small strong phases even though their prediction comes with a large uncertainty. In the framework of ref. [79] only absolute values of penguin-to-tree ratios are predicted from QCDF whereas the corresponding strong phases can assume arbitrary values between 0 and π [83]. In this way, large CP asymmetries can be generated even without a large NP contribution and also the fact that $A_{\rm CP}(B^- \to \pi^0 K^-)$ and $A_{\rm CP}(\bar{B}^0 \to \pi^+ K^-)$ have opposite sign is no longer puzzling because the phases of the various tree and penguin topologies are uncorrelated. In contrast, our calculation reduces the 2.5σ SM discrepancy in $\Delta A_{\rm CP}$ only marginally. From fig. 10 we can read off that the vast majority of the allowed points are outside the 2.2σ region. Only a few rather fine-tuned points are between 2.2σ and 2σ.

5 Conclusion

In this article we studied the possibility of probing isospin-violating NP in hadronic B decays. We proposed to study the EW penguin sector of the effective weak Hamiltonian via the decays $\bar{B}_s \to \phi\pi^0$ and $\bar{B}_s \to \phi\rho^0$ and we provided a detailed phenomenological analysis of these two modes in correlation to other hadronic B decays.

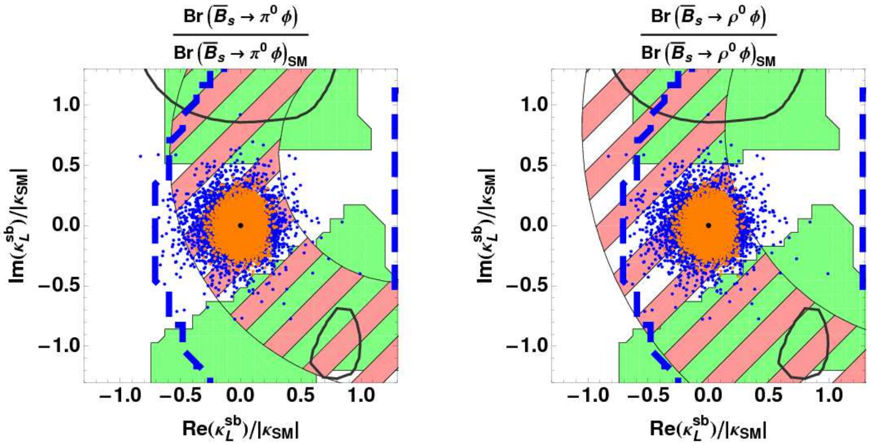

Figure 11: Zoom of the upper plots in fig. 6. On top we add the κ_L^{sb} values resulting from chargino-induced flavour-violating Z couplings in a parameter scan as defined in the table in fig. 10 with the same colour coding as in fig. 10

Our analysis is motivated by discrepancies found in $B \to \pi K$ decays, which are to date the best-measured hadronic $b \to s$ decays. In particular, the $2.5\,\sigma$ discrepancy found in the observable $\Delta A_{\rm CP}$ can be interpreted as a sign of NP in the EW penguin sector of the theory. We demonstrated in a model-independent analysis that this discrepancy can easily be resolved by an additional NP contribution to the EW penguin operators $Q_7^{(\prime)}, ..., Q_{10}^{(\prime)}$ if it is of the same order of magnitude as the leading SM coefficient $C_9^{\rm SM}$. An exception are parity-symmetric scenarios where the contributions to PP decays cancel. Whereas the solution in the case of NP in $C_9^{(\prime)}$ is, as expected, due to a new contribution to the colour-allowed EW penguin amplitude, we pointed out that, in the case of NP in $C_7^{(\prime)}$, the solution mainly comes about via a weak annihilation contribution in the QCDF framework which has a surprisingly large imaginary part. In particular we found for the case of equal new contributions to C_7 and C_9 that, even though these contributions tend to cancel in the EW penguin amplitude, the ΔA_{CP} discrepancy can still be solved via the EW penguin annihilation amplitude, a fact that has not been noticed so far. For various scenarios we performed frequentist fits to $B \to \pi K$ data. We found the fit to work well for NP in $C_9^{(\prime)}$ while NP in $C_7^{(\prime)}$ is only poorly constrained from $B \to \pi K$ alone. Especially in this case, the PV counterparts $B \to \rho K$ and $B \to \pi K^*$, which carry a different interplay of chiralities, give valuable additional information. We find that present experimental data already set strong constraints: a new EW penguin amplitude can be at most ~ 5 times larger than the SM one; on the other hand a new amplitude of about the same size as the SM one is required to solve the ΔA_{CP} discrepancy.

Whether the discrepancy in $\Delta A_{\rm CP}$ is really a manifestation of NP is however not clear because the experimental data are still not conclusive due to the large uncertainties in the theory prediction and the still somewhat low statistics of the measurements.

The long-standing problem of large theoretical hadronic uncertainties in hadronic decays can, however, be partially addressed exploiting the large variety of hadronic decay channels. In the case at hand, the best test is provided by the $\bar{B}_s \to \phi\pi^0$ and $\bar{B}_s \to \phi\rho^0$ modes, which are purely isospin-violating decays and are dominated by the EW penguin amplitude. Since these decays are not related to other hadronic B decays via flavour symmetries, their analysis requires a determination of the hadronic matrix elements from first principles and we used the QCDF approach to this end. From the full QCDF results we derived simple approximate expressions (eqs. (21)-(23), (33)) which reproduce the $\bar{B}_s \to \phi\pi^0, \phi\rho^0$ amplitudes with high accuracy for arbitrary scenarios with NP in $C_7^{(\prime)}, ..., C_{10}^{(\prime)}$. By quoting these formulae we facilitate the study of these decays without an extensive implementation of the QCDF framework.

In this work we performed the first analysis of the impact of NP in EW penguins on the $\bar{B}_s \to \phi\pi^0, \phi\rho^0$. A new EW penguin amplitude of the same size as the SM one can easily enhance the $\bar{B}_s \to \phi\pi^0$ and $\bar{B}_s \to \phi\rho^0$ branching ratios by an order of magnitude. We performed a quantitative analysis parameterising NP in EW penguins in a model-independent way at the level of the Wilson coefficients. For various scenarios we investigated the maximum enhancement of the $\bar{B}_s \to \phi\pi^0, \phi\rho^0$ branching ratios with respect to the result of our $B \to K\pi$ fits and with respect to constraints from other hadronic B decays. The results displayed in tab. 3 show that in many cases a large enhancement is possible. Particular exceptions are parity-symmetric models which have no impact on the VV decay $\bar{B}_s \to \phi\rho^0$ and scenarios with (approximately) equal contributions to $C_7^{(\prime)}$ and $C_9^{(\prime)}$ which cancel in $\bar{B}_s \to \phi\pi^0$.

A survey of concrete NP models has been performed in section 4, where we considered a modified Z^0 penguin, a model with an additional $U(1)'$ gauge symmetry and the MSSM. In such models additional constraints arise from the semileptonic decays $\bar{B} \to X_s e^+e^-$ and $\bar{B} \to K^* l^+ l^-$ and from B_s-$\bar{B}_s$ mixing. In case of the modified-Z^0-penguin scenario we found that the semileptonic constraints still allow for NP to an extent which is sufficient to resolve the ΔA_{CP} discrepancy. On the other hand, they prevent the $\bar{B}_s \to \phi\pi^0, \phi\rho^0$ decays from developing an enhancement which beats the hadronic uncertainties of the SM prediction. Therefore, a large effect measured in these decays would rule out the modified Z coupling. The semileptonic constraints can for example be avoided in a model with an additional Z' boson whose couplings to leptons can be switched off. Our analysis showed that in this scenario constraints from hadronic B decays and B_s-$\bar{B}_s$ mixing can be fulfilled simultaneously only at the $2\,\sigma$ level. The tight constraints from B_s-$\bar{B}_s$ mixing limit a potential enhancement of $\bar{B}_s \to \phi\pi^0, \phi\rho^0$ to a factor ~ 5. Furthermore the occurrence of such a measurable enhancement requires a large $g_{U(1)'}$ coupling and/or a light Z' boson. Finally we found that in the MSSM it is not possible to obtain a new contribution larger than about 25% in C_9 and about 8% in C_7, which is clearly not enough to generate a large ΔA_{CP} or a significant enhancement of the B_s decays. The ΔA_{CP} discrepancy can be reduced only marginally in this way. Only a few rather fine-tuned parameter points reduce it from 2.5σ to 2σ.

We stress again that the decays $\bar{B}_s \to \phi\pi^0, \phi\rho^0$ are highly sensitive to isospin-violating

NP. Their measurement would complement the analysis of $B \to K\pi$ decays and could shed light on the "$\Delta A_{\rm CP}$ puzzle". For this reason we strongly encourage experimental efforts to measure these decays at LHCb and at future Super-B factories.

Acknowledgements

We would like to thank U. Nierste for initiating the project and for a careful reading of the manuscript. We are grateful to him and to M. Beneke for useful discussions and suggestions. Furthermore we thank S. Khalil for helpful communications on [78] and [79]. This work is supported by the DFG Sonderforschungsbereich/Transregio 9 "Computergestützte Theoretische Teilchenphysik" and by the EU contract No. MRTN-CT-2006-035482, "FLAVIAnet". L.V. acknowledges the TTP Karlsruhe and the CERN Theory group for hospitality, and the Alexander-von-Humboldt Foundation for support. L.H. and D.S. acknowledge the support by Ev. Studienwerk Villigst and by Cusanuswerk, respectively, and by the DFG Graduate College *High Energy Physics and Particle Astrophysics*. L.H. is further supported by the Federal Ministry of Education and Research (BMBF) under constract No. 05H09WWE.

Appendices

A General framework for the calculation of hadronic B decays

Throughout this work, we study hadronic B decays into two light mesons using the framework of QCD factorisation [12–16]. This framework is based on the well-known effective weak Hamiltonian for $\Delta B = 1$ transitions given in (5) and described in section A.1. Matrix elements of this Hamiltonian are calculated in an expansion in $\Lambda_{\rm QCD}/m_B$. We give a few details concerning the generalisation of QCDF to a Hamiltonian containing operators with flipped chiralities in section A.2 and specify our input parameters in section A.3. In section A.4 we collect expressions for obtaining various observables from the QCDF-calculated amplitudes.

A.1 The effective weak Hamiltonian

The starting point for the analysis of hadronic B decays is the parameterisation of high-energy transition in terms of effective four-quark operators multiplied by short-distance coefficients. In the SM, this leads to the effective weak Hamiltonian in eq. (5). The short-distance coefficients C_i are calculated in the $\overline{\rm MS}$ renormalisation scheme at the scale $\mu_{\rm EW} \sim m_W$. Their low-scale values at $\mu_{\rm EW} \sim m_b$ are obtained from renormalisation group equations (RGE). In the SM, only C_1 is $\mathcal{O}(1)$, while C_2 and the QCD penguin coefficients $C_{3,...,6}$ arise at order $\mathcal{O}(\alpha_s)$ and the electroweak penguin coefficients arise at order $\mathcal{O}(\alpha)$, albeit partly enhanced by factors of $x_{tW} = m_t^2/m_W^2$ and/or $1/\sin^2\theta_W$. The complete analytical expressions for these coefficients are written down e.g. in [63].

Besides the SM operators, we also consider the possibility that New Physics gives rise to the so-called "mirror" penguin operators Q_i', obtained from Q_i by a global exchange of left- and right-handed chiralities of the quark fields, $(V-A) \leftrightarrow (V+A)$. We thus replace in eq. (5)

$$C_i Q_i \longrightarrow C_i Q_i + C_i' Q_i'. \tag{58}$$

Given the enhancement of $C_7(\mu_{\rm EW})$ and $C_9(\mu_{\rm EW})$ by x_{tW} and/or $1/\sin^2\theta_W$, we follow the modified RGE scheme presented in [14] for the SM coefficients and consider the enhanced terms as leading order coefficients, i.e.

$$C_7^{\rm LO}(m_W) = \frac{\alpha}{4\pi}\frac{x_{tW}}{3} \quad , \quad C_9^{\rm LO}(m_W) = \frac{\alpha}{4\pi}\left[\frac{x_{tW}}{3} + \frac{2}{3\sin\theta_W^2}(10B_0(x_{tW}) - 4C_0(x_{tW}))\right] \tag{59}$$

with the loop functions $B_0(x)$ and $C_0(x)$ from [63]. To be consistent we neglect at the same time electromagnetic corrections to the QCD penguin coefficients as well as any mixing of $C_7, \ldots, C_{10}$ into $C_1, ..., C_6$. Since this treatment improves the RGE evolution for $C_7, ..., C_{10}$ and since it is exactly these coefficients we are interested in, it is well suited for our analysis. By contrast, for the NP contributions we use the standard treatment for the leading order RGE.

A.2 Operator matrix elements in QCDF

From the effective Hamiltonian (5) the decay amplitude for the process $\bar{B} \to M_1 M_2$ can be calculated as

$$\mathcal{A}^{(h)}_{\bar{B}\to M_1 M_2} = \langle M_1^{(h)} M_2^{(h)} | \mathcal{H}_{\rm eff} | \bar{B} \rangle, \tag{60}$$

where h refers to a helicity amplitude in case of a decay into two vector mesons, $\bar{B} \to V_1^h V_2^h$ with $h = 0, +, -$.

In QCDF the matrix elements of the effective Hamiltonian are organised in terms of flavour amplitudes α_i which are directly related to the topologies of the underlying weak transition, for example colour-allowed EW penguin, colour-suppressed tree etc. Analogous amplitudes β_i represent the corresponding weak annihilation transitions. The topological amplitudes α_i in turn can be decomposed into coefficients a_i which are in direct correspondence to the operators Q_i in the effective Hamiltonian. At NLO these coefficients a_i contain the perturbative non-factorisable vertex-, penguin- and spectator-scattering corrections governed by the factorisation formula. For a complete description we refer to [15]. The expressions given there can easily be generalised to account for the mirror operators by adding a topological amplitude α'_i to each of the α_i [84]. A similar generalisation applies to the annihilation amplitudes β_i. Here we only need to add the expressions for $\alpha'_{3\mathrm{EW},4\mathrm{EW}}$, which read

$$\alpha'^p_{3\mathrm{EW}}(M_1M_2) = \begin{cases} -a'^p_9(M_1M_2) + a'^p_7(M_1M_2), & \text{if } M_1M_2 = PP, \\ a'^p_9(M_1M_2) + a'^p_7(M_1M_2), & \text{if } M_1M_2 = PV, \\ a'^p_9(M_1M_2) - a'^p_7(M_1M_2), & \text{if } M_1M_2 = VP, \\ -a'^p_9(M_1M_2) - a'^p_7(M_1M_2), & \text{if } M_1M_2 = V^0V^0, \\ -f^{M_1}_\pm \left(a'^p_9(M_1M_2) + a'^p_7(M_1M_2)\right), & \text{if } M_1M_2 = V^\pm V^\pm, \end{cases}$$

$$\alpha'^p_{4\mathrm{EW}}(M_1M_2) = \begin{cases} -a'^p_{10}(M_1M_2) - r^{M_2}_\chi\, a'^p_8(M_1M_2), & \text{if } M_1M_2 = PP, \\ a'^p_{10}(M_1M_2) + r^{M_2}_\chi\, a'^p_8(M_1M_2), & \text{if } M_1M_2 = PV, \\ a'^p_{10}(M_1M_2) - r^{M_2}_\chi\, a'^p_8(M_1M_2), & \text{if } M_1M_2 = VP, \\ -a'^p_{10}(M_1M_2) + r^{M_2}_\chi\, a'^p_8(M_1M_2), & \text{if } M_1M_2 = V^0V^0, \\ f^{M_1}_\pm \left(-a'^p_{10}(M_1M_2) + r^{M_2}_\chi\, a'^p_8(M_1M_2)\right), & \text{if } M_1M_2 = V^\pm V^\pm \end{cases} \tag{61}$$

with $f^{M_1}_\pm = F^{B\to M_1}_\mp(0)/F^{B\to M_1}_\pm(0)$ being a ratio of form factors, such that $f^{M_1}_+ \sim m_B/\Lambda_{\mathrm{QCD}}$ and $f^{M_1}_- \sim \Lambda_{\mathrm{QCD}}/m_B$ in the heavy-quark limit [16]. The NLO expressions for the coefficients a'_i are equivalent to the ones for the coefficients a_i from [15] up to the replacement $C_i \to C'_i$. Additionally in the transverse amplitudes of $B \to VV$ decays one has to flip the helicities, i.e. the expressions for a^+_i are needed for a'^-_i and vice versa.

The pattern of signs appearing in eq. (61) is a consequence of the fact that matrix elements of the mirror operators are related to the SM ones by parity

$$\langle M_1M_2|Q_i|\bar{B}\rangle \;=\; -\eta_{M_1M_2}\,\langle M_1M_2|Q'_i|\bar{B}\rangle, \tag{62}$$

which implies that the amplitudes involve the coefficients $a^{(\prime)}_i$ only in the combinations [53]

$$a^p_i(M_1,M_2) \;-\; \eta_{M_1M_2}\, a'^p_i(M_1,M_2). \tag{63}$$

Here $\eta_{M_1M_2} = \pm 1$ is the parity of the final state. For PP and longitudinal VV final states, we have $\eta_{M_1M_2} = 1$ whereas for PV final states $\eta_{M_1M_2} = -1$. In this manner left-handed and right-handed NP give rise to different signatures and correlations among PP, PV or VV decays. Exploiting this feature can be very important in order to probe the chirality structure of a potential NP model.

A.3 Input parameters and tree to penguin ratios in $B \to \pi K$, $B \to \pi\pi$

In the framework of QCDF the decay amplitudes depend on quite a few input parameters such as form factors, Gegenbauer moments of light-cone distribution amplitudes, etc. In

QCD scale and running quark masses [GeV]				
$\Lambda^{(5)}_{\overline{\rm MS}}$	$m_b(m_b)$	$m_c(m_b)$	m_s	m_q/m_s
0.231	4.2	1.3±0.2	0.090± 0.020	0.0413

CKM parameters				
λ	$\lvert V_{cb}\rvert$	$\lvert V_{ub}/V_{cb}\rvert$	γ	$\sin(2\beta)$
0.225	0.0415 ± 0.0010	$0.085^{+0.025}_{-0.015}$	$(70 \pm 10)^\circ$	0.673 ± 0.23

B meson parameters				
		B^-	$\bar{B}^0$	$\bar{B}^0_s$
Lifetime	τ[ps]	1.638	1.525	1.472
Decay constant	f_B[MeV]	210 ± 20		240 ± 20
	λ_B[MeV]	200^{+250}_{-0}		200^{+250}_{-0}

Pseudoscalar-meson decay constants and Gegenbauer moments		
	π	K
f[MeV]	131	160
$\alpha_1, \alpha_{1,\perp}$	0	0.06 ± 0.06
$\alpha_2, \alpha_{2,\perp}$	0.20 ± 0.15	0.20 ± 0.15

Vector-meson decay constants and Gegenbauer moments			
	ρ	K^*	ϕ
f[MeV]	209 ± 1	218 ± 4	221 ± 3
$f^\perp$[MeV]	165 ± 9	185 ± 10	186 ± 9
$\alpha_1, \alpha_{1,\perp}$	0	0.06 ± 0.06	0
$\alpha_2, \alpha_{2,\perp}$	0.1 ± 0.2	0.1 ± 0.2	0 ± 0.3

Pseudoscalar-meson form factor at $q^2 = 0$			
	$B \to \pi$	$B \to K$	$B_s \to \bar{K}$
F_0	0.25 ± 0.05	0.34 ± 0.05	0.31 ± 0.05

Vector-meson form factor at $q^2 = 0$			
	$B \to \rho$	$B \to K^*$	$B_s \to \phi$
A_0	$0.30^{+0.07}_{-0.03}$	0.39 ± 0.06	$0.38^{+0.10}_{-0.02}$
F_+	0.00 ± 0.06	0.00 ± 0.06	0.00 ± 0.06
F_-	0.55 ± 0.06	0.68 ± 0.07	$0.65^{+0.14}_{-0.00}$

Table 8: Summary of the theoretical input parameters for hadronic B decays into two light mesons. All scale-dependent quantities refer to $\mu = 2\,\mathrm{GeV}$ unless otherwise stated. The values represent the most up-to-date values taken from [15,16,85–89].

tab. 8 we provide a list of up-to-date values. We use the updated value of $\Lambda^{(5)}_{\overline{\rm MS}}$ as obtained at 2 loop in [90]; as of $\lambda_B = \lambda_{B_s}$ we assume the lower value 200 MeV as suggested by exclusive hadronic decays, see [16,86,88,91]. Particular attention deserves the choice of $X_{H,A}$, i.e. the numbers which parameterise our ignorance of non-perturbative physics occurring in spectator scattering and weak annihilation due to the exchange of soft gluons. For X_H we use the definition of [15],

$$X_H = (1+\rho_H e^{i\phi_H}) \ln \frac{m_B}{\Lambda_h}, \tag{64}$$

with a non-perturbative scale $\Lambda_h = 500$ MeV. The default value is $\rho_H = 0$ and we estimate the uncertainty setting $\rho_H = 1$ and freely varying ϕ_H between 0 and 2π. In the light of experimental data, X_A requires more attention. The reasoning goes as follows.

A good test of the QCDF hypothesis is to look at the πK-penguin to $\pi\pi$-tree ratio [15], which can be directly related to experimental observables:

$$\left|\frac{\hat{\alpha}_4^c(\pi\bar{K})}{\alpha_1(\pi\pi)+\alpha_2(\pi\pi)}\right| \simeq \left|\frac{V_{ub}}{V_{cb}}\right| \frac{f_\pi}{f_K} \left[\frac{\Gamma(B^-\to\pi^-\bar{K}^0)}{\Gamma(B^-\to\pi^-\pi^0)}\right]^{1/2} \overset{\text{exp.}}{=} 0.100^{+0.030}_{-0.018}. \tag{65}$$

To a good approximation this ratio relates a pure QCD-penguin decay to a pure tree decay and allows to eliminate the uncertainty from the heavy-to-light form factor. Since the tree decay $B^-\to\pi^-\pi^0$ suffers from small uncertainties in QCDF and is expected to receive negligible contributions from NP, eq. (65) probes the accuracy of the QCDF prediction for the penguin amplitude $\hat{\alpha}_4^c(\pi\bar{K})$. In absence of sizeable NP contributions to QCD penguins it constrains the uncalculable weak-annihilation contribution β_3^c, which is responsible for the lion's share of the theoretical uncertainty in the penguin amplitude. Though subleading in $\Lambda_{\rm QCD}/m_B$, β_3^c is known to be numerically enhanced.

Using the parameters in tab. 8 and expressing β_3^c via the complex $\mathcal{O}(1)$ parameter X_A as in ref. [15] with

$$X_A = (1+\rho_A e^{i\phi_A}) \ln \frac{m_B}{\Lambda_h} \tag{66}$$

with the default value $\rho_A = 0$, we find

$$\left|\frac{\hat{\alpha}_4^c(\pi\bar{K})}{\alpha_1(\pi\pi)+\alpha_2(\pi\pi)}\right| \overset{\text{SM}}{=} 0.078^{+0.025}_{-0.015}, \tag{67}$$

which is slightly smaller than older results. Repeating the analysis of [15] for the PV and VV modes we obtain fig. 12. The plots show the experimental central values and uncertainties of the ratio in eq. (65) (circles around the origin) for $B\to\pi K$ and three related decays. They are combined with "limaçon" curves representing the corresponding theory predictions where the phase ϕ_A is freely varied between 0 and 2π while we set $\rho_A = 1$ $(1.5, 2)$ for PP and PV modes and $\rho_A = 0.6$ $(1.0, 1.5)$ for VV modes to obtain the blue (purple, yellow) curves. The red dots correspond to $\rho_A = 0, 1, 1.5$ ($\rho_A = 0, 0.6, 1.0$ for VV modes) with ϕ_A fixed as in the scenario "S4" in [15] for PP and PV modes and $\phi_A = -40°$ for VV.

These results lead us to the conclusion that, in the light of present data, we prefer to change the widely used treatment with $\rho_A = 0$ as default and $\rho_A = 1$ ($\rho_A = 0.6$ for VV) for the variation of ϕ_A in order to have a more conservative estimate of the theoretical uncertainty. Nevertheless we confirm that $\rho_A \leq 2$ is a reasonable upper bound for weak-annihilation contributions in QCDF. We adopt $\rho_A = 1.5$ ($\rho_A = 1.0$ for VV modes) as our default value, keeping the default for ϕ_A as above, and estimate the uncertainty with ρ_A unchanged and $\phi_A \in [0, 2\pi)$.

A.4 Calculating observables in hadronic B decays

Starting from a decay amplitude $\mathcal{A}(\bar{B} \to M_1 M_2)$ the corresponding decay rate can be calculated as

$$\Gamma(\bar{B} \to M_1 M_2) = \frac{S}{16\pi m_B} |\mathcal{A}(\bar{B} \to M_1 M_2)|^2, \tag{68}$$

with a symmetry factor S. We have $S = 1/2$ if M_1 and M_2 are identical and $S = 1$ otherwise. For decays into two vector mesons, where three different helicity amplitudes exist, one replaces $|\mathcal{A}(\bar{B} \to M_1 M_2)|^2$ by a sum over the three possible helicities of the final state, $\sum_{h=0,-,+} |\mathcal{A}^h(\bar{B} \to V_1 V_2)|^2$. The branching ratios are easily calculated from $\mathrm{Br}(\bar{B} \to M_1 M_2) = \Gamma(\bar{B} \to M_1 M_2)/\Gamma_{\mathrm{tot}}$ with Γ_{tot} being the total decay width of the $\bar{B}$ meson. Our theoretical predictions always refer to CP-averaged branching ratios defined as

$$\overline{\mathrm{Br}}(\bar{B} \to \bar{f}) = \frac{1}{2} \left(\mathrm{Br}(\bar{B} \to \bar{f}) + \mathrm{Br}(B \to f) \right), \tag{69}$$

where $\bar{f}, f$ stand for the final state $M_1 M_2$ and its CP-conjugated state. The CP-conjugated decay rate is calculated by replacing $\mathcal{A}$ in eq. (68) by the corresponding CP-conjugated amplitude. This amounts to a change of sign for all the weak phases while strong phases are unchanged.

The direct CP asymmetries read

$$A_{\mathrm{CP}} = \frac{\mathrm{Br}(\bar{B} \to \bar{f}) - \mathrm{Br}(B \to f)}{\mathrm{Br}(\bar{B} \to \bar{f}) + \mathrm{Br}(B \to f)} \tag{70}$$

and the longitudinal polarisation fraction $f_L(\bar{B} \to M_1 M_2)$ is defined as

$$f_L(\bar{B} \to M_1 M_2) = \frac{|\mathcal{A}^0(\bar{B} \to V_1 V_2)|^2}{\sum_{h=0,-,+} |\mathcal{A}^h(\bar{B} \to V_1 V_2)|^2}. \tag{71}$$

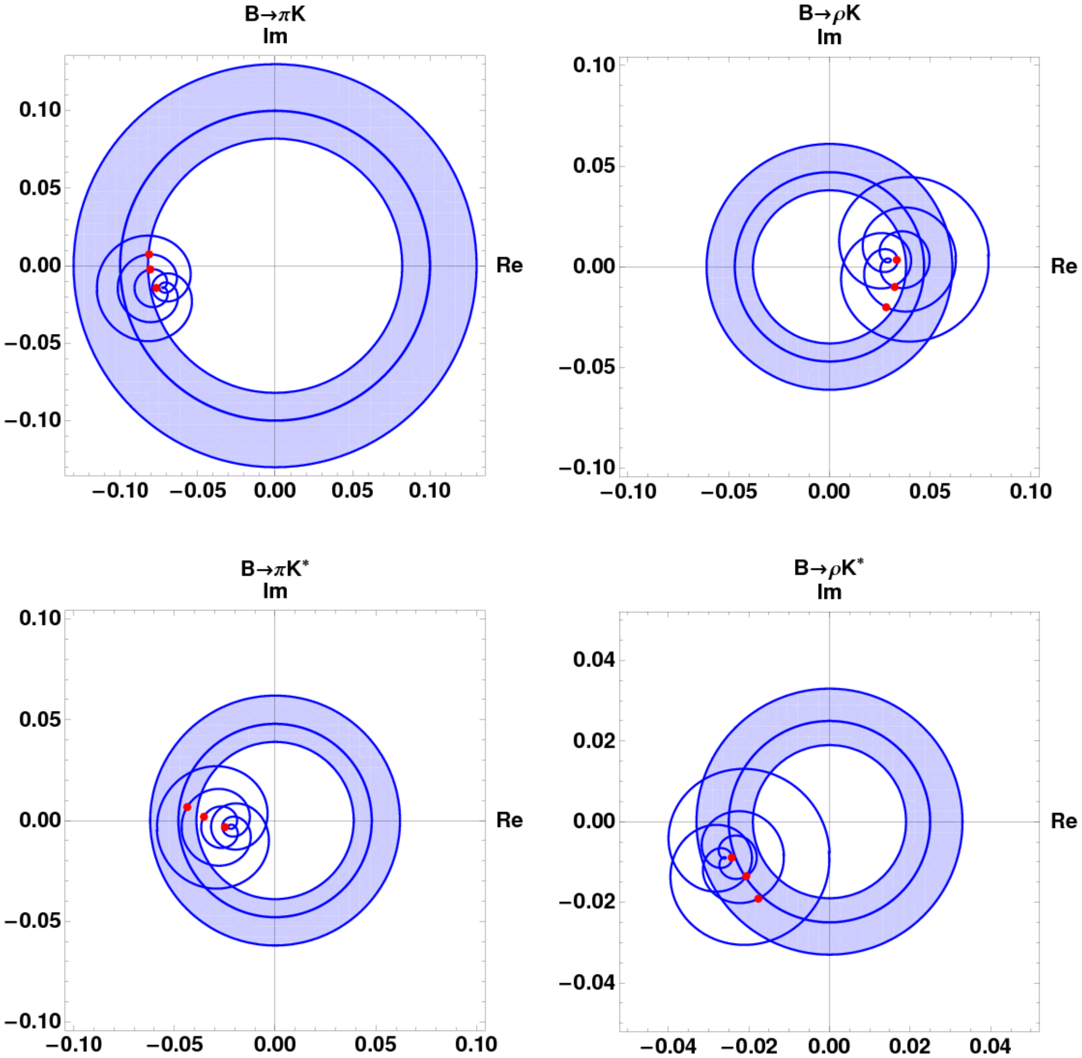

Figure 12: Experimental and theoretical values of the penguin-to-tree ratio defined in eq. (65). For explanations see text.

B Isospin-violating observables in $B \to \pi K$

In this appendix we present the observables which are sensitive to isopin violation in the $B \to \pi K$ decay modes and which we use to calculate our $2\,\sigma$ constraints.

First, one has ratios of any two different decay rates. Using the parameterisation (10) and neglecting terms which are quadratic in the r_i as well as the annihilation contribution $r_{\rm EW}^{\rm A}$ which has only a small real part, one has 6 different ratios which read [10,11]

$$
\begin{aligned}
R_c^B &\equiv 2\,\frac{\overline{\rm Br}(B^- \to \pi^0 K^-)}{\overline{\rm Br}(B^- \to \pi^- \bar{K}^0)} \simeq 1 \,+\, 2\,{\rm Re}(r_{\rm EW} + r_{\rm EW}^{\rm C}) -\, 2\,{\rm Re}(r_{\rm T} + r_{\rm C})\cos\gamma\,, \\
R_n^B &\equiv \frac{1}{2}\,\frac{\overline{\rm Br}(\bar{B}^0 \to \pi^+ K^-)}{\overline{\rm Br}(\bar{B}^0 \to \pi^0 \bar{K}^0)} \simeq 1 \,+\, 2\,{\rm Re}(r_{\rm EW} + r_{\rm EW}^{\rm C}) -\, 2\,{\rm Re}(r_{\rm T} + r_{\rm C})\cos\gamma\,, \\
R_c^K &\equiv 2\,\frac{\tau_0}{\tau_-}\,\frac{\overline{\rm Br}(B^- \to \pi^0 K^-)}{\overline{\rm Br}(\bar{B}^0 \to \pi^+ K^-)} \simeq 1 \,+\, 2\,{\rm Re}(r_{\rm EW}) -\, 2\,{\rm Re}(r_{\rm C})\cos\gamma\,, \\
R_n^K &\equiv \frac{1}{2}\,\frac{\tau_0}{\tau_-}\,\frac{\overline{\rm Br}(B^- \to \pi^- \bar{K}^0)}{\overline{\rm Br}(\bar{B}^0 \to \pi^0 \bar{K}^0)} \simeq 1 \,+\, 2\,{\rm Re}(r_{\rm EW}) -\, 2\,{\rm Re}(r_{\rm C})\cos\gamma\,, \\
R_c^\pi &\equiv \frac{\tau_0}{\tau_-}\,\frac{\overline{\rm Br}(B^- \to \pi^- \bar{K}^0)}{\overline{\rm Br}(\bar{B}^0 \to \pi^+ K^-)} \simeq 1 \,+\, 2\,{\rm Re}(r_{\rm T})\cos\gamma -\, 2\,{\rm Re}(r_{\rm EW}^{\rm C}), \\
R_n^\pi &\equiv \frac{\tau_0}{\tau_-}\,\frac{\overline{\rm Br}(B^- \to \pi^0 K^-)}{\overline{\rm Br}(\bar{B}^0 \to \pi^0 \bar{K}^0)} \simeq 1 -\, 2\,{\rm Re}(r_{\rm T} + 2 r_{\rm C})\cos\gamma \,+\, 2\,{\rm Re}(2 r_{\rm EW} + r_{\rm EW}^{\rm C})\,,
\end{aligned}
\tag{72}
$$

where τ_0 and τ_- are the life times of the neutral and charged B mesons, respectively. NP in EW penguins as in (13) enters the ratios $R_{c,n}^{B,K,\pi}$ through

$$
\begin{aligned}
{\rm Re}(r_{\rm EW}) &\to {\rm Re}(r_{\rm EW}) + {\rm Re}(\tilde{r}_{\rm EW})\cos\delta_z, \\
{\rm Re}(r_{\rm EW}^{\rm C}) &\to {\rm Re}(r_{\rm EW}^{\rm C}) + {\rm Re}(\tilde{r}_{\rm EW}^{\rm C})\cos\delta_z.
\end{aligned}
\tag{73}
$$

Experimental data on the $R_{c,n}^{B,K,\pi}$ can be used to constrain the NP contributions $\tilde{r}_{\rm EW}$ and $\tilde{r}_{\rm EW}^{\rm C}$. Note that the $R_{c,n}^{B,K,\pi}$ involve different combinations of $\tilde{r}_{\rm EW}$ and $\tilde{r}_{\rm EW}^{\rm C}$ and thus they are sensitive to different linear combinations of the electroweak penguin coefficients $C_7^{(\prime)}, ..., C_{10}^{(\prime)}$. Therefore, it depends on the specific NP scenario in consideration which of the $R_{c,n}^{B,K,\pi}$ give the best constraints.

Beyond being responsible for the universal QCD penguin contribution, isospin relations account for the approximate equation

$$
\Gamma(B^- \to \pi^- \bar{K}^0) - 2\,\Gamma(B^- \to \pi^0 K^-) \,\approx\, 2\,\Gamma(\bar{B}^0 \to \pi^0 \bar{K}^0) - \Gamma(\bar{B}^0 \to \pi^+ K^-) \tag{74}
$$

known as Lipkin sum rule [92]. In the strict isospin limit both sides of this equation vanish identically. This is reflected in the fact that $R_{c,n}^B$ in (72) are both equal to one, apart from isospin-violating terms of order $\mathcal{O}(r_i)$. These linear terms are generated by the interference of the isospin-violating parts of the amplitude with the QCD penguin part. The special property of (74) is now that these interference terms on the left- and righthand side of the approximate equation cancel each other. For this reason (74) can be used to construct a purely isospin-violating observable, namely

$$R \equiv 2\,\frac{\tau_-\,\overline{\mathrm{Br}}(\bar{B}^0 \to \pi^0 \bar{K}^0) \,+\, \tau_0\,\overline{\mathrm{Br}}(B^- \to \pi^0 K^-)}{\tau_-\,\overline{\mathrm{Br}}(\bar{B}^0 \to \pi^+ K^-) \,+\, \tau_0\,\Gamma(B^- \to \pi^- \bar{K}^0)} \;=\; 1 \,+\, \mathcal{O}(r_i^2)\,. \tag{75}$$

In a similar way it is possible to construct observables with a high sensitivity to isospin violation out of the direct CP asymmetries. To this end we consider the two differences

$$\begin{aligned}
\Delta A_{\mathrm{CP}}^- &\equiv A_{\mathrm{CP}}(B^- \to \pi^0 K^-) \,-\, A_{\mathrm{CP}}(\bar{B} \to \pi^+ K^-) \,=\, \Delta A_{\mathrm{CP}} \\
\Delta A_{\mathrm{CP}}^0 &\equiv A_{\mathrm{CP}}(B^- \to \pi^- \bar{K}^0) \,-\, A_{\mathrm{CP}}(\bar{B} \to \pi^0 \bar{K}^0).
\end{aligned} \tag{76}$$

In the parameterisation (10) and in the presence of NP in electroweak penguins (13) one finds $\Delta A_{\mathrm{CP}}^0 = \Delta A_{\mathrm{CP}}^-$ up to terms quadratic in the r_i. The observable ΔA_{CP}^- is given in (15) and represents the famous ΔA_{CP} showing a 2.5σ discrepancy with current data. A precise measurement of ΔA_{CP}^0 could therfore shed light on the ΔA_{CP} discrepancy.

Since $\pi^0 K_s$ is a CP-eigenstate into which both the B^0 and the $\bar{B}^0$ meson can decay, we have mixing-induced CP violation in this decay channel. The corresponding observable S_{CP} is defined via the time-dependent CP asymmetry as

$$\frac{\mathrm{Br}(\bar{B}^0(t) \to f) - \mathrm{Br}(B^0(t) \to f)}{\mathrm{Br}(\bar{B}^0(t) \to f) + \mathrm{Br}(B^0(t) \to f)} \equiv S_{\mathrm{CP}} \sin(\Delta m_B t) - C_{\mathrm{CP}} \cos(\Delta m_B t), \tag{77}$$

where $C_{\mathrm{CP}} = -A_{\mathrm{CP}}$ is the direct CP asymmetry, up to a sign. Although $S_{\pi K}$ is not sensitive to isospin-violation in particular, it will be affected by a solution of the "ΔA_{CP}-puzzle" via a NP contribution $\tilde{r}_{\mathrm{EW}}$. The reason is that $\tilde{r}_{\mathrm{EW}}$ has to come with a large new weak phase δ in order to have substantial impact on ΔA_{CP}. Including the new electroweak contributions and neglecting $\mathrm{Re}(r_{\mathrm{EW}}^{\mathrm{A}})$ we find

$$S_{\mathrm{CP}}(\bar{B}^0 \to \pi^0 \bar{K}^0) \simeq \sin 2\beta + 2\mathrm{Re}\,(r_{\mathrm{C}}) \cos 2\beta \sin\gamma - 2\mathrm{Re}(\tilde{r}_{\mathrm{EW}} + \tilde{r}_{\mathrm{EW}}^{C}) \cos 2\beta \sin\delta. \tag{78}$$

We collect the theoretical and experimental results for the observables defined here, as well as the CP-averaged branching ratios and direct CP asymmetries in tab. 1.

Finally we give the QCDF expressions of the ratios r_i used above:

$$r_{\mathrm{T}} = -\left|\frac{\lambda_u^{(s)}}{\lambda_c^{(s)}}\right| \frac{\alpha_1(\pi K)}{\hat{\alpha}_4^c(\pi K)}, \qquad r_{\mathrm{C}} = -\left|\frac{\lambda_u^{(s)}}{\lambda_c^{(s)}}\right| \frac{A_{K\pi}}{A_{\pi K}} \frac{\alpha_2(K\pi)}{\hat{\alpha}_4^c(\pi K)},$$

$$r_{\mathrm{EW}} = \frac{3}{2} \frac{A_{K\pi}}{A_{\pi K}} \frac{\alpha_{3,\mathrm{EW}}^c(K\pi)}{\hat{\alpha}_4^c(\pi K)}, \qquad r_{\mathrm{EW}}^{C} = \frac{3}{2} \frac{\alpha_{4,\mathrm{EW}}^c(\pi K)}{\hat{\alpha}_4^c(\pi K)}, \qquad r_{\mathrm{EW}}^{A} = \frac{3}{2} \frac{\beta_{3,\mathrm{EW}}^c(\pi K)}{\hat{\alpha}_4^c(\pi K)}. \tag{79}$$

C The fit

The basic idea of our fit is quite simple: we calculate within a NP scenario the expected values for a set of observables as a function of NP parameters q_i. We then compare these values at each point of a grid in the $\{q_i\}$ parameter space to experimental data. The points for which the experimental and the theoretical results are closest are most likely to be realised, i.e. they represent the q_i-values for which the theoretical prediction describes best the experimental measurements. Technically, this comparison is performed by evaluating at each grid point the χ^2 function

$$\chi^2(\{q_i\}) = \sum_j \frac{(x_{j\,\mathrm{theo}}(\{q_i\}) - x_{j\,\mathrm{exp}})^2}{\sigma^2_{j\,\mathrm{exp}}}, \tag{80}$$

where the sum runs over different observables x_j. In this notation $x_{j\,\mathrm{theo}}$ represents the theoretical prediction of the observable and $x_{j\,\mathrm{exp}}$ is the corresponding experimental mean value. $\sigma_{j\,\mathrm{exp}}$ stands for the 1σ experimental uncertainty (symmetric around the mean).

The non-trivial part of the analysis is the implementation of the theoretical error. Here we follow the Rfit scheme [7]. Our basic assumption is that experimental data approximatively yield a Gaussian distribution of an observable but a theoretical calculation does not. The latter depends on a set of input parameters like form factors, decay constants etc. for which no probability distribution is known. The Rfit scheme corresponds to a frequentist approach and it assumes no particular distribution for the theory parameters, only that they are constrained to certain allowed ranges. The theoretical and experimental uncertainties are then combined in the following χ^2 function:

$$\chi^2 = \sum_j \begin{cases} \frac{(|x_{j\,\mathrm{exp}} - x_{j\,\mathrm{theo}}| - \sigma_{j\,\mathrm{theo}})^2}{\sigma^2_{j\,\mathrm{exp}}} & \text{if } |x_{j\,\mathrm{exp}} - x_{j\,\mathrm{theo}}| > \sigma_{j\,\mathrm{theo}}, \\ 0 & \text{otherwise.} \end{cases} \tag{81}$$

Here we suppress the dependence on the parameters $\{q_i\}$. Since we often encounter asymmetric theory intervals, notated as $(x_{i\,\mathrm{theo}})^{+\sigma_{i\,\mathrm{theo,\,sup}}}_{-\sigma_{i\,\mathrm{theo,\,inf}}}$, we generalise eq. (81) to

$$\chi^2 = \sum_j \begin{cases} \frac{(x_{j\,\mathrm{theo}} - \sigma_{j\,\mathrm{theo,\,inf}} - x_{j\,\mathrm{exp}})^2}{\sigma^2_{j\,\mathrm{exp}}} & \text{if } x_{j\,\mathrm{exp}} < (x_{j\,\mathrm{theo}} - \sigma_{j\,\mathrm{theo,\,inf}}), \\ \frac{(x_{j\,\mathrm{exp}} - (x_{j\,\mathrm{theo}} + \sigma_{j\,\mathrm{theo,\,sup}}))^2}{\sigma^2_{j\,\mathrm{exp}}} & \text{if } x_{j\,\mathrm{exp}} > (x_{j\,\mathrm{theo}} + \sigma_{j\,\mathrm{theo,\,sup}}), \\ 0 & \text{otherwise.} \end{cases} \tag{82}$$

We calculate $\sigma_{j\,\mathrm{theo,\,sup}}$ and $\sigma_{j\,\mathrm{theo,\,inf}}$ using the theory input given in tab. 8 and Appendix A.3, adding the resulting uncertainties in quadrature.

Using the χ^2 function in eq. (82) it is possible to define confidence levels (CLs) by means of the function

$$\mathrm{CL}(\{q_i\}) = \frac{1}{\sqrt{2^{N_\mathrm{dof}}}\Gamma(N_\mathrm{dof}/2)} \int_{\Delta\chi^2(\{q_i\})}^{\infty} e^{-t/2} t^{N_\mathrm{dof}/2-1} dt, \tag{83}$$

where $\Delta\chi^2$ is the χ^2 function after subtraction of its minimum: $\Delta\chi^2 = \chi^2 - \min(\chi^2)$. $N_{\rm dof}$ is the number of degrees of freedom of free model parameters. Setting CL $= 1 - 68.27/100$, CL $= 1 - 95.45/100$, CL $= 1 - 99.73/100$ and CL $= 1 - 99.99/100$ we find the $1\,\sigma$, $2\,\sigma$, $3\,\sigma$ and $5\,\sigma$ confidence levels respectively.

In our fits we only include quantities which are derived from *independently* measured observables, i.e. $\Delta A^0_{\rm CP}$, $\Delta A^-_{\rm CP}$, $S_{\rm CP}(\bar{B}^0 \to \pi^0 \bar{K}^0)$ and one out of the three categories of ratios $R^{(B,K,\pi)}$ (see Appendix B). Thereby we select the category which is most sensitive to the NP scenario under consideration. In this way we can on the one hand avoid to overweight a particular observable in the fit and on the other hand avoid that the fit is pulled to large q_i-values by discrepancies of quantities carrying only a small sensitivity on NP. We note here that, since the $R^{(B,K,\pi)}_{(c,n)}$ are ratios of branching fractions, which we assume to be Gaussian in experiment, their probability distributions derived from experimental data are not exact Gaussians as required by eqs. (81-83). Comparing fits to ratios of branching fractions to fits to the differences of the corresponding branching ratios (which follow a Gaussian distribution), we checked that the qualitative outcome of the fits in terms of preferred regions in the complex q_i-planes is not tarnished but that the contour lines are sharpened due to the reduction of theoretical uncertainties in the ratios.

D SUSY contributions to penguin coefficients

In this section we quote our results for the initial conditions of the Wilson coefficients $C_{3,..,10}$, $C_{7\gamma}$ and C_{8g} and of their mirror counterparts at the SUSY mass scale. We decompose the Wilson coefficients $C_{3,..,10}$ into contributions C_g from gluon penguins, C_γ from photon penguins, C_Z from Z penguins and $C^{\rm LL1}_{B_q}$, $C^{\rm LL2}_{B_q}$, $C^{\rm LR1}_{B_q}$, $C^{\rm LR1}_{B_q}$ $(q = u, d)$ from box diagrams:

$$C_3 = -\frac{1}{3}C_g + \frac{1}{s_W^2}C_Z + \frac{1}{2}C^{\rm LL1}_{B_u} + C^{\rm LL1}_{B_d}, \qquad C_4 = C_g + \frac{1}{2}C^{\rm LL2}_{B_u} + C^{\rm LL2}_{B_d}, \tag{84}$$

$$C_5 = -\frac{1}{3}C_g + \frac{1}{2}C^{\rm LR1}_{B_u} + C^{\rm LR1}_{B_d}, \qquad C_6 = C_g + \frac{1}{2}C^{\rm LR2}_{B_u} + C^{\rm LR2}_{B_d}, \tag{85}$$

$$C_7 = C_\gamma + 4C_Z + C^{\rm LR1}_{B_u} - C^{\rm LR1}_{B_d}, \qquad C_8 = C^{\rm LR2}_{B_u} - C^{\rm LR2}_{B_d}, \tag{86}$$

$$C_9 = C_\gamma - \frac{4c_W^2}{s_W^2}C_Z + C^{\rm LL1}_{B_u} - C^{\rm LL1}_{B_d}, \qquad C_{10} = C^{\rm LL2}_{B_u} - C^{\rm LL2}_{B_d}, \tag{87}$$

The corresponding FCNCs are mediated either by chargino-(up-)squark loops or by gluino-(down-)squark loops. We do not consider neutralino-(down-)squark exchange since it is suppressed with respect to the gluino contributions involving the strong coupling.

We neglect additional operators arising from $b \to s\bar{b}b$ transitions because they contribute to B decays only in higher orders. Moreover we neglect box diagrams with more than one flavour-violating squark line. As for the squarks of the first two generations we assume approximate degeneracy of the corresponding elements of $\hat{m}^2_{\tilde{Q}}$, likewise for $\hat{m}^2_{\tilde{u}}$ and $\hat{m}^2_{\tilde{d}}$. Yukawa couplings of the first two generations are set to zero. In this way the box diagrams depend on common masses $m_{\tilde{u}_L} = m_{\tilde{d}_L}$ ($m_{\tilde{u}_R}$ and $m_{\tilde{d}_R}$) for the left-handed (right-handed) squarks of the first and second generation.

We use the conventions of the SUSY Les Houches Accords [80,81] with only one exception: The CKM matrix is denoted as V whereas the chargino mixing matrices are named $\mathcal{U}$ and $\mathcal{V}$ instead of U and V.

D.1 Chargino contributions

We use the loop functions written down in [93,94] and the mass ratio

$$x_{u_r c_m} = \left(\frac{m_{\tilde{u}_r}}{m_{\tilde{\chi}^+_m}}\right)^2. \tag{88}$$

Generation indices $i, j = 1, 2, 3$, squark indices $r, s = 1, ..., 6$ and chargino indices $m, n = 1, 2$ are always summed over in the following. We abbreviate the chargino-quark-squark couplings by

$$\Gamma^L_{rim} = (g\mathcal{R}^{u*}_{ri}\mathcal{V}_{m1} - \mathcal{R}^{u*}_{r,i+3}\mathcal{V}_{m2}Y_{u_i}), \qquad \Gamma^R_{rim} = Y_b\,\mathcal{R}^{u*}_{ri}\,\mathcal{U}^*_{m2} \tag{89}$$

Neglecting Yukawa couplings of the first two generations we find that $C'_{3,..,10} = 0$. The coefficients $C_{3,..,10}$ are constructed from

$$C_\gamma = \frac{\alpha}{24\sqrt{2}G_F\pi V_{33}V^*_{32}(m_{\tilde{\chi}^+_m})^2} V_{j3}V^*_{i2}\Gamma^L_{rim}\Gamma^{L*}_{rjm}h^{(0)}_3(x_{u_r c_m}), \tag{90}$$

$$C_g = \frac{\alpha_s}{32\sqrt{2}G_F\pi V_{33}V^*_{32}(m_{\tilde{\chi}^+_m})^2} V_{j3}V^*_{i2}\Gamma^L_{rim}\Gamma^{L*}_{rjm}h^{(0)}_4(x_{u_r c_m}), \tag{91}$$

$$\begin{aligned} C^{\rm LL1}_{B_u} =& \frac{\alpha}{24 s_W^2\sqrt{2}G_F\pi V_{33}V^*_{32}} V_{j3}V^*_{i2}m_{\tilde{\chi}^+_m}m_{\tilde{\chi}^+_n}\mathcal{U}_{n1}\mathcal{U}^*_{m1}\Gamma^L_{rin}\Gamma^{L*}_{rjm} \\ & D_0(m^2_{\tilde{d}_L}, m^2_{\tilde{u}_r}, m^2_{\tilde{\chi}^+_m}, m^2_{\tilde{\chi}^+_n}), \end{aligned} \tag{92}$$

$$C^{\rm LL1}_{B_d} = \frac{\alpha}{48 s_W^2\sqrt{2}G_F\pi V_{33}V^*_{32}} V_{j3}V^*_{i2}\mathcal{V}_{m1}\mathcal{V}^*_{n1}\Gamma^L_{rin}\Gamma^{L*}_{rjm}D_2(m^2_{\tilde{u}_L}, m^2_{\tilde{u}_r}, m^2_{\tilde{\chi}^+_m}, m^2_{\tilde{\chi}^+_n}), \tag{93}$$

$$\begin{aligned} C_Z =& \frac{\alpha}{48 g^2\pi V_{33}V^*_{32}} V_{j3}V^*_{i2}\Gamma^L_{rin}\Gamma^{L*}_{sjm}\left(\delta_{mn}C_2(m^2_{\tilde{\chi}^+_m}, m^2_{\tilde{u}_s}, m^2_{\tilde{u}_r})\sum_{k=1}^{3}\mathcal{R}^u_{rk}\mathcal{R}^{u*}_{sk} + \right. \\ & \left. \delta_{sr}\left\{2C_0(m^2_{\tilde{u}_s}, m^2_{\tilde{\chi}^+_m}, m^2_{\tilde{\chi}^+_n})m_{\tilde{\chi}^+_m}m_{\tilde{\chi}^+_n}\mathcal{U}_{n1}\mathcal{U}^*_{m1} - C_2(m^2_{\tilde{u}_s}, m^2_{\tilde{\chi}^+_m}, m^2_{\tilde{\chi}^+_n})\mathcal{V}_{m1}\mathcal{V}^*_{n1}\right\}\right). \end{aligned} \tag{94}$$

The remaining box coefficients vanish. The magnetic and chromo-magnetic coefficients are given by

$$C_{7\gamma} = \frac{1}{8\sqrt{2}G_F V_{33}V_{32}^*(m_{\tilde{\chi}_m^+})^2} V_{j3}V_{i2}^*\Gamma_{rim}^L \left(\frac{m_{\tilde{\chi}_m^+}}{m_b}\Gamma_{rjm}^{R*}h_2^{(0)}(x_{u_r c_m}) - \Gamma_{rjm}^{L*}h_1^{(0)}(x_{u_r c_m}) \right), \quad (95)$$

$$C_{8g} = \frac{1}{8\sqrt{2}G_F V_{33}V_{32}^*(m_{\tilde{\chi}_m^+})^2} V_{j3}V_{i2}^*\Gamma_{rim}^L \left(\frac{m_{\tilde{\chi}_m^+}}{m_b}\Gamma_{rjm}^{R*}h_6^{(0)}(x_{u_r c_m}) - \Gamma_{rjm}^{L*}h_5^{(0)}(x_{u_r c_m}) \right). \quad (96)$$

D.2 Gluino contributions

Here we use the loop functions written down in [95,93] and

$$F_{10}(x) = \frac{3 - 3x + (2 + x)\log(x)}{12(x-1)^2}. \quad (97)$$

These functions depend on the mass ratio

$$x_{gd_s} = \left(\frac{m_{\tilde{g}}}{m_{\tilde{d}_s}} \right)^2. \quad (98)$$

Writing

$$G_{si}^L = \mathcal{R}_{si}^d, \qquad G_{si}^R = \mathcal{R}_{s,i+3}^{d*} \quad (99)$$

we split the 6×6 down-squark mixing matrix $\mathcal{R}$ into a lefthanded and a righthanded 6×3 block G^L and G^R. With a sum over all indices understood, we find ($q = u, d$)

$$C_\gamma = -\frac{4\sqrt{2}\alpha\alpha_s}{27G_F V_{33}V_{32}^* m_{\tilde{d}_s}^2} G_{s2}^{L*}G_{s3}^L\, F_6(x_{gd_s}), \quad (100)$$

$$C_g = \frac{\alpha_s^2}{2\sqrt{2}G_F V_{33}V_{32}^* m_{\tilde{d}_s}^2} G_{s2}^{L*}G_{s3}^L \left(C_F F_6(x_{gd_s}) - C_A F_{10}(x_{gd_s}) \right), \quad (101)$$

$$C_Z = -\frac{2\alpha\alpha_s}{9g^2 V_{33}V_{32}^*} \sum_{i=1}^{3} G_{r3}^L G_{si}^R G_{ri}^{R*} G_{s2}^{L*} C_2(m_{\tilde{g}}^2, m_{\tilde{d}_r}^2, m_{\tilde{d}_s}^2), \quad (102)$$

$$C_{B_q}^{\text{LL1}} = \frac{\alpha_s^2\, G_{r3}^L G_{r2}^{L*}}{108\sqrt{2}G_F V_{33}V_{32}^*} \left(20 m_{\tilde{g}}^2 D_0(m_{\tilde{g}}^2, m_{\tilde{g}}^2, m_{\tilde{d}_r}^2, m_{\tilde{q}_L}^2) + D_2(m_{\tilde{g}}^2, m_{\tilde{g}}^2, m_{\tilde{d}_r}^2, m_{\tilde{q}_L}^2) \right), \quad (103)$$

$$C_{B_q}^{\text{LL2}} = -\frac{\alpha_s^2\, G_{r3}^L G_{r2}^{L*}}{36\sqrt{2}G_F V_{33}V_{32}^*} \left(4 m_{\tilde{g}}^2 D_0(m_{\tilde{g}}^2, m_{\tilde{g}}^2, m_{\tilde{d}_r}^2, m_{\tilde{q}_L}^2) - 7 D_2(m_{\tilde{g}}^2, m_{\tilde{g}}^2, m_{\tilde{d}_r}^2, m_{\tilde{q}_L}^2) \right), \quad (104)$$

$$C_{B_q}^{\mathrm{LR1}} = -\frac{\alpha_s^2\, G_{r3}^L G_{r2}^{L*}}{54\sqrt{2} G_F V_{33} V_{32}^*} \left(m_{\tilde{g}}^2 D_0(m_{\tilde{g}}^2, m_{\tilde{g}}^2, m_{\tilde{d}_r}^2, m_{\tilde{q}_R}^2) + 5 D_2(m_{\tilde{g}}^2, m_{\tilde{g}}^2, m_{\tilde{d}_r}^2, m_{\tilde{q}_R}^2) \right), \tag{105}$$

$$C_{B_q}^{\mathrm{LR2}} = -\frac{\alpha_s^2\, G_{r3}^L G_{r2}^{L*}}{18\sqrt{2} G_F V_{33} V_{32}^*} \left(7 m_{\tilde{g}}^2 D_0(m_{\tilde{g}}^2, m_{\tilde{g}}^2, m_{\tilde{d}_r}^2, m_{\tilde{q}_R}^2) - D_2(m_{\tilde{g}}^2, m_{\tilde{g}}^2, m_{\tilde{d}_r}^2, m_{\tilde{q}_R}^2) \right). \tag{106}$$

The magnetic and chromo-magnetic coefficients are

$$C_{7\gamma} = \frac{4\sqrt{2}\alpha_s \pi}{9 G_F V_{33} V_{32}^* m_{\tilde{d}_s}^2} \left(\frac{m_{\tilde{g}}}{m_b} G_{s2}^{L*} G_{s3}^R F_4(x_{gd_s}) - G_{s2}^{L*} G_{s3}^L F_2(x_{gd_s}) \right), \tag{107}$$

$$\begin{aligned} C_{8g} = &\frac{\sqrt{2}\alpha_s \pi}{2 G_F V_{33} V_{32}^* m_{\tilde{d}_s}^2} \left(\frac{m_{\tilde{g}}}{m_b} G_{s2}^{L*} G_{s3}^R (C_A F_3(x_{gd_s}) - (2C_F - C_A) F_4(x_{gd_s})) \right. \\ &\left. - G_{s2}^{L*} G_{s3}^L (C_A F_1(x_{gd_s}) - (2C_F - C_A) F_2(x_{gd_s})) \right), \end{aligned} \tag{108}$$

with the group factors $C_F = \frac{4}{3}$ and $C_A = 3$.

The coefficients of the respective mirror operators are obtained by exchanging all L and R indices in the above results.

References

[1] R. Godang *et al.*, "Observation of exclusive two-body B decays to kaons and pions," *Phys. Rev. Lett.*, vol. 80, pp. 3456–3460, 1998.

[2] D. Cronin-Hennessy *et al.*, "Observation of $B \to K^{\pm}\pi^0$ and $B \to K^0\pi^0$, and evidence for $B \to \pi^+\pi^-$," *Phys. Rev. Lett.*, vol. 85, pp. 515–519, 2000.

[3] M. Gronau and J. L. Rosner, "Combining CP asymmetries in $B \to K\pi$ decays," *Phys. Rev.*, vol. D59, p. 113002, 1999.

[4] S. Baek and D. London, "Is there still a $B \to \pi K$ puzzle?," *Phys. Lett.*, vol. B653, pp. 249–253, 2007.

[5] R. Fleischer, S. Recksiegel, and F. Schwab, "On Puzzles and Non-Puzzles in $B \to \pi\pi$, πK Decays," *Eur. Phys. J.*, vol. C51, pp. 55–61, 2007.

[6] E. Barberio *et al.*, "Averages of $b-$hadron and $c-$hadron Properties at the End of 2007," 2008.

[7] A. Hocker, H. Lacker, S. Laplace, and F. Le Diberder, "A New approach to a global fit of the CKM matrix," *Eur. Phys. J.*, vol. C21, pp. 225–259, 2001.

[8] A. J. Buras, R. Fleischer, S. Recksiegel, and F. Schwab, "The $B \to \pi K$ puzzle and its relation to rare B and K decays," *Eur. Phys. J.*, vol. C32, pp. 45–54, 2003.

[9] A. J. Buras, R. Fleischer, S. Recksiegel, and F. Schwab, "$B \to \pi\pi$, new physics in $B \to \pi K$ and implications for rare K and B decays," *Phys. Rev. Lett.*, vol. 92, p. 101804, 2004.

[10] T. Yoshikawa, "A possibility of large electro-weak penguin contribution in $B \to K\pi$ modes," *Phys. Rev.*, vol. D68, p. 054023, 2003.

[11] S. Mishima and T. Yoshikawa, "Large electroweak penguin contribution in $B \to K\pi$ and $\pi\pi$ decay modes," *Phys. Rev.*, vol. D70, p. 094024, 2004.

[12] M. Beneke, G. Buchalla, M. Neubert, and C. T. Sachrajda, "QCD factorization for $B \to \pi\pi$ decays: Strong phases and CP violation in the heavy quark limit," *Phys. Rev. Lett.*, vol. 83, pp. 1914–1917, 1999.

[13] M. Beneke, G. Buchalla, M. Neubert, and C. T. Sachrajda, "QCD factorization for exclusive, non-leptonic B meson decays: General arguments and the case of heavy-light final states," *Nucl. Phys.*, vol. B591, pp. 313–418, 2000.

[14] M. Beneke, G. Buchalla, M. Neubert, and C. T. Sachrajda, "QCD factorization in $B \to \pi K, \pi\pi$ decays and extraction of Wolfenstein parameters," *Nucl. Phys.*, vol. B606, pp. 245–321, 2001.

[15] M. Beneke and M. Neubert, "QCD factorization for $B \to PP$ and $B \to PV$ decays," *Nucl. Phys.*, vol. B675, pp. 333–415, 2003.

[16] M. Beneke, J. Rohrer, and D. Yang, "Branching fractions, polarisation and asymmetries of $B \to VV$ decays," *Nucl. Phys.*, vol. B774, pp. 64–101, 2007.

[17] M. Neubert, "Rescattering effects, isospin relations and electroweak penguins in $B \to \pi K$ decays," *Phys.Lett.*, vol. B424, pp. 152–160, 1998.

[18] D. Zeppenfeld, "SU(3) Relations for B Meson Decays," *Zeit. Phys.*, vol. C8, p. 77, 1981.

[19] M. Gronau, O. F. Hernandez, D. London, and J. L. Rosner, "Decays of B mesons to two light pseudoscalars," *Phys.Rev.*, vol. D50, pp. 4529–4543, 1994.

[20] D. M. Asner *et al.*, "Search for exclusive charmless hadronic B decays," *Phys. Rev.*, vol. D53, pp. 1039–1050, 1996.

[21] S. Chen *et al.*, "Measurement of charge asymmetries in charmless hadronic B meson decays," *Phys. Rev. Lett.*, vol. 85, pp. 525–529, 2000.

[22] A. Bornheim *et al.*, "Measurements of charmless hadronic two-body B meson decays and the ratio $\mathcal{B}(B \to DK)/\mathcal{B}(B \to D\pi)$," *Phys. Rev.*, vol. D68, p. 052002, 2003.

[23] P. Chang *et al.*, "Observation of the decays $B^0 \to K^+\pi^-\pi^0$ and $B^0 \to \rho^- K^+$," *Phys. Lett.*, vol. B599, pp. 148–158, 2004.

[24] B. Aubert *et al.*, "Improved Measurements of the Branching Fractions for $B^0 \to \pi^+\pi^-$ and $B^0 \to K^+\pi^-$, and a Search for $B^0 \to K^+K^-$," *Phys. Rev.*, vol. D75, p. 012008, 2007.

[25] B. Aubert *et al.*, "Observation of $B^+ \to \bar{K}^0 K^+$ and $B^0 \to K^0 \bar{K}^0$," *Phys. Rev. Lett.*, vol. 97, p. 171805, 2006.

[26] K. Abe *et al.*, "Observation of B decays to two kaons," *Phys. Rev. Lett.*, vol. 98, p. 181804, 2007.

[27] K. Abe *et al.*, "Measurements of branching fractions for $B \to K\pi$ and $B \to \pi\pi$ decays with 449 million $B\bar{B}$ pairs," *Phys. Rev. Lett.*, vol. 99, p. 121601, 2007.

[28] M. Morello, "Branching fractions and direct CP asymmetries of charmless decay modes at the Tevatron," *Nucl. Phys. Proc. Suppl.*, vol. 170, pp. 39–45, 2007.

[29] B. Aubert *et al.*, "Study of $B^0 \to \pi^0\pi^0$, $B^\pm \to \pi^\pm\pi^0$, and $B^\pm \to K^\pm\pi^0$ Decays, and Isospin Analysis of $B \to \pi\pi$ Decays," *Phys. Rev.*, vol. D76, p. 091102, 2007.

[30] B. Aubert *et al.*, "Evidence for Direct CP Violation from Dalitz-plot analysis of $B^\pm \to K^\pm\pi^\mp\pi^\pm$," *Phys. Rev.*, vol. D78, p. 012004, 2008.

[31] S. W. Lin *et al.*, "Difference in direct charge-parity violation between charged and neutral B meson decays," *Nature*, vol. 452, pp. 332–335, 2008.

[32] B. Aubert *et al.*, "Measurement of CP Asymmetries and Branching Fractions in $B^0 \to\to \pi^+\pi^-$, $B^0 \to K^+\pi^-$, $B^0 \to \pi^0\pi^0$, $B^0 \to K^0\pi^0$ and Isospin Analysis of $B \to \pi\pi$ Decays," 2008.

[33] B. Aubert *et al.*, "Measurement of time dependent CP asymmetry parameters in B^0 meson decays to ωK^0_S, $\eta' K^0$ and $\pi^0 K^0_S$," *Phys. Rev.*, vol. D79, p. 052003, 2009.

[34] M. Fujikawa *et al.*, "Measurement of CP asymmetries in $B^0 \to K^0\pi^0$ decays," *Phys. Rev.*, vol. D81, p. 011101, 2010.

[35] A. J. Buras, R. Fleischer, S. Recksiegel, and F. Schwab, "New aspects of $B \to \pi\pi, \pi K$ and their implications for rare decays," *Eur. Phys. J.*, vol. C45, pp. 701–710, 2006.

[36] M. Gronau and J. L. Rosner, "Rate and CP-asymmetry sum rules in $B \to K\pi$," *Phys. Rev.*, vol. D74, p. 057503, 2006.

[37] M. Gronau and J. L. Rosner, "Sum rule for rate and CP asymmetry in $B^+ \to K^+\pi^0$," *Phys. Lett.*, vol. B644, pp. 237–240, 2007.

[38] R. Fleischer, "$B_{s,d} \to \pi\pi, \pi K, KK$: Status and Prospects," *Eur. Phys. J.*, vol. C52, pp. 267–281, 2007.

[39] C. S. Kim, S. Oh, and Y. W. Yoon, "Is there any puzzle of new physics in $B \to K\pi$ decays?," *Phys. Lett.*, vol. B665, pp. 231–236, 2008.

[40] T. Feldmann, M. Jung, and T. Mannel, "Is there a non-Standard-Model contribution in non-leptonic $b \to s$ decays?," *JHEP*, vol. 08, p. 066, 2008.

[41] R. Fleischer, S. Jager, D. Pirjol, and J. Zupan, "Benchmarks for the New-Physics Search through CP Violation in $B^0 \to \pi^0 K_S$," *Phys. Rev.*, vol. D78, p. 111501, 2008.

[42] S. Baek, C.-W. Chiang, and D. London, "The $B \to \pi K$ Puzzle: 2009 Update," *Phys. Lett.*, vol. B675, p. 59, 2009.

[43] S. Baek, C.-W. Chiang, M. Gronau, D. London, and J. L. Rosner, "Diagnostic for new physics in $B \to \pi K$ decays," *Phys. Lett.*, vol. B678, pp. 97–100, 2009.

[44] A. J. Buras, R. Fleischer, S. Recksiegel, and F. Schwab, "Anatomy of prominent B and K decays and signatures of CP- violating new physics in the electroweak penguin sector," *Nucl. Phys.*, vol. B697, pp. 133–206, 2004.

[45] A. J. Buras, R. Fleischer, S. Recksiegel, and F. Schwab, "The $B \to \pi\pi, \pi K$ puzzles in the light of new data: Implications for the standard model, new physics and rare decays," *Acta Phys. Polon.*, vol. B36, pp. 2015–2050, 2005.

[46] C. S. Kim, S. Oh, and C. Yu, "A critical study of the $B \to K\pi$ puzzle," *Phys. Rev.*, vol. D72, p. 074005, 2005.

[47] K. Abe *et al.*, "Search for charmless hadronic decays of B mesons with the SLD detector," *Phys. Rev.*, vol. D62, p. 071101, 2000.

[48] R. Fleischer, "Search for the angle γ in the electroweak penguin dominated decay $B_s \to \pi^0\phi$," *Phys. Lett.*, vol. B332, pp. 419–427, 1994.

[49] G. Zweig, "CERN Report No. 8419 TH 412; reprinted in Developments in the Quark Theory of Hadrons, edited by D. B. Lichtenberg and S. P. Rosen (Hadronic Press, Massachusetts, 1980)." 1964.

[50] S. Okubo, "Phi meson and unitary symmetry model," *Phys. Lett.*, vol. 5, pp. 165–168, 1963.

[51] J. Iizuka, K. Okada, and O. Shito, "Systematics and phenomenology of boson mass levels. 3," *Prog. Theor. Phys.*, vol. 35, pp. 1061–1073, 1966.

[52] J. Iizuka, "Systematics and phenomenology of meson family," *Prog. Theor. Phys. Suppl.*, vol. 37, pp. 21–34, 1966.

[53] A. L. Kagan, "Right-handed currents, CP violation, and $B \to VV$," 2004.

[54] A. J. Buras and M. Munz, "Effective Hamiltonian for $B \to X_s e^+ e^-$ beyond leading logarithms in the NDR and HV schemes," *Phys. Rev.*, vol. D52, pp. 186–195, 1995.

[55] G. Buchalla and A. J. Buras, "QCD corrections to rare K and B decays for arbitrary top quark mass," *Nucl. Phys.*, vol. B400, pp. 225–239, 1993.

[56] S. Glenn *et al.*, "Search for inclusive $b \to s\ell^+\ell^-$," *Phys. Rev. Lett.*, vol. 80, pp. 2289–2293, 1998.

[57] B. Aubert *et al.*, "Measurement of the $B \to X_s \ell^+\ell^-$ branching fraction with a sum over exclusive modes," *Phys. Rev. Lett.*, vol. 93, p. 081802, 2004.

[58] K. Abe *et al.*, "Improved measurement of the electroweak penguin process $B \to X_s\ell^+\ell^-$," 2004.

[59] M. Iwasaki *et al.*, "Improved measurement of the electroweak penguin process $B \to X_s\ell^+\ell^-$," *Phys. Rev.*, vol. D72, p. 092005, 2005.

[60] C. Bobeth, G. Hiller, and G. Piranishvili, "CP Asymmetries in bar $B \to \bar{K}^*(\to \bar{K}\pi)\bar{\ell}\ell$ and Untagged $\bar{B}_s$, $B_s \to \phi(\to K^+K^-)\bar{\ell}\ell$ Decays at NLO," *JHEP*, vol. 07, p. 106, 2008.

[61] U. Egede, T. Hurth, J. Matias, M. Ramon, and W. Reece, "New observables in the decay mode $\bar{B} \to \bar{K}^{*0}\ell^+\ell^-$," *JHEP*, vol. 11, p. 032, 2008.

[62] W. Altmannshofer *et al.*, "Symmetries and Asymmetries of $B \to K^*\mu^+\mu^-$ Decays in the Standard Model and Beyond," *JHEP*, vol. 01, p. 019, 2009.

[63] G. Buchalla, A. J. Buras, and M. E. Lautenbacher, "Weak Decays Beyond Leading Logarithms," *Rev. Mod. Phys.*, vol. 68, pp. 1125–1144, 1996.

[64] A. J. Buras, M. Misiak, and J. Urban, "Two-loop QCD anomalous dimensions of flavour-changing four-quark operators within and beyond the standard model," *Nucl. Phys.*, vol. B586, pp. 397–426, 2000.

[65] V. Lubicz and C. Tarantino, "Flavour physics and Lattice QCD: averages of lattice inputs for the Unitarity Triangle Analysis," *Nuovo Cim.*, vol. 123B, pp. 674–688, 2008.

[66] A. Abulencia *et al.*, "Observation of $B_s^0 - \bar{B}_s^0$ oscillations," *Phys. Rev. Lett.*, vol. 97, p. 242003, 2006.

[67] A. Lenz and U. Nierste, "Theoretical update of $B_s - \bar{B}_s$ mixing," *JHEP*, vol. 0706, p. 072, 2007.

[68] A. Lenz *et al.*, "Anatomy of New Physics in $B-\bar{B}$ mixing," *arXiv:1008.1593 [hep-ph]*, 2010.

[69] P. Langacker and D. London, "Mixing Between Ordinary and Exotic Fermions," *Phys.Rev.*, vol. D38, p. 886, 1988.

[70] Y. Grossman, M. Neubert, and A. L. Kagan, "Trojan penguins and isospin violation in hadronic B decays," *JHEP*, vol. 10, p. 029, 1999.

[71] G. Buchalla, G. Hiller, and G. Isidori, "Phenomenology of nonstandard Z couplings in exclusive semileptonic $b \to s$ transitions," *Phys. Rev.*, vol. D63, p. 014015, 2000.

[72] W. Altmannshofer, A. J. Buras, D. M. Straub, and M. Wick, "New strategies for New Physics search in $B \to K^* \nu\bar{\nu}$, $B \to K\nu\bar{\nu}$ and $B \to X_s \nu\bar{\nu}$ decays," *JHEP*, vol. 04, p. 022, 2009.

[73] P. Langacker, "The Physics of Heavy Z' Gauge Bosons," *Rev. Mod. Phys.*, vol. 81, pp. 1199–1228, 2009.

[74] V. Barger *et al.*, "Family Non-universal $U(1)'$ Gauge Symmetries and $b \to s$ Transitions," *Phys. Rev.*, vol. D80, p. 055008, 2009.

[75] Q. Chang, X.-Q. Li, and Y.-D. Yang, "Constraints on the nonuniversal Z' couplings from $B \to \pi K, \pi K^*$ and ρK Decays," *JHEP*, vol. 05, p. 056, 2009.

[76] V. Barger *et al.*, "$b \to s$ Transitions in Family-dependent $U(1)'$ Models," *JHEP*, vol. 12, p. 048, 2009.

[77] T. G. Rizzo, "Gauge kinetic mixing and leptophobic Z' in E(6) and SO(10)," *Phys. Rev.*, vol. D59, p. 015020, 1999.

[78] K. Huitu and S. Khalil, "New Physics contribution to $B \to K\pi$ decays in SCET," *Phys. Rev.*, vol. D81, p. 095008, 2010.

[79] S. Khalil, A. Masiero, and H. Murayama, "$B \to K\pi$ Puzzle and New Sources of CP Violation in Supersymmetry," *Phys. Lett.*, vol. B682, pp. 74–77, 2009.

[80] P. Skands *et al.*, "SUSY Les Houches accord: Interfacing SUSY spectrum calculators, decay packages, and event generators," *JHEP*, vol. 07, p. 036, 2004.

[81] B. Allanach, C. Balazs, G. Belanger, M. Bernhardt, F. Boudjema, *et al.*, "SUSY Les Houches Accord 2," *Comput.Phys.Commun.*, vol. 180, pp. 8–25, 2009.

[82] M. Imbeault, S. Baek, and D. London, "The $B \to \pi K$ Puzzle and Supersymmetry," *Phys. Lett.*, vol. B663, pp. 410–415, 2008.

[83] S. Khalil private communication.

[84] M. Beneke, X.-Q. Li, and L. Vernazza, "Hadronic B decays in the MSSM with large $\tan\beta$," *Eur. Phys. J.*, vol. C61, pp. 429–438, 2009.

[85] M. Beneke and S. Jager, "Spectator scattering at NLO in non-leptonic B decays: Tree amplitudes," *Nucl. Phys.*, vol. B751, pp. 160–185, 2006.

[86] M. Beneke and S. Jager, "Spectator scattering at NLO in non-leptonic B decays: Leading penguin amplitudes," *Nucl. Phys.*, vol. B768, pp. 51–84, 2007.

[87] M. Bartsch, G. Buchalla, and C. Kraus, "$B \to V_L V_L$ Decays at Next-to-Leading Order in QCD," 2008.

[88] M. Beneke, T. Huber, and X.-Q. Li, "NNLO vertex corrections to non-leptonic B decays: Tree amplitudes," *Nucl. Phys.*, vol. B832, pp. 109–151, 2010.

[89] C. Amsler *et al.*, "Review of particle physics," *Phys. Lett.*, vol. B667, p. 1, 2008.

[90] S. Bethke, "The 2009 World Average of $\alpha_s(M_Z)$," *Eur. Phys. J.*, vol. C64, pp. 689–703, 2009.

[91] G. Bell and V. Pilipp, "$B^- \to \pi^-\pi^0/\rho^-\rho^0$ to NNLO in QCD factorization," *Phys. Rev.*, vol. D80, p. 054024, 2009.

[92] H. J. Lipkin, "A useful approximate isospin equality for charmless strange B decays," *Phys. Lett.*, vol. B445, pp. 403–406, 1999.

[93] A. J. Buras, T. Ewerth, S. Jager, and J. Rosiek, "$K^+ \to \pi^+\nu\bar{\nu}$ and $K_L \to \pi^0\nu\bar{\nu}$ decays in the general MSSM," *Nucl. Phys.*, vol. B714, pp. 103–136, 2005.

[94] C. Bobeth, A. J. Buras, and T. Ewerth, "$\bar{B} \to X_s l^+ l^-$ in the MSSM at NNLO," *Nucl. Phys.*, vol. B713, pp. 522–554, 2005.

[95] S. Bertolini, F. Borzumati, A. Masiero, and G. Ridolfi, "Effects of supergravity induced electroweak breaking on rare B decays and mixings," *Nucl. Phys.*, vol. B353, pp. 591–649, 1991.